UNIVERSITY OF CATANIA

DEPARTMENT OF CHEMICAL SCIENCES

INTERNATIONAL PhD IN CHEMICAL SCIENCES – XXXIII CYCLE

Debora Concetta Santonocito

Lipid Nanoparticles as Tools for the Administration of Active Natural Products Aimed to the Treatment of Nervous System Disorders

_____

PhD Thesis

_____

Tutor: PhD Coordinator:

Prof. Carmelo Puglia   Prof. Salvatore Sortino

Contents

Chapter 1

Chapter 2

Chapter 3

Chapter 4

Chapter 1

1.1. Natural compounds: advantages and disadvantages in clinical practice

In the last decade, the attention on natural products, especially those derived from plants, has been increased due to their safe toxicological profile and their numerous applications in the pharmaceutical field. Scientific research has undergone numerous advances, in particular about some properties shown by natural substances, in order to find innovative therapeutic solutions for human health. The consumption of products of natural origin is remarkable, according to the perceptions of current consumers which everything that is "natural is good". This belief is guaranteed by the millennial use of these natural compounds; in fact their therapeutic properties are traditionally known since the beginning of civilization, as there were no other "therapeutic" remedies available. Natural compounds have been long and widely used in the prevention and treatment of nervous system disorders [J. *Zhang et al., 2019*]. Numerous sacred texts of ancient and scientific Indian literature such as Rigveda, Yajurveda, Samaveda and Atharvanaveda have served as references to herbal medicines for the treatment of various disorders of the nervous system [*P. Srivastava et al., 2016*]. Although many synthetic neuroactive drugs have been developed over the centuries, the researchers have focused their attention on phytochemicals due to their minimal side effects and multi-target characteristics [*M. Rasool et al., 2014*].

Among the promising phytocompounds for the treatment of nervous system disorders deserve special attention:

- Curcumin, isolated from the rhizome of *Curcuma Longa*, is in use for several centuries as therapeutic agent. It has a series of biological activities such as antioxidant, anti-inflammatory and anti-amyloid [*N. Aftab et al., 2010; R.D. Shytle et al., 2009; N.K. Gowda et al.; 2009*].

- Astaxanthin is a fat-soluble orange-red color pigment extracted from the *Haematococcus pluvialis*, a unicellular biflagellate green microalgae. Astaxanthin exhibits a powerful antioxidant activity and

possesses many valuable therapeutical functions, such as anti-aging, anticancer [*P.N. Prabhu et al., 2009; D.N. Tripathi et al., 2010; P. Palozza et al., 2009*] and neuroprotective effect [*A. Satoh et al., 2009*].

- Capsaicin is a molecule present in numerous different species of red chilli pepper (*Capsicum*) whose "spicy" taste derives from the concentration of this compound. It was first isolated from paprika and cayenne in the late 19th century [*J.C. Thresh, 1876*]. Capsaicin has been used medicinally for centuries, but recently it has been extensively studied fot its antioxidant, anti-inflammatory and analgesic properties [*D.A. Simone et al., 1989; J.D. Brederson et al., 2013; A. Galano et al., 2012; C.S. Kim et al., 2003*].

- Mangiferin is an interesting natural compound extracted from the plant of *Mangifera indica L.* A number of ancient Indian scriptures have highlighted the nutritive and medicinal value of different parts of the mango tree. It has a wide scope therapeutic properties, including anti-inflammatory [*A. Sá-Nunes et al., 2006*] and antioxidant [*E. Joubert et al., 2008*] activities for the potential treatment of eye diseases.

- N-Palmitoylethanolamide is an endogenous fatty acid amide belonging to the family of N-acylethanolamines (NAEs) and it was isolated for the first time from purified lipid fractions of soybeans, egg yolk and peanut meal [*O.H. Coburn et al., 1954; O.H. Ganley et al., 1958*]. It has a potent anti-inflammatory activity, which can be exploited in different pathological conditions and in a variety of biological systems including retina [*I. Matias et al., 2006; S. Petrosino et al., 2010; D. Tronino et al., 2016*]. There are, in fact, several reports highlighting that PEA can exert beneficial effects in several retinal diseases such as diabetic retinopathy and glaucoma [*C. Costagliola et al., 2014*].

Notwithstanding this appreciable renaissance of natural substances, their potential therapeutic properties are strongly compromise due to stability and bioavailability issues. These unfavorable features are mainly represented by poor water solubility, low gastrointestinal permeability and a not

8

optimal biological stability during the storage period (low shelf life). The last phenomenon, in particular, is responsible for a reduction in the dose of the drug and consequently the therapeutic effect of the phytocompound [*F. Sansone et al., 2011*].

Moreover, most drugs currently used for CNS disorders are lipid-soluble; their low solubility is a critical issue in clinical practice, since it often results in low bioavailability [*W.A. Banks, 2009*].

Therefore, innovative strategies are required in order to overcome the limits of these interesting natural active compounds and to allow their potential application in therapeutic field.

Recently, nanomedicine is attracting considerable attention due to its potential advantages to enhance pharmacokinetics as well as pharmacodynamics activity of plant origin constituents.

1.2. Lipid-based nanocarriers (LNCs)

The advent of nanotechnology has made important innovations in the field of biological research and clinical practice.

The history of nanoparticles in pharmaceutical research began with polymeric nanoparticles, carriers with submicron dimensions made up of biodegradable and non-biodegradable polymers. Advantages of these carriers are site-specific targeting and controlled release of the drugs [*E. Allèmann et al., 1993; S.A. Wissing et al., 2003*]. However, they showed significant problems, such as the cytotoxicity of polymers used and a complex industrial scale-up [*K. Vega-Villa et al., 2008*]. Therefore, these nanoparticles are not suitable for the pharmaceutical market. Alternative nanoparticles made from solid lipids called Lipid-based Nanocarriers (LNCs) have been used as a new colloidal carrier since 1990 [*B. Choongjin et al., 2014*]. LNCs are colloidal carrier systems composed by a lipid matrix and they are divided into a first (Solid Lipid Nanoparticles - SLNs) and a second generation (Nanostructured Lipid Carriers - NLCs) [*R.H. Müller et al., 2000; C. Schwarz et al., 1999; H. Rajashree et al., 2011*].
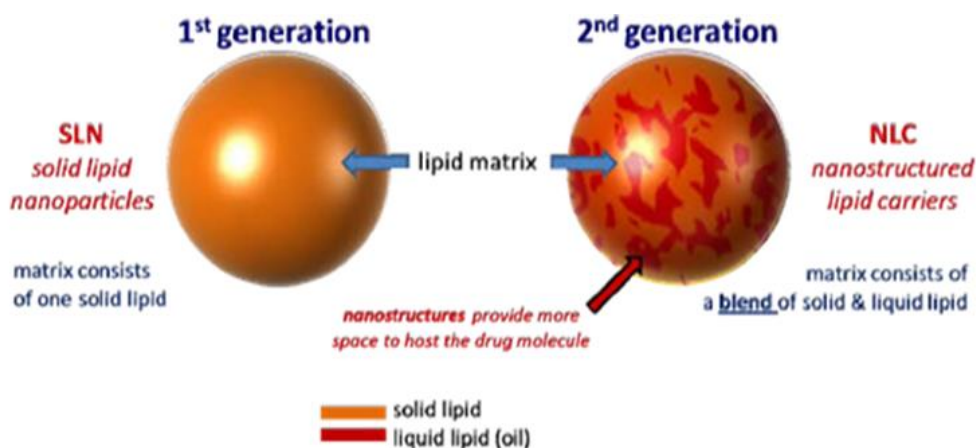
Figure 1. Schematic representation of SLN and NLC.

1.3. Solid Lipid Nanoparticles (SLNs)

SLNs are colloidal carriers made from solid lipids and stabilized by surfactant with a mean diameter ranging from 50 and 1000 nm. They are formulated using biodegradable lipids that are Generally Recognized As Safe (GRAS). The matrix of SLNs includes of solid lipids such as triglycerides (trimyristin, tripalmitin, tristearin), glyceryl behenate, glyceryl palmitostearate, fatty acids (stearic acid) or the wax (cetyl palmitate) [*E. Esposito, 2005; M. Sentjurc et al., 2003*]. Usually, lipid concentration ranges between 0.1 and 30% [*J. Pardeike et al., 2009*], while surfactant added for physical stabilization, had a concentration ranging from 0.5 to 5%. The most used emulsifiers are poloxamer 188, polysorbate 80, soybean and egg lecithin. SLNs are able to solubilize hydrophilic and lipophilic molecules in a physiologic environment, controlling their delivery and protecting them from degradation [*A. Zur Mühlen et al., 1998*]. Compared with others systems (nanoemulsions, polymeric nanoparticles and liposomes), SLNs have many benefits such as ease of preparation, low cost, high-scale production, excellent physical stability, chemical versatility, no toxicity of lipid carrier system and biodegradability of lipids [*C. Puglia et al., 2016*]. The encapsulation of the drugs into these nano-carriers increases their solubility, stability, cell uptake, specificity, tolerability, and therapeutic index. SLNs are obtained only from solid lipids at room temperature, presenting highly

10

organized structures "symmetric brick wall model" and forming perfect crystals [*Rajashree et al., 2011*]. SLN structure depends on the chemical characteristics of drug and excipients. As reported in figure 2, drug can be encapsulated within the SLN in different ways, obtaining three different types of nanoparticles [*W.Z. Mehnert et al., 1997; S.A. Wissing et al., 2004*]:

- The SLN Type I, or "homogeneous matrix model", in which the drug is dispersed in the solid solution;

- The SLN Type II, or "drug-enriched shell model", in which the shell is drug-enriched;

- The SLN type III, or "drug-enriched core model", in which the lipid core is drug-enriched.
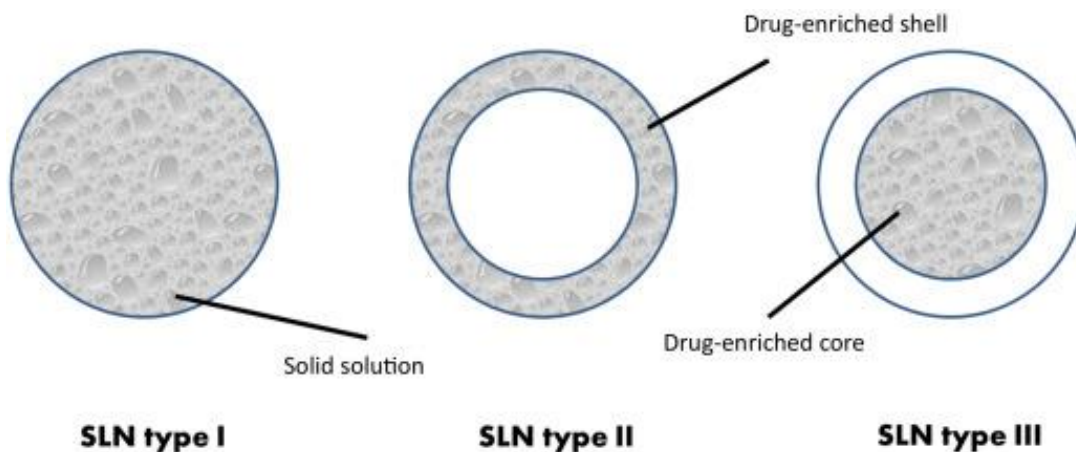
Figure 2. SLN type: (I) homogeneous matrix model; (II) drug- enriched shell model; (III)drug-enriched core-model.

Although SLNs represent an innovative and excellent drug delivery systems, they showed some limitations, such as the poor loading capacity and the physical instability during storage, due to expulsion of the loaded drug by their crystalline structure [*B. Fonseca-Santos et al., 2020*].

1.4. Nanostructured Lipid Carriers (NLCs)

In order to overcome SLN limitations, a second generation of lipid nanoparticles was developed, the so-called NLC or "Nanostructured lipid carriers". The innovation of these carriers consists in the composition of a solid/liquid two-phase hybridized lipid matrix, thus minimizing the phenomenon of expulsion of active compound [*R.H. Muller et al., 2002*]. This combination of both lipids leads to the formation of disordered structures "welsh natural stone wall model", generating an imperfect crystal structure (Figure 3) that provides larger spaces, enabling a high drug loading [*R.H. Muller et al., 2005*].
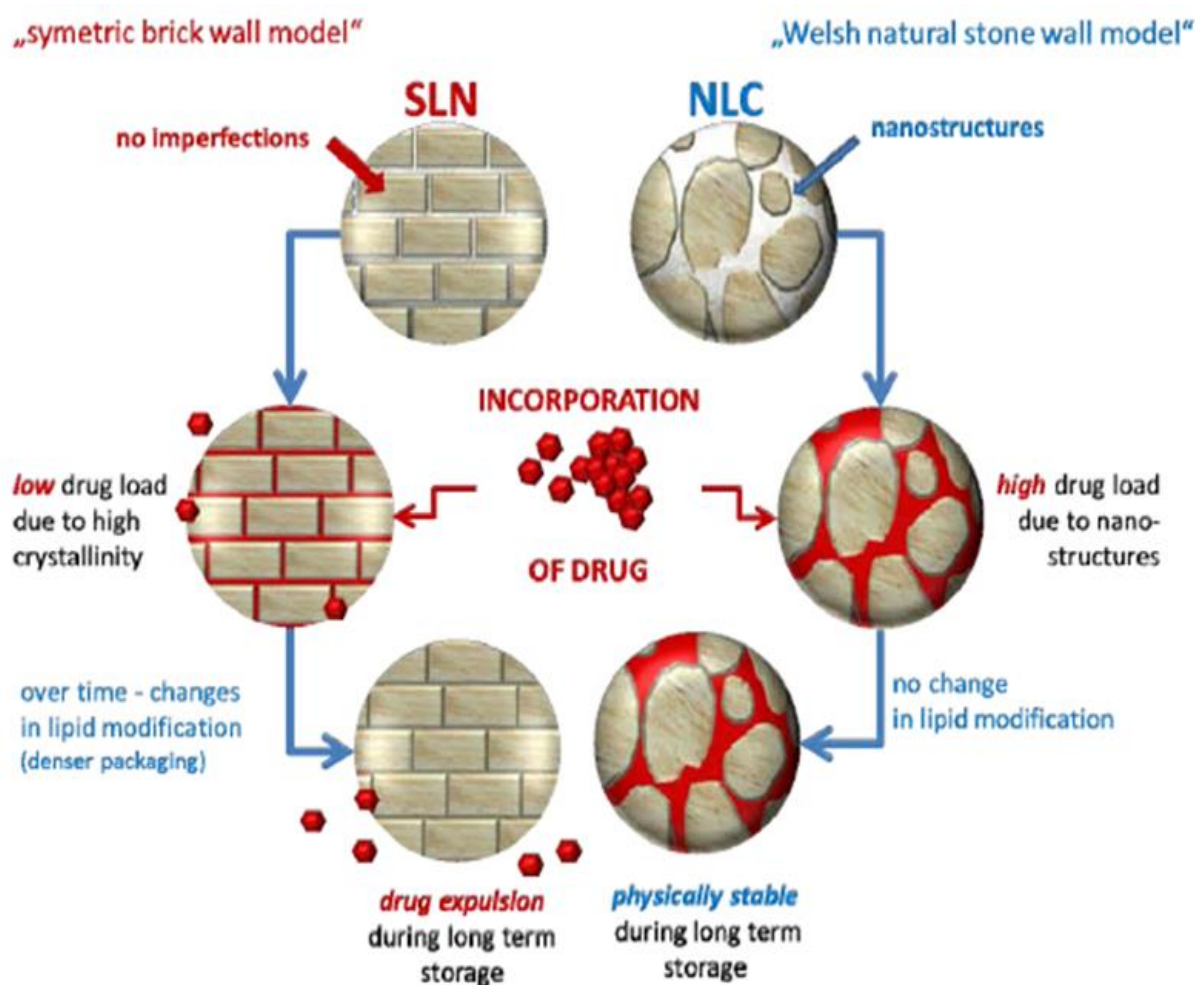
Figure 3. SLN structure vs NLC structure.

There are different types of NLCs, based on their composition: imperfect NLC, amorphous NLC and multiple NLC [*B. Fonseca-Santos et al., 2020; S.S. Shidhaye et al., 2008; D. Puri et al., 2010*].

- Imperfect type NLC (I): spatially different lipids, e.g. glycerides composed of different fatty acids are mixed. Using these lipids leads to larger distances between the fatty acid chains of the glycerides and general imperfections in the crystal and thus to more room for the encapsulation of drug. The highest drug load could be achieved by mixing solid lipids with small amounts of liquid lipids (oils).

- Amorphous type NLC (II): Drug expulsion is caused by ongoing crystallisation of the solid lipid; this can be prevented by using a mixing of special lipids (e.g. hydroxyoctacosanylhydroxystearate and isopropylmyristate) which avoid the crystallisation [*V. Jenning et al., 2000; V. Jenning et al.,2000*].

- Multiple type NLC (III): This type of NLC can be regarded as an analogue to W/O/W emulsions since it is an oil-in-solid lipid-in-water dispersion. Solid lipid is mixed with an higher amounts of oil; this leads to the formation of oily nanocompartments within the solid lipid matrix [*V. Jenning et al., 2001; V. Jenning et al., 2000; V. Jenning et al.,2000*]. In addition, the high amount of oil promotes the dissolution of drugs since many of them show greater solubility in oils than in solid lipids [*S.A Wissing et al., 2004*].
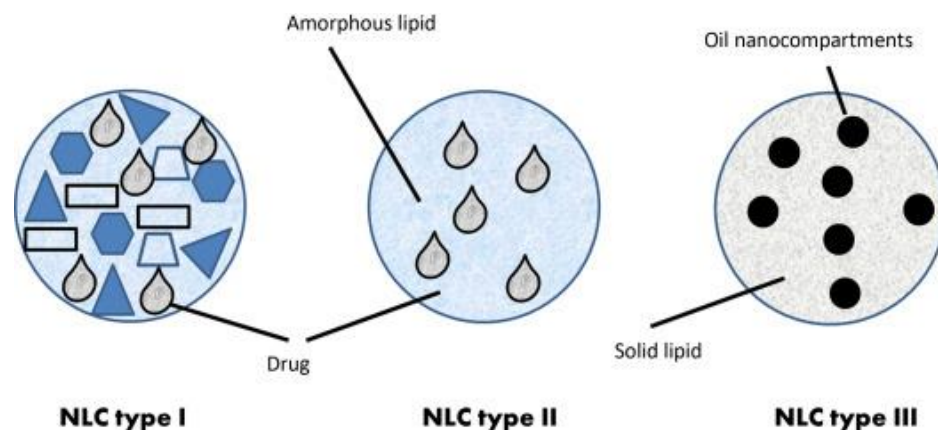
Figure 4. NLC type: (I) imperfect type NLC, (II) amorphous type NLC and (III) multiple type NLC.

Compared to SLNs, NLCs show a higher drug loading, flexible release profile and avoid/minimize potential expulsion of drug during storage [*W. Mehnert et al., 2001*].

1.5.Preparation of lipid-based nanocarriers

Lipid nanoparticles are prepared by different methods such as high-pressure homogenization with hot or cold homogenization, high shear homogenization and ultrasound, solvent evaporation technique [*W. Mehnert et al., 2001; F. Corrias et al., 2011*]. The production technique is the crucial point to obtain a good final product.

High-pressure homogenization (HPH) technique is the most used in the pharmaceutical field because it has many advantages, compared to other methods, such as easy scale up, lack of organic solvents and short production time. Lipid nanoparticles can be produced by either a hot or cold high pressure homogenization technique [*D. Puri et al., 2010*].

Hot homogenization method: the drug was dissolved in the melted lipid (5–10°C above the melting point) and the drug-lipid mixture is dispersed in a hot surfactant solution at the same temperature to form a pre-emulsion, which was subsequently homogenized. This method has significant disadvantages, such as drug degradation, lipid transition and drug loss due to the water content [*C. Nastruzzi et al., 2004; S.A. Wissing et al, 2004*].

Cold homogenization method: the melted lipid containing the drug is rapidly cooled using liquid nitrogen or dry ice. After solidification, the solid solution was crushed to obtain lipid microparticles. The lipid microparticles are then dispersed in a cold surfactant solution and homogenized at room temperature. This method was developed to overcome the problems of hot homogenization; moreover, it is suitable for thermolabile and hydrophilic drugs [*S. Das et al., 2011*].

LNCs can also be produced by *solvent evaporation* method [*D. Puri et al., 2010*]. The lipid is dissolved in an organic solvent (e.g. ethanol) and this lipid phase is emulsified in an aqueous

surfactant solution. After evaporation of the solvent, the lipid precipitates forming nanoparticles. The main disadvantage is the use of organic solvents.

High shear homogenization method (HSH) and *ultrasonication* (US) are recognized as the most suitable procedure to produce lipid nanoparticles due to their easy scalability and avoidance of organic solvents [*D.P. Gaspar et al., 2017*]. For both techniques, the lipid phase is heated to approximately 5-10°C above solid lipid melting point and it dispersed to a surfactant solution by high shear homogenization or ultrasonic. Afterwards, the samples are cooled to room temperature or lower temperatures to form the LNCs by lipid crystallization [*R.B. Rigon et al., 2016; S.J. Lim et al., 2004*]. However, there are some disadvantages of these methods, such as a low dispersion of nanoparticles due to the presence of microparticles in the HSH technique or the metal contamination from probe erosion during sonication can affect the physical stability of the SLNs [*V. Vijayan et al., 2013*]. Therefore, it has been demonstrated that a strategy to overcome these drawbacks and to obtain LNCs characterized by small size and a low polydispersion index, such as in the case of parenteral and / or ocular administration, is represented by the coupling of short cycles of HSH and US [*C. Puglia et al., 2020*].

1.6. Characterization of lipid-based nanocarriers

The average size of the nanoparticles was measured by *Photon Correlation Spectroscopy* (PCS) [*A. Liparulo et al., 2020*]. The measurement method is based on the principle of dynamic light diffusion. The analysis system provides six different light between 11 and 90° that allow to characterize samples containing particles of different sizes. Photonic correlation spectroscopy, also called *Dynamic Light Scattering* (DLS), is a technique used to measure the light flow of light scattered in a liquid, measuring the fluctuations in the intensity of the scattered light due to the Brownian particle motions. The temporal fluctuations of the diffused intensity are analyzed by a correlator and this correlation function is obtained from the translational diffusion coefficient (DT); from this coefficient it is

possible to obtain the hydrodynamic ray of the particles (RH), through the Stokes-Einstein equation (Equation 1):

$$D_T = \frac{k_b T}{6\pi\eta R_H}$$

The Zeta Potential is an indicator of the stability of a dispersed system. This parameter is determined using the technique called *Electrophoretic Light Scattering* (ELS), which it measures the electrophoretic mobility of particles in dispersion or in solution. Mobility is converted into zeta potential to allow a comparison of materials under different experimental conditions. The principle used is the electrophoresis. The dispersion, placed in a special cuvette, is introduced into a cell containing two electrodes. An electric field is applied to the electrodes and the particles having a net charge will migrate to the opposite charge electrode with a velocity proportional to the zeta potential. This velocity is measured with the laser- Doppler anemometry technique. The frequency shifts of an incident laser beam, caused by these moving particles, is measured as the mobility of the particles, from this derive the zeta potential. Good results are obtained for potential values of $\pm$ 25 mV. The instrument carries out three measures with an average value.

1.6.1. Determination of drug loading

A range of approaches can be used for determination of drug encapsulated in the lipid system, such as centrifugation, filtration and tangential fitration.

Although centrifugation or ultracentrifugation techniques are commonly used, the impact of the centrifugation force can cause caking and difficulties in redispersing nanoparticles.

Instead filtration, also called dead-end filtration, can cause nanoparticles to stick together or adhere to the membrane surface, thus leading to a considerable decrease in filtrate flux. Recently, the use of Tangential Flow Filtration (TFF) system allowed to overcome these problems. This technique is a

filtration method where the filtered fluid flows tangentially to the filter surface (Figure 5). It can be applied to a wide range of biological fields such as immunology, protein chemistry, molecular biology, biochemistry, and microbiology. In the nanotechnology field, it is typically used to separate the unentrapped drug from the nanoparticle suspension [*C. Puglia et al., 2019; C. Puglia et al., 2016; C. Puglia et al., 2017*].
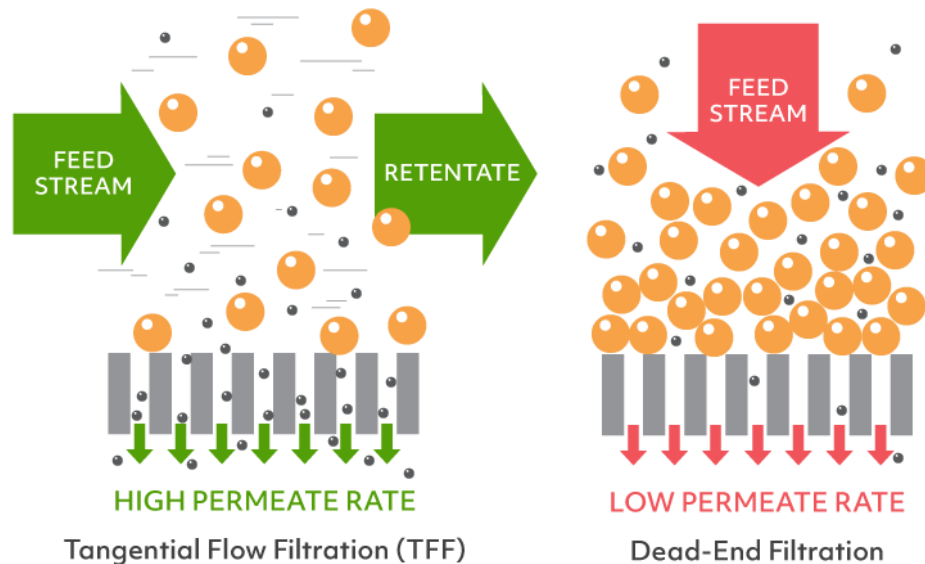
Figure 5. Comparison of Tangential Flow Filtration and Normal Dead-end Filtration.

TFF is a techinique based on the use of polymeric membranes with highly defined pore sizes to separate molecules according to size. Depending on membrane porosity, it can be classified as a microfiltration or ultrafiltration process. Microfiltration uses membranes with pore sizes typically between 0.1 μm and 10 μm, while ultrafiltration is performed with much smaller pore sizes ranging between 0.001 and 0.1 μm.

TFF system is composed of a pump used to promote the flow of the feed stream through the membrane surfaces. A key role of this filtration method is that the filtrate slips away on the filtering surface; thus, preventing the membrane fouling. Therefore, TFF allows continuously working, constant flow and total product recovery [*Musumeci T. et al., 2018*]. During the TFF process one portion of

nanoparticle suspension passes through the membrane (permeate), while the remainder (retentate) is recirculated back to the feed reservoir.

Drug incorporation efficiency can be expressed both as encapsulation effciency (E.E.%) and drug loading (D.L.%), calculated from equations 2-3 reported below:

E.E. (%) = (Mass of drug in nanoparticles)/(Mass of drug fed to the system)

D.L. (%) = (Mass of drug in nanoparticles)/(Mass of nanoparticles)

1.7. Stability of lipid-based nanocarriers

A crucial point for the use of LNCs as colloidal drug carriers is their physical (aggregation / fusion of particles) and / or chemical (drug loss, microbiological contamination) stability due to their storage for long periods in aqueous medium [*C. Freitas et al., 1995; M.D. Coffin et al., 1992*]. LNCs are dispersions having typically water contents of 70–99.9%; moreover, they are composed of 0.1% (w/w) to 30% (w/w) solid lipid dispersed in an aqueous medium stabilized with 0.5% (w/w) to 5% (w/w) surfactant [*J. Pardeike et al., 2009*]. Surfactants are chosen according to the route of administration and, usually, they are used in combination to prevent the formation of agglomerates of particles. Therefore, the choice and concentration of the surfactant are essential to avoid nanoparticle aggregation. Another problem is chemical stability in the case of drugs susceptible to hydrolysis. To overcome these problems, it is highly desirable to obtain a freeze-dried SLN formulation.

Freeze drying, also called lyophilization, can transform colloidal suspensions into stable solid cakes for long term storage. It has numerous advantages such as high stability of the system due to the absence of water, maintenance of the chemical-physical characteristics of the nanoparticle system and low transport and storage costs due to the small volumes. Lyophilization is a complex process that generates stress sources itself, which can destabilize the nanoparticle formulation. A key role of

the freeze-drying process is played by the cryoprotectant which is able to immobilize the nanoparticles within its glass matrix, preventing their aggregation and protecting them against the mechanical stress of ice crystals. For this reason, cryoprotectants have been used to decrease SLN aggregations due to the stress during this process [*W. Abdelwahed et al., 2006*]. Sugars are the most cryoprotectants (e.g. glucose, mannitol and trehalose) used in freeze drying of nanoparticles [*C. Schwarz et al., 1997; W. Mehnert et al 2001*]. The level of stabilization afforded by sugars generally depends on their concentrations; increasing the cryoprotectant concentration to a certain level may eventually reach a limit of stabilization or even destabilize system [*W. Abdelwahed, 2015; M.J. Pikal et al., 1990*]. If an excipient cannot protect the nanoparticles during the lyophilization, it is not likely to be an effective cryoprotectant. For product quality is important the reconstitution performance of the lyophilizate after storage.

As previously described, zeta potential (ZP) is an indicator of the stability of a dispersed system. This parameter is determined using the Electrophoretic Light Scattering technique, which measures the electrophoretic mobility of particles in dispersion or molecules in solution. This mobility is converted into zeta potential using Smoluchowski equation (Equation 4):

$$\vartheta = \left(\frac{\varepsilon \cdot E}{\eta} \right) \xi$$

where ϑ is the electrophoretic mobility, η is viscosity, ε is dielectric constant and E is electric field. Potential values of $\pm$ 25 mV predict good long-term stability.

In order to assess the physical stability of nanoparticle formulation, Turbiscan analyzer is employed. This technique has been reported as a reliable technology to evaluate the occurrence of instability phenomena related to particle aggregation and/or migration. It consists of the simultaneous measurement of the intensity of the transmitted (T) and backscattered (BS) light from the sample to

detect destabilization process (Figure 6). In fact, it enables fast and sensitive identification of destabilization mechanisms (such as creaming, sedimentation, flocculation, coalescence).
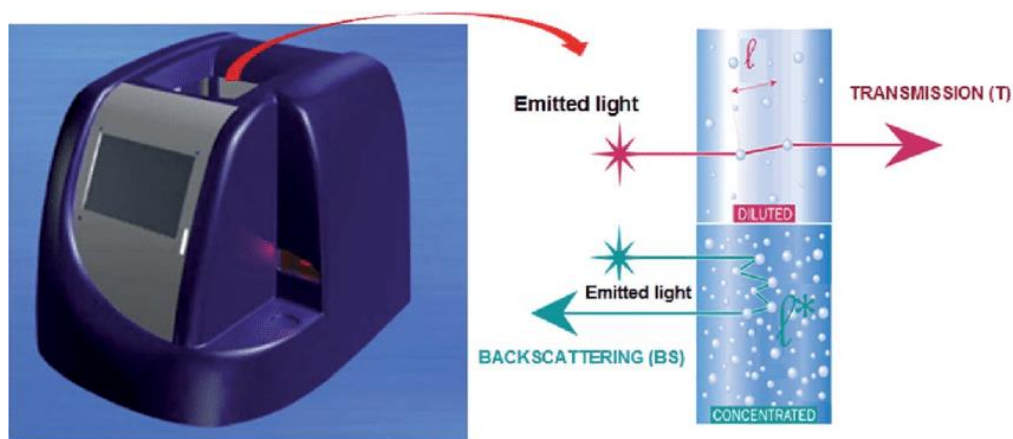
Figure 6. Measurement principle diagram of the Turbiscan.

A temperature-controlled measurement cell allows either stability monitoring at specific storage temperatures or accelerating destabilization process. The main advantage of this technology is the ability to analyze samples ranging from very diluted to highly concentrated, thus allowing to test formulations with concentration ranges inaccessible with other techniques. The measurement method is based on the principle of multiple light scattering technology. The Turbiscan analyzer uses a near-infrared light source (wavelength = 880 nm) to examine a sample. Two fixed detectors capture the transmission and backscattering signals as a function of position and time. These signals are dependent on the particle size and concentration. The output is a series of intensity profiles that describe the evolution of the sample, providing information on particle migration (sedimentation and creaming) and on particle size changes (coalescence and flocculation).

Chapter 2

2.1. Administration route of lipid-based nanocarriers

LNCs show many advantages such as biocompatibility, non-toxicity, preservation of the drug from degradation, small size and controlled release of the encapsulated drug. Therefore, these carriers are suitable for all routes of drug administration.

LNCs are widely developed and characterized for their applications by various routes such as oral, pulmonary and dermal.

-Dermal drug delivery: LNCs show an excellent tolerability due to the use of excipient recognized as safe (GRAS). The structural similarities of these lipids with those composing skin make these carriers promising tools for topical administration of drugs. Thanks to this peculiarity and their biocompatibility, LNCs enable the skin penetration and achieve drug targeting by different mechanisms such as intercellular, intracellular or follicular route. Moreover, their small size between 50 and 1000 nm make them suitable for topical administration.

-Pulmonary drug delivery: This administration route show many advantages due to the unique physiological features of the lungs such as the large alveolar surface area, extensive vascularization, low thickness epithelial barrier and relatively low proteolytic activity, as well as the avoidance of first-pass hepatic metabolism [*Y. Z. Li et al., 2010*].

On the contrary, this route of administration has limits due to the existing barriers [*U. Pison et al., 2006*]. In the upper bronchi, absorption is prevented due to the thickness of the mucus and the reduced surface area. In addition, the ciliary movement tends to expel the particles that are deposited in the bronchial epithelium. The size of the particles inhaled by aerosol influences lung absorption. Thanks to their chemical-physical characteristics such as particle size and biocompatibility, SLNs are carriers suitable for lung delivery as they have the ability to deposit in the lungs. Moreover, with these systems it is possible to ensure a prolonged release and a quick transport.

- *Oral drug delivery:* The bioavailability of orally administered drugs is usually limited by their low solubility and dissolution rate. LNCs are able to enhance the oral bioavailability of many drugs by maintaining a solubilized state of the drug and facilitating the formation of micelles due to induction of endogenous secretion phospholipids and bile salts [*Z. Zhang et al., 2009*]. A further advantage of these systems is the possibility to deliver protein and peptide drugs, which are impossible to administer orally, as demonstrated by several studies [*C.Y. Zhuang et al., 2010; A. Hanafy et al., 2007*].

- *Ocular drug delivery*: Ophthalmic drug delivery for the treatment of the posterior eye segment diseases, is still a great challenge. The efficacy of topical administration into the eyes by conventional solutions and suspensions is limited by a series of pre-corneal drug removal mechanisms which oppose to trans-corneal drug absorption [*C. Puglia et al., 2015*] and physiological barriers [*E.M. Del Amo et al., 2008; C. Bucolo et al., 2012*]; in fact, the ocular bioavailability of drugs is less than 5–10%. Therefore, frequent instillations of eye drops are necessary to achieve the expected therapeutic effect; this, especially in chronic therapy, decreases the patient compliance [*L. Battaglia et al., 2016*]. Therefore, conventional therapy for the treatment of the posterior eye segment diseases occurs through the administration by transcleral/periocular route, which includes peribulbar, retrobulbar and subconjunctival injections or the application of ocular implants (Figure 7). These therapies show numerous disadvantages as they require high costs that significantly affect the National Health System (NHS) [*P. Romero-Aroca et al., 2016*], involve an invasive procedure and show serious ocular complications [*K.M. Sampat et al., 2010*].
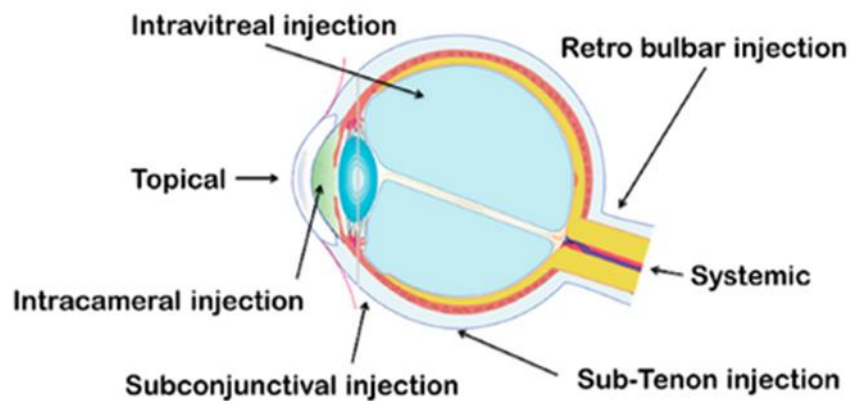
Figure 7. Route of ocular administration.

Nowadays, there is an increasing need to find a therapy for the retinal diseases, such as diabetic retinopathy, age-related macular degeneration and optic neuropathy.

Recently, the development of lipid-based nanocarriers, in particular the NLC, has made it possible to prolong corneal residence time and improve the ocular bioavailability of ophthalmic drugs [*R. Pignatello et al., 2011; Y. Duan et al., 2015; S. Yu et al., 2015; E. Sanchez-Lopez et al., 2017*].

- *Parenteral administration:* Parenteral delivery is the drug administration by injection, infusion, and implantation. It is important in emergency situations such as cardiac arrest and anaphylactic shock. This administration route exhibits several advantages, such as first-pass metabolism avoidance, better bioavailability, and reliable dosage. Unfortunately, the parenteral administration of LNCs is limited by the presence of the Mononuclear Phagocytic System (MPS) and the Reticulo Endothelial System (RES) [*M.M. Frank et al., 1991; R.J. Johnson, 2004*]. These endogenous systems recognize the nanocarriers as extraneous and carry them in the liver, spleen, lungs and bone marrow (opsonization) [*L. Illum et al., 1986; R. Gref et al., 1995; Z. Panagi et al., 2001*].

In the last years, the ocular and parenteral administration routes are receiving increased attention as a drug delivery for the potential treatment of nervous system disorders.

2.2. The nervous system

The nervous system is the most complex system of our body. It is divided into peripheral (PNS) and central nervous system (CNS), the latter being composed of the brain and spinal cord that constitute the control center of all functions body (Figure 8) [*A.M. Cardoso et al., 2016*].
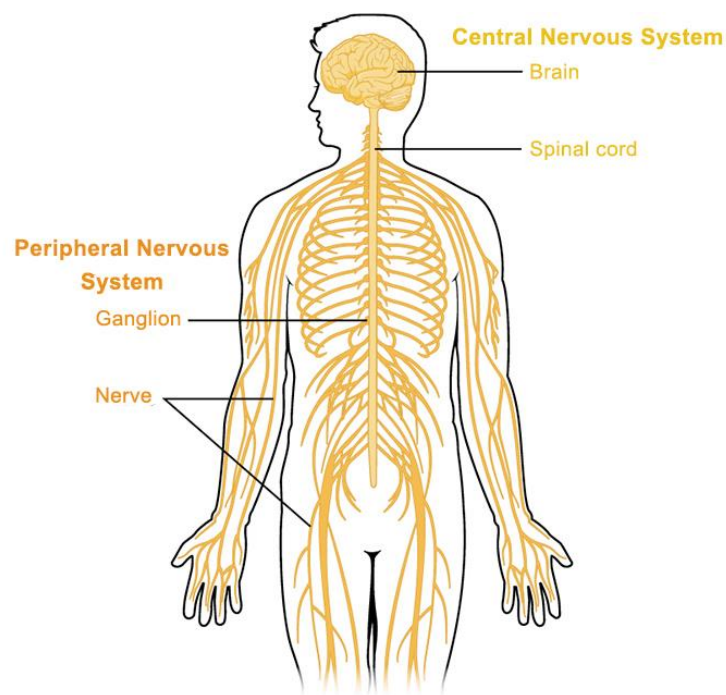
Figure 8. Schematic representation of the nervous system.

The brain microenvironment, essential for its normal function, is ensured by the Blood–Brain Barrier (BBB), a physical physiological barrier between the brain and the blood stream that allows the maintenance of CNS stability. This barrier is composed of specialized Brain Endothelial Cells (BECs), which are continuously joined by tight junctions and surrounded by a basement membrane, pericytes, and astrocytes [*B.W. Chow et al., 2015*]. The BBB represents the major obstacle to reach CNS. Due to this complex anatomy, most of the current therapeutic strategies remain ineffective for the CNS treatment.

Over the last years, the incidence of CNS disorders has greatly increased due to demographic changes of population and growth of average life expectancy [*B.A. Silva et al., 2007*]. These pathologies represent a serious problem, not only concerning the high costs of treatment, but in addition, the quality of life of the patient. These diseases, such as Alzheimer's disease, are characterized by a gradual motor and sensorial loss, as well as deficits of perceptual functions and behaviour associated due to neuronal death [*R. Pal et al., 2015*].

2.2.1. Alzheimer's disease

Alzheimer's disease (AD) is a neurodegenerative disorder characterized by cognitive impairments. The classical symptoms of the disease include gradual deterioration of memory and language. This disease is characterized by the presence of extracellular amyloid-β (Aβ) plaques and intraneuronal tau neurofibrillary tangles in the cerebral cortex [*J.A. Loureiro et al., 2017*]. The main cause of the pathogenetic process of AD consists in a marked oxidative stress at the level of the encephalic cells affected by the neurodegenerative process [*E. Zanforlin et al., 2017*]. Nowadays, there is no effective pharmacotherapy for the treatment of AD. Recent research and epidemiological studies indicate that the normalization of antioxidant capacity could represent a very promising therapeutic for the treatment of neurodegenerative disorders such as AD. In recent years, research has made a significant effort to develop innovative therapies based on natural compounds, as old synthetic drugs cause numerous side effects.

2.2.1.1. Natural compounds for the potential treatment of Alzheimer's disease

There are a number of natural antioxidants, such as curcumin and astaxanthin, which possess numerous therapeutic properties for the treatment of various diseases such as Alzheimer's disease.

Curcumin (1,7-bis (4-hydroxy-3-methoxyphenyl) -1,6-heptadiene-3,5-dione; CUR) is a yellow polyphenol (Figure 9), extracted from rhizomes by _Curcuma Longa_, which has been used for centuries in traditional medicine for the treatment of various diseases [_B.B. Aggarwal et al., 2009_].
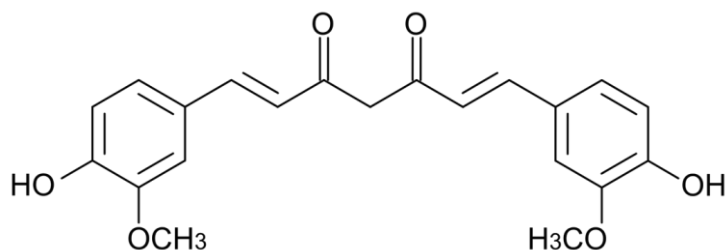
Figure 9. Chemical structure of curcumin.

All curcuminoids are excellent antioxidants that, unlike others, are able both to prevent the formation of free radicals and to neutralize the free radicals already existing. In fact, they are considered effective bioprotectors due to this dual activity. These free radicals are reactive oxygen species (ROS) and reactive nitrogen species (RNS) [_I. Chattopadhyay et al., 2004_] that are physiologically generated by cells as a "waste product" during the activity of the mitochondrial electron transport chain.

In pathological conditions, such as cancer, chronic inflammation, cancer and neurological disorders, their accumulation causes the so-called "oxidative stress" due to an imbalance between the excessive production of oxidizing factors (such as free radicals) and the decrease in antioxidant defenses.

The damage caused by free radicals mainly affect DNA and mitochondria; moreover, the ROS activates NF-κB which sets in motion the transcription of a cascade of pro-inflammatory cytokines (TNF-α, IL-1β, IL-2, IL-6, chemokines—IL-8) and adhesion molecules, such as ICAM-1, that are central mediators in the inflammatory response [_A. Panico et al., 2015; L. Crascì et al., 2018; P. Ninfali et al., 2005_].

Furthermore, CUR enhances the natural antioxidant systems of cells, increasing glutathione levels - one of the most important endogenous antioxidants - promoting liver detoxification and inhibiting the formation of nitrosamines [*R.K. Maheshwari et al., 2006*].

Due to its excellent antioxidant [*H.Y. Lee et al., 2017*] and anti-inflammatory properties [*M.A. Panaro et al., 2020; E. Esposito et al., 2013*], CUR plays a significant beneficial and regulatory pleiotropic role in various pathological conditions such as AD. Oxidative stress may increase the production and aggregation of Aβ and accelerate the phosphorylation and polymerization of tau, thus promoting disease progression [*Y. Zhao et al., 2013*]. In fact, CUR has been studied for its ability to prevent the formation and accumulation of Aβ, the main cause of AD. An *in vivo* study showed that intragastric CUR administration reduced the formation of Aβ, in AD mice model, by reducing the expression of the enzyme BACE1. This enzyme which cleaves the AβPP into Aβ. [*K. Zheng et al., 2017; C. Taghibiglou et al., 2017*].

Moreover, CUR has shown to exert others important activities, including anticoagulant, antithrombotic, antihypertensive, antidiabetogenic, hypocholesterolemic, antiviral and hepatoprotective [*M. Mandal et al., 2020*]. It could also be effective in the treatment of malaria and in the prevention of cervical cancer. Furthermore, it can interfere with the replication of HIV [*S. Prasad et al., 2015*] and it acts as a radical scavenger, inhibiting lipid peroxidation [*H. Hatcher et al., 2008*]. Although it has numerous potential therapeutic properties, CUR shows many disadvantages when administered *in vivo* such as poor bioavailability, absorption and a very fast metabolism and elimination [*T. Jiang et al., 2020; P. Anand et al., 2007*] due to its high lipophilicity.

Another powerful natural antioxidant is <u>Astaxanthin</u> (3,3′-dihydroxy-β, β′-carotene-4,4′-dione; AST), a molecule obtained from a particular green alga *Haematococcus Pluvialis*.

It is a carotenoid belonging to the family of the Xanthophylls and it is responsible for the coloring of some fish, including salmon and shellfish [*I. Higuera et al., 2006*]. The remarkable scavenger activity of AST is due to its chemical structure which traps radicals in the polyene chain (Figure 10). It is a

highly lipophilic molecule, but the presence of two terminal hydrophilic groups determines a slight solubility in water.
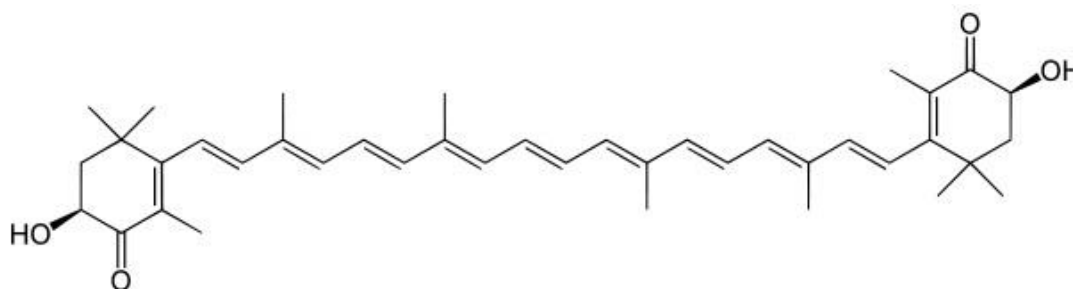
Figure 10. Chemical structure of astaxanthin.

This dual nature and its small size allow it to easily permeate cell membranes. In fact, it is a carotenoid that carry out its antioxidant and anti-inflammatory actions at the level of the eyes, the brain and the CNS, as it manages to cross the blood-brain barrier and the blood-retinal barrier.

Therefore, it is used in treatments such as cataracts, macular degeneration, blindness, dementia and Alzheimer [*R. Yamagishi et al., 2014; S. Piermarocchi et al., 2012; Z. Li et al., 2013*]. Many studies indicated that AST is a promising biologically active compound for the treatment of AD. Wang and coworkers reported that AST protected neuroblastoma cells against Aβ-induced oxidative cell death through induction of the antioxidant enzyme HO-1 expression [*H.-Q. Wang et al., 2010*]. Moreover, it reduced ischemia-related injury in brain tissue, mainly through the inhibition of oxidative stress [*S. Fakhri et al., 2019*].

Although AST expresses a high pharmacological potential, it is often not used terapeutically due to poor drug stability. The presence of C = C double bonds in the chemical structure of carotenoids makes the molecule sensitive to oxidation, to air and to the photo-oxidation. All these factors can cause their conversion into a mixture of stereoisomers (with trans-cis isomerization). Furthermore, AST is sensitive to thermal degradation and it is poor-water solubility [*M. Li et al., 2016*].

Therefore, although CUR and AST could be used to treat important CNS pathologies involving a deficit of antioxidant defenses such as AD, their use in clinical practice is limited by their instability problems. This obstacle can be overcome by encapsulating these compounds in the stealth lipid nanoparticles suitable for systemic administration.

2.2.1.2. Stealth systems for parenteral administration route

As previously described, parenteral administration is one of the most commonly used routes for drug administration at the CNS level. Unfortunately, the use of LNCs through systemic administration is limited by the opsonization process (Figure 11).

Opsonization is one of the many mechanisms that the immune system uses to fight pathogens [*D. Mevorach et al., 2000*]. It is an immune process which uses opsonins to tag foreign pathogens for elimination by phagocytes. Opsonization can occur by antibodies or the complement system [*L. Thau et al., 2020*].

- Antibodies are part of the adaptive immune system and are produced by plasma cells in response to a specific antigen. They have variable regions, also known as antigen-binding sites that allow the antibody to fit like "a lock and key" into the epitopes of specific antigens. Once the antigen-binding sites are bound to the epitopes on the antigen, the stem region of the antibody binds to the receptor on the phagocytes. There are different type of immunoglobulin(Ig): A, M, G, D and E.

- The complement system improves the ability of antibodies and phagocytic cells to fight invading organisms. It is composed of over 30 proteins and, among these, the most important is C3. When a pathogen is detected, C3 protein is activated on the surface of the microbe and a ligand is formed which provides a firm bond between organisms and phagocytic cells. This

stimulates efficient engulfment by phagocytic cells and most microbes are rapidly killed once they are ingested.
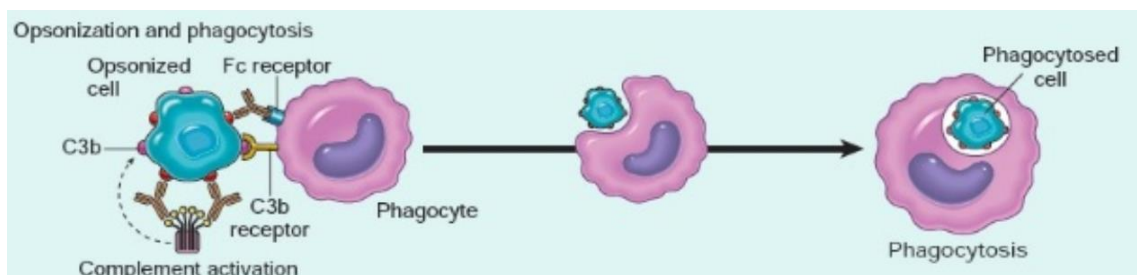
Figure 11. Opsonization process.

Opsonization can be exploited to target chemotherapy drugs to localize MPS tumors [*S.A. Wissing et al., 2004*]. Carrying these carriers into other organs is not a simple task, cause their short half-life (3-5 min) after intravenous administration.

One of the most used strategy to prolong the systemic residence of these carriers is based on the modification of the nanoparticle surface and the realization of "stealth" systems (pSLNs) able to avoid the defense line represented by the macrophages [*G. Kaul et al., 2002*]. This can be get by modifying nanoparticles with a synthetic derivatization process using flexible hydrophilic polymers (Figure 12), such as polethylene glycol (PEG) [*S.A. Wissing et al., 2004; I. Brigger et al., 2002*].
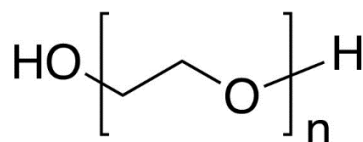
Figure 12. Chemical structured of poly-ethilene glycol (PEG).

PEG is a hydrophilic polymer widely used to improve the stability of drug carriers. It is non-toxic, non-immunogenic, non-antigenic and FDA-approved. This surface modification of nanocarriers with

PEG is known as PEGylation. PEGylation of the nanoparticles is a strategy that confers them stealth properties by creating a hydrophilic steric barrier that delays opsonization and rapid recognition by the RES and MPS (Figure 13) [*D.E. Owens III et al., 2006*]; thus enabling the nanoparticles to circulate longer in the blood and to reach the target site [*H. Yuan et al., 2013; Y.W. Naguib et al., 2014; T. Betancourt et al., 2009; A. Arranja et al., 2016; S. Kommareddy et al., 2007; R. Gref et al., 1994*]. In addition, the large conformational freedom provided by the flexibility of PEG renders interpenetration of foreign matters into the PEG corona thermodynamically unfavorable [*A. Vonarbourg et al., 2006*].
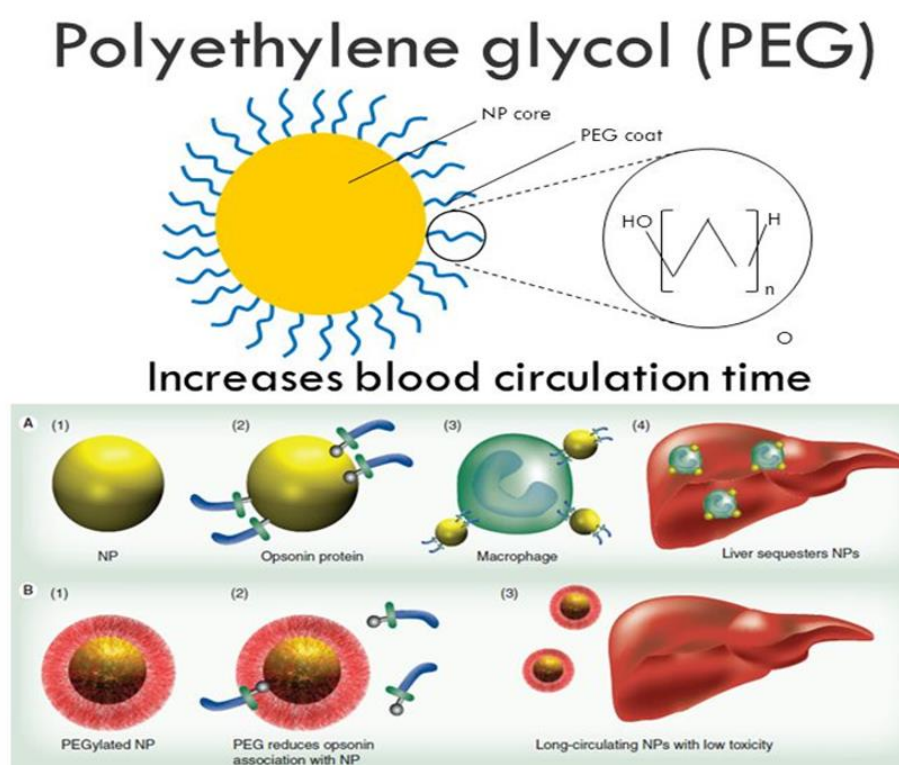
Figure 13. PEGylation strategy.

This strategy has been successful used for other important drug delivery systems. Many studies have proved that the PEGylation not only stabilizes the SLNs, but also modulates their kinetics of cellular absorption. As reported in literature, PEGylation improves pharmacokinetic profile of nanoparticles.

Kommareddy and coworkers confirmed that thiolated gelatin nanoparticles modified with the PEG had a half-life 5 times greater (15 hs) than unmodified nanoparticles (3 hs) [*S. Kommareddy et al., 2007*]. The same results were achieved with PEGylated PGLA nanoparticles [*R. Gref et al., 1994*].

Consequently, it increases the intracellular concentration of the drug delivered by pSLN, resulting in an increase in therapeutic efficacy. This can be exploited in chemotherapy to circumvent the resistance of cancer cells and increase patient survival and care [*A. Arranjia et al., 2016; X. Lui et al., 2015*]. Therefore, PEGylation of nanocarriers increases intracellular bioavailability and therapeutic efficacy of the drug [*X. Hu et al., 2015*].

Another strategy to realize "stealth" systems is to coat the nanoparticle surface with surfactants, such poloxamers (Figure 14) [*E. Esposito et al., 2017*]. This hydrophilic coating modifies the SLN biodistribution, improving blood circulation times and deposition in non-RES organs [*T.M. Göppert et al., 2005*]. Among the different surfactants used to modify the particle distribution, polysorbate 80 belonged to the most effective surfactants to enhance the CNS concentration [*A. Ambruosi et al., 2005*].
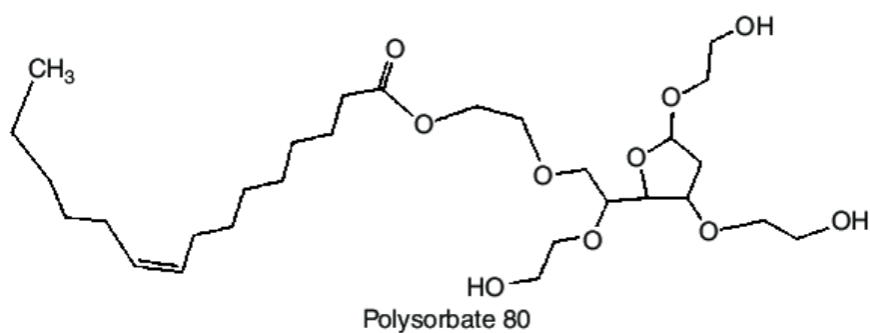
Figure 14. Chemical structure of polysorbate 80 (P80).

Therefore, these strategies alter SLN biodistribution, enhancing blood circulation time and deposition in non- RES organs such as the CNS.

2.2.2.Neuropathic pain

An injury to the nerves of the peripheral nervous system (peripheral neuropathy) or the structures of the CNS causes a chronic painful sensation called neuropathic pain or neuralgia.

The perception of pain (nociception) involved particular receptors, called nociceptors, that transduce mechanical, thermal and / or chemical signals into action potentials which are then transmitted to the CNS to be processed. TRPV1 vanilloid channel receptor is the most studied nociceptor.

TRPV1 receptors are widely expressed in areas involved in pain transmission both in central (CNS) and peripheral nervous systems (PNS) [*M.J. Caterina, 2007; S. Spampinato et al., 2011*]. In the CNS, TRPV1 receptors are also involved in the modulation of synaptic plasticity as well as in epilepsy and cognition [*M. Fu et al., 2009*]. Regarding the PNS, TRPV1 receptors are located in sensory ganglia and in small sensory C and Aδ fibers [*M.J. Caterina, 2007; G.J. Michael et al., 1999*], thus representing a potential target for the modulation of pain sensitivity [*L. Basso et al., 2019; H. Lee et al., 2019*]. Up-regulation of TRPV1 expression occurs during inflammation and in pathological pain states, such as neuropathic pain [*D. Vilceanu et al., 2010*]. On the contrary, a down-regulation of the TRPV1 expression has been observed in neuropathic pain caused by injury [*G.J. Michael et al., 1999*]. Therefore, TRPV1 receptors represent the target site to treat the neuropathic pain.

2.2.2.1.Natural compound for the potential treatment of neuropathic pain

Capsaicin (CPS), the pungent ingredient of hot peppers, is a highly selective agonist of TRPV1 with a nanomolar affinity [*F. Yang et al., 2017*]. TRPV1 receptor is a non-selective ligand-gated cation channel formed by six membrane-spanning domains assembled as homo or hetero-tetramers activated by heat, low pH, and endogenous lipids (Figure 15) [*D.E. Clapham et al., 2001; N. Kedei et al., 2001; A. Ferrer-Montiel et al., 2004*].
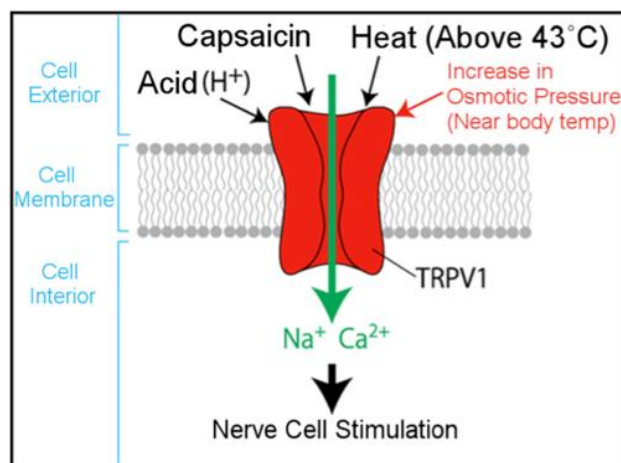
Figure 15. Schematic representation of the TRPV1 receptor.

During exposure to CPS, TRPV1 receptors might undergo to phosphorylation/dephosphorylation processes that contribute to phosphorylation-mediated TRPV1 desensitization or tachyphylaxis, a mechanism that account for acute TRPV1 desensitization. Moreover, prolonged exposure to CPS induces TRPV1 endocytosis and lysosomal degradation resulting in a loss of function known as "nociceptor defunctionalization". TRPV1 defunctionalization is also characterized by a reversible reduction in intra-epidermal nerve fibers, a mechanism that contributes to long-term nociceptors desensitization [*P. Holzer et al., 2008; K.R. Bley et al., 2010*].

Although, defunctionalization of TRPV1 receptors has been used for the treatment of thermal hyperalgesia in chronic pain conditions, evidence points for a physiological role of TRPV1 receptors where a long-term blockade or the down-regulation of this receptor might have detrimental effects [*D.A. Simone et al., 1998*]. Therefore, it results of noteworthy interest the formulation of a drug delivery system able to produce a CPS slow release thus preventing TRPV1 internalization and degradation.

The best strategy to obtain a controlled release of CPS, preventing the long term down-regulation of TRPV1 and preserving the physiologic role of this receptor, is the inclusion of the drug into lipid nanoparticles.

2.2.3.Posterior eye segment

Optic nerve and retina are considered integral parts of the CNS; in fact, the retina has been described as the "window to the brain". The nervous tunica (retina) together with the ciliary body, the choroid and iris represent the posterior segment of the eye [*C. Puglia et al., 2015*]. It is the site of many ocular diseases such as diabetic retinopathy, age-related macular and optic neuropathy.

Although the drug delivery to the posterior eye segment is still a great challenge due to its complex anatomy, the development of lipid-based nanocarriers has made it possible to prolong corneal residence time and improve the ocular bioavailability of drugs.

These systems, in particular the NLCs, possess important advantages for ocular application, such as controlled drug release, high drug loading, good bioavailability and excellent tolerability [*C. Puglia et al., 2015; J. Araújo et al., 2011*]. Scientific evidence has frequently demonstrated the NLC's ability to improve the interaction with the ocular mucosa, prolonging the corneal residence time of the loaded drug, thus producing not only an increase of the ocular bioavailability but also a reduction of the local and systemic side effects. NLCs are therefore currently studied as delivery systems for the treatment of the most important ocular disorders, from the common ocular inflammation or infection to important diseases affecting the posterior eye segment [*Q. Luo et al., 2011; S.P. Balguri et al., 2016; D. Tronino et al., 2016*].

2.2.3.1. Eye disorders

Many ophthalmic diseases are associated with oxidative stress, such as cataract and diabetic retinopathy [*D.C. Beebe et al., 2010*], as overproduction of reactive oxygen species (ROS) affects neurons and retinal vessels. ROS are a free radical usually involved in the redox mechanisms of body. In physiological conditions, ROS are maintained in equilibrium, however their overproduction can lead to biological process called oxidative stress. The latter causes a production of chemically reactive

species, which induce a variety of proinflammatory mediators, such as VEGF and TNF-α [*L.P. Aiello et al., 1995; G.A. Limb et al., 1999*]. Moreover, it is considered the main pathogenesis of diabetic retinopathy (DR).

Diabetic retinopathy (DR) is a chronic disease and is the most common diabetes-related complication. It is one of the most frequent causes of loss of sight [*G.D. Calderon et al., 2017*] and visual impairment and it is strongly influenced by many factors such as: diabetes duration, poor glycemic control and hypertension [*R. Williams et al., 2004*]. In diabetes, sustained hyperglycemia acts as a trigger for a variety of events leading in vascular dysfunction. Vascular alterations in DR are related to several biochemical and immunological mechanisms that promote pro-inflammatory cytokines release such as TNF-α. The expression of several inflammatory biomarkers is regulated at the level of gene transcription through the activation of proinflammatory transcription factors, such as Nuclear Factor-kappa-B (NF-kB). Activation of NF-kB leads to the modulation of many cytokines such as TNF-α. The first changes detectable in DR are loss of pericytes, capillary basement membrane thickening, edema, and formation of microaneurysms. These structural and functional changes cause microvascular occlusion, neovascularization, and neurodegeneration [*J. Tang et al., 2011*]. As oxidative stress and inflammation represent the key factors in the onset and progression of DR, antioxidant and anti-inflammatory compounds represent promising approach for the treatment of DR. Several studies [*S.J. Kim et al., 2016; R. Liu et al., 2012*] demonstrated the important role of the natural anti-inflammatories and antioxidants, such as N-palmitoylethanolamide and mangiferin, for the potential treatment of eye diseases.

2.2.3.2. Natural compound for the potential treatment of retinal diseases

N- palmitoylethanolamide (PEA) is an important natural anti-inflammatory. It is a lipophilic compound naturally present in a large variety of foods such as eggs, soy, peas, peanuts; among these, soybeans represent the main source (about 7μg / g) [*O.H. Coburn et al., 1954; O.H. Ganley et al.,*

1958]. PEA is an endogenous fatty acid amide belonging to the family of N- acylethanolamines (NAEs) (Figure 16).
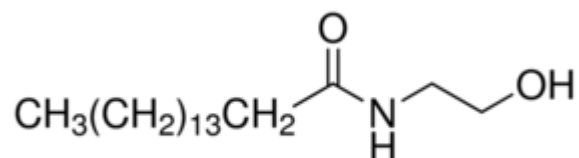
Figure 16. Chemical structure of N-palmitoylethanolamide.

It has an important anti-inflammatory and neuroprotective action which can be exploited in different pathological conditions and in a variety of biological systems, including retina [*D. Tronino et al., 2016; I. Matias et al., 2006; S. Petrosino et al., 2010*]. Pescosolido and coworkers showed that PEA is able to reduce ocular inflammation [*N. Pescosolido et al., 2011*]. Moreover, several studies demonstrated the beneficial role of PEA in retinal diseases such as diabetic retinopathy, preserving the integrity of the blood–retinal barrier [*I. Matias et al., 2006; I. Paterniti et al., 2015; C. Puglia et al., 2018*]. The pharmacological properties of PEA involve effects upon mast cells, CB2-like cannabinoid receptors, ATP-sensitive K^+-channels, TRP channels and NF-kB, and the nuclear receptor peroxisome proliferator-activated receptor α (PPARα) [*J. Lo Verme et al., 2005; G. D'Agostino et al., 2007*]. The latter receptor plays a key role in the inflammatory response. The activation of the PPAR-α receptor is important both in the regulation of the genes involved in cellular and inflammatory metabolic processes, and in the reduction of the synthesis of pro-inflammatory molecules, such as IL-6 and prostaglandins, which is expressed through a reduced nuclear transcription factor activity (NF-kB) [*P.R. Devchand et al., 1999; R. Kostadinova et al., 2005*]. The limits of PEA (poor solubility and high instability) justify its nanoencapsulation into drug delivery systems (NLC) for the promising treatment of eye disorders.

Another important natural compound is _Mangiferin_ (2-b-D-glucopyranosyl-1, 3, 6, 7-tetrahydroxyxanthone, MGN). It is a polyphenol mainly extracted from the leaves, stem barks and fruits of _Mangifera indica L._, which has shown a wide scope therapeutic properties, including antibacterial [_C. Engels et al., 2009_], anti-inflammatory [_A. Sá-Nunes et al., 2006_], especially potent antioxidant [_E. Joubert et al., 2008_] and antidiabetic [_Y. Li et al., 2008_] performances for the potential treatment of eye diseases. MGN is a C-glucosyl-xanthone which has the following chemical structure:
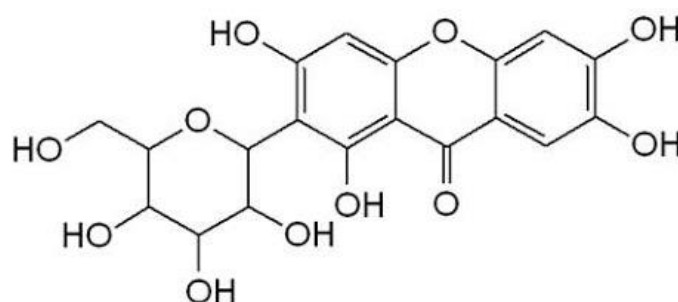
Figure 17. Chemical structure of mangiferin.

It has four hydroxyl groups responsible for its antiradical and antioxidant properties; it is also able to chelate iron and, therefore, prevents the generation of hydroxyl radicals in Fenton-type reactions [_G.L. Pardo-Andreu et al., 2006_]. Rodriguez and coworkers showed that MGN exerted an important role in the protection of erythrocytes from ROS production, contributing to the integrity and functionality of these cells [_J. Rodríguez et al., 2006_].

Additionally, some studies showed the anti-inflammatory activity of _Mangifera Indica L._ [_B.L. Dhananjaya et al., 2016; D. Impellizzeri et al., 2015_]. TNF (Tumor Necrosis Factor) is one of the main cytokines involved in the first phase of inflammation and is responsible for the production of other cytokines, such as IL-β and IL-6. Other elements implicated in inflammatory processes are some transcription factors, among which the nuclear transcription factor κB (NF-κB). It is a protein

complex which is normally present in the cytoplasm in an inactive state, complexed with its inhibitory subunit, IκBα.

The phosphorylation of IκBα, throught activation of the enzyme IκB kinase (IKK), leading to nuclear translocation and the activation of NF-κB which initiates the synthesis of new pro-inflammatory cytokines. Some researchers suggested that MGN manages to inhibit NF-κB activation [*A. Sarkar et al., 2004*]. Therefore, MGN could be administered for the potential treatment of retinal diseases, such as diabetic retinopathy, thanks to its antioxidant and anti-inflammatory activities.

Unfortunately, its use in clinical practice is compromised due to its low aqueous solubility (0.111 mg/mL) [*R.N. Tharanathan et al., 2006; M. Pleguezuelos-Villa et al., 2019; J. Acosta et al., 2016*]. For this reason, it is necessary to formulate an ophthalmic drug delivery system to increase aqueous solubility of MGN and to reach the posterior eye segment through topical administration. Therefore, NLCs represent an innovative strategy in order to overcome the unfavorable features of this interesting natural active compound and to consent their potential application in therapeutic field.

Chapter 3

3.Aim of thesis

The aim of my research project is to find efficient formulation strategies to obtain stable and homogeneous lipid nanoparticles loaded with natural compounds for the treatment of nervous system disorders. The encapsulation of these molecules in nanocarriers increases solubility, stability, cell uptake, specificity, tolerability, therapeutic index and selective release. These strategies allow to deliver these compounds to the target site and to overcome the complex anatomy of nervous system and the instability problems of natural compounds.

The nervous system disorders can involve the CNS, PNS and retina; the latter is considered the "window to the brain".

Among these disorders, whose clinical use is complex, deserve special attention:

- *CNS pathologies* involving a deficit of antioxidant defenses, such as Alzheimer's disease. Therefore, my PhD thesis was finalized to the formulation of innovative drug delivery systems able to maximize the CNS concentration of CUR and AST, two powerful natural antioxidants that could be used to treat Alzheimer's disease.

To prolong the blood circulation time and avoid the opsonization, I have explored many strategies in order to formulate stealth systems (sSLNs) loaded with CUR and AST suitable for the parenteral administration. I have decided to apply the "sSLN strategy" since these systems show important advantages such as stability, reduced toxicity due to the use of biodegradable and biocompatible lipids, controlled release of drug and increased bioavailability that allows their administration by parenteral route.

The strategies to realize "stealth" systems are to coat the nanoparticles surface with hydrophilic polymer (PEG) or surfactant such as polysorbate 80. The obtained sSLNs were characterized in term of technological parameters (PDI, mean particle size and PZ), stability over time and cytotoxicity.

Furthermore, the antioxidant effect of CUR and AST was evaluated through the ORAC assay, based on the absorbency capacity of the radical oxygen.

Finally, the pharmacological activity of CUR-pSLNs and AST-p80SLNs have been evaluated by *in vivo* assay in which the memory performances were observed.

- *neuropathic pain* through the modulation of TRPV1 receptor. Capsaicin is a natural agonist highly selective of TRPV1 used for the treatment of thermal hyperalgesia in chronic pain conditions. Since prolonged exposure to CPS induces TRPV1 defunctionalization, the aim was to formulate CPS loaded lipid nanocarriers (CPS-SLNs) in order to optimize CPS release, thus preventing TRPV1 internalization and degradation.

CPS-SLNs were formulated and characterized by *in vitro* studies. Activation of TRPV1 receptors after CPS-SLN administration was evaluated by measuring spontaneous pain induced by local injection into the plantar surface of the mouse hind-paw. Moreover, expression of TRPV1 in the skin was evaluated by western blot analysis in CPS-SLN injected mice and compared to a standard CPS solution.

- *retinal diseases*, such as diabetic retinopathy. Finally, I have explored many strategies in order to formulate stable lipid nanoparticles for the treatment of the eye diseases. The development of the NLCs, has made it possible to prolong corneal residence time and improve the ocular bioavailability of ophthalmic drugs. In particular, I have focused my efforts on the determination of the best formulation parameters necessary to obtain valid and stable nanocarriers loaded with PEA and MGN, suitable for ocular administration. Although both natural compounds show important therapeutic properties, their use in clinical practice is compromised due to their poor physicochemical properties.

Therefore, their nanoencapsulation could be a strategy to improve their ocular bioavailability. PEA-NLCs were prepared by high shear homogenization coupled to ultrasound (HSH-US) method. They were characterized by Dynamic Light Scattering (DLS) in terms of average size (M.D.), polydispersion index (PDI) and zeta potential (PZ); in addition, the characterization study included the evaluation of the thermal behavior of the nanoparticles by DSC (Differential Scanning Calorimetry). Pharmacokinetic studies have been conducted to evaluate the distribution of the drug in the eye. Moreover, the pharmacological activity has been evaluated by *in vivo* assay in which a reduction of TNF-α levels was observed, a pro-inflammatory cytokine involved in the pathogenesis of diabetic retinopathy. Regarding the MGN-NLCs, the nanocarriers were prepared and formulated by the same technique used for PEA-NLCs. The antioxidant activity of MGN was evaluated by ORAC assay. Finally, the obtained formulations were analyzed in term of ocular tolerance and *ex vivo* permeation.

Chapter 4

4.1. Materials

Compritol 888 ATO (COMP, MW 414.7 g/mol), a mixture of mono-, di-, and triglycerides of behenic acid, Precirol ATO 5 (Glyceryl palmitostearate), and Cetyl palmitate (Hexadecyl palmitate, MW 480,85 g/mol) were obtained from Gattefossè (Milan, Italy); Lecinol S-10, hydrogenated lecithin, was obtained from Nikko Chemical (Italy) and Lutrol F68 (MW 8400 g/mol) were provided by BASF ChemTrade GmbH (Burgbernheim, Germany). DSPE-PEG2000 (1,2-distearoyl-sn-glycero-3-phosphoethanolamine- N-[amino (polyethyleneglycol)- 2000] ammonium salt) was a gift from Lipoid GmbH (Ludwigshafen, Germany). Curcumin (CUR, MW 368.38 g/mol), Astaxanthin (AST, MW 596.84 g/mol), Capsaicin (CPS, MW 305.41 g/mol), Trolox (MW 250.29 g/mol), AAPH (2,2'-azobis(2-methylpropionamidine) dihydrochloride, MW 271.19 g/mol), Stearic Acid (MW 284,48 g/mol), Mangiferin (MGN, MW 422.33 g/mol), Cytosine arabinoside, 1-(4,5-Dimethylthiazol-2-yl)-3,5-diphenylformazan (MTT), Streptozotocin (STZ), Dimethyl Sulfoxide (DMSO) and other chemicals were from Sigma-Aldrich (Milan, Italy). Softisan© 100 (Hydrogenated Coco-Glycerides) was a gift of Sasol (Witten, Germany). Tween 80 was provided from Polichimica S.r.l (Bologna, Italy). Fluorescein disodium salt (MW 332.31 g/mol) was obtained from Acros Organics. Dulbecco's Modified Eagles Medium (DMEM), heat inactivated Foetal Bovine Serum (FBS), Penicillin/Streptomycin solution, 200 mM L-glutamine, collagenase, 0.05% trypsin-0.02% EDTA solution were from Invitrogen (ThermoScientific, Milan, Italy). Miglyol 812 (MIG), which is a mixture of caprylic/capric triglycerides, was obtained from Eigenmann & Veronelli S.p.A. (Milan, Italy) and micronized PEA was a kind gift from Epitech Group (Milan, Italy). MCF-7 human breast cancer cell line was purchased from Cell Bank Interlab Cell Line Collection (Genova, Italy). The transgenic mice TgCRND8 were generated and supplied by the group of Dr. P St George Hyslop (Center for research in neurodegenerative Diseases, Toronto, Canada) and then the colony was bred in the animal house Ce.S.A.L. (Centro Stabulazione Animali da Laboratorio), University of Florence.

4.2. Active natural products for the treatment of CNS disorders

4.2.1. MTT assay: lipid screening to deliver CUR and AST

The choice of the most suitable lipid matrix to formulate sSLNs loaded with CUR and AST was carried out by *in vitro* assay. This study investigated the effect on cell viability of different blank SLNs formulated using different lipid matrices such as stearic acid, Compritol, and Precirol on adult primary stem cells (Primary Adult Stem Cell Human Dental Pulp, DPSCs) [*S. Gronthos et al., 2000; G. Bonaventura et al., 2019*].

The Dental Pulp Stem Cells (DSPCs) were isolated from human teeth. Freshly extracted teeth were immediately cracked open, and pulp tissue was collected, minced into small fragments of 1 mm, and then digested in 3 mg/ml collagenase type I for 1 h at 37°C. The tissue pellet, after filtration by using a 70-μm filter, was resuspended in DMEM containing 15% (v/v) FBS, 2mM L-glutamine, 50 mg/mL, penicillin (50 U/mL), and plated in 75 cm^2 flasks at a final density of 2 x 10^6 cells or placed at the final density of 0.5 x 10^4 cells/well of a 96-multiwell plates. When the cultures were about 80-85% confluent, cells were trypsinized by using 00.05% trypsin-0.02% EDTA solution. After centrifugation, cells were resuspended in fresh basic complete media, plated at 1:4 density ratio in 75 cm^2 flasks, incubated at 37°C in humidified atmosphere containing CO_2 (95-5%), and the medium was replaced every 2 or 3 days.

The DSPC cell culture was suspended in the specific complete culture medium and placed in 96-multiwell plates and placed for at 37° C in a humidified atmosphere and CO_2 (95-5%). In order to establish the optimal lipid matrix to formulate CUR-pSLNs, cell cultures were treated for 24 h.

Cell survival analysis was performed by MTT reduction assay, evaluating mitochondrial dehydrogenase activity. Cells were set up 0.5 x 10^4 cells per well of a 96-multiwell, flat-bottomed, 200-mL microplate and maintained at 37°C in a humidified CO_2 (95-5%) air mixture. At the end of treatment time, 20 mL of 0.5% MTT in (pH 7.4) PBS were added to each microwell. After 1 h of

incubation with the reagent, the supernatant was removed and replaced with 100 mL of DMSO. The optical density of each well was measured with a microplate spectrophotometer reader (Titertek Multiskan; Flow Laboratories, Helsinki, Finland) at $\lambda = 570$ nm. Results were normalized with DMSO control (0.05%) and expressed as a percentage of cell viability inhibition.

The obtained data were statistically analyzed using One-Way analysis of variance (ANOVA) followed by a post hoc Holm–Sidak test to estimate significant differences among groups. Data were reported as mean ± SD of four separated experiments in duplicate, and differences between groups were considered to be significant at *$p < 0.05$.

4.2.2. Stealth SLNs preparation

The stealth systems (s-SLNs) loaded with CUR and AST were formulated using two different strategies using polyethylene glycol (pSLNs) [*S.A. Wissing et al., 2004; I. Brigger et al., 2002*], and polysorbate 80 (p80SLNs) [*E. Esposito et al., 2017*].

Curcumin-loaded SLNs using the PEGylation strategy were formulated using Compritol® 888 ATO (glycerol behenate) as lipid phase and Lutrol F68® (Poloxamer 188) as surfactant. Non-stealth nanoparticles loaded with curcumin (CUR-SLNs) were prepared by the *solvent evaporation* method with slight modifications [*C.F. Luo et al., 2013; A.J. Shuhendler et al., 2012*]. Firstly, CUR (99 mg), Compritol 888 ATO (60 mg) and injectable soya lecithin (60 mg) were solubilized and melted in ethanol (10 mL) at 70 °C. For preparation of PEGylated SLNs (CUR-pSLNs), 15 mg of DSPE- PEG 2000 was added to lipid phase. The melted lipid phase was dispersed in the hot (70° C) surfactant solution (Lutrol F68, 0.5% w/v) under stirring at 695 rpm. The hot dispersion was then cooled in an ice-bath (2- 3° C) for 5 min. Finally, the organic solvent was removed by vacuum. Blank nanoparticles were prepared by the same procedure without adding CUR.

As regard the modification strategy with polysorbate 80, CUR-p80SLNs were prepared by different protocols (*solvent evaporation* and *solvent diffusion* methods) and using different lipid matrices (Compritol 888 ATO, cetyl palmitate). In order to modify the surface of the nanoparticles, P80 (20% w/w with respect to the lipid weight) was added to the SLN stirring at 250 rpm for 30 min.

Astaxanthin-loaded SLNs were formulated using the same strategies. PEGylated SLNs loaded with AST (AST-pSLNs) were prepared by *solvent-diffusion* technique, using stearic acid as lipid phase and Lutrol F68® (Poloxamer 188) as surfactant. The lipid matrix most suitable for the encapsulation of AST was stearic acid [*P.C. Bhatt et al., 2015*]. The choice to use this lipid was further confirmed by the *in vitro* assay previously described. Briefly, stearic acid (0,005 g), DSPE- PEG_{2000} (0,8 mg) and AST (AST 4,2 mg) were solubilized in ethanol (1,2 ml) and melted at 70°C. The aqueous phase was constituted by hydroxypropylmethyl cellulose (0,05 g), soy lecithin (0,05 g), Lutrol F68 (0,05 g) and distilled water (5,8 ml). The melted lipid phase was dispersed in the hot (70°C) aqueous phase by using a high- speed stirrer (Ultra-Turrax T25, IKA-Werke GmbH &Co. Kg, Staufen, Germany) at 15.000 rpm for 8 min, maintaining the temperature at least 10°C above the lipid melting point. The obtained pre-emulsion was ultrasonified by using a Labsonic2000 (B. Braun, Melsunen, Germany) for 10 min. Then the hot dispersion was cooled in an ice bath for 5 min. Finally the organic solvent was removed by under vacuum. AST-loaded pSLNs were prepared by the same procedure with the addition of AST (1 µM).

As regard the AST-p80SLNs (AST 4,2 mg), SLNs were prepared by the same protocol without the addition of DSPE- PEG_{2000}. In order to modify the surface of the nanoparticles, P80 (20% w/w with respect to the lipid weight) was added to the SLN stirring at 250 rpm for 30 min.

4.2.3. Stealth SLNs characterization

The average size (Z-Ave) and polidispersity index (PDI) of the nanoparticles were measured by Dynamic Light Scattering (DLS). A Zeta Sizer Nano-ZS90 (Malvern Instrument Ltd., Worcs, England), equipped with a solid-state laser having a nominal power of 4.5 mW with a maximum output of 5 mW 670 nm, was employed. Analyses were performed using a 90° scattering angle at 20 ± 0.2 °C. Samples were prepared diluting 100 μL of SLN suspension with 900 μL of distilled water. Each value was measured at least in triplicate.

The Zeta Potential (ZP, ξ) was measured by Electrophoretic Light Scattering (ELS) using the Zeta Sizer Nano-ZS90 (Malvern Instrument Ltd., Worcs, England). It is an indicator of the stability of a dispersed system. The instrument used for the measurement gave us indications about the electrophoretic mobility of particles in dispersion or in solution. The instrument carried out three sets of measures up to 100 to achieve an average value. Samples were suspended in distilled water and the measurements were recorded at 25 °C. Each value was measured at least in triplicate.

Additionally, the morphology of nanoparticles loaded with CUR and AST was investigated using Transmission Electron Microscopy (TEM; JEOL JEM-101).

4.2.4. Determination of drug loading

The unentrapped drugs (CUR and AST) were determined by filtration using a Pellicon XL™ tangential ultrafiltration system (Millipore, Milan, Italy). It is equipped with a polyethersulfone Biomax 1000 membrane with a 1.000.000 molecular weight cut off (MWCO). An amount of each lyophilized nanoparticles was solubilized in dichloromethane and the CUR and AST content were measured by UV spectrophotometry at 424 and 492 nm, respectively (Lambda 52, PerkinElmer, MA, USA). Calibration curves for the validated UV assays of drug were performed on six solutions in the concentration range 10–100 μg/ml ($r^2 > 0.99$). Each point represented the average of three

measurements and the error was calculated as standard deviation (±SD). Drug incorporation efficiency was calculated from the equation 5:

Drug recovery (%)=Mass of active in nanoparticles /Mass of active fed to the system×100

Possible lipid interferences during UV determination of drug were also studied between the standard curves of drug alone and in presence of lipids. The differences observed were within the experimental error, thus inferring that no lipid interference occurred.

4.2.5. In vitro release study

The amounts of CUR and AST released from SLNs were calculated through the permeability test. This test was carried out using the vertical Franz cells consisting of a receptor and a donor compartment. The receptor compartment (4.5 mL) was filled with phosphate buffer solution (PBS, pH 7.4) and placed in a bath at 37 °C, under magnetic stirring. The testing samples (200 µL) were placed in the donor cell maintaining a complete and intimate contact with the surface of a cellulose acetate membrane (0.2 µm pore size, 25 mm diameter, Sartorius; Göttingen, Germany). At predetermined intervals, samples (200 µL) at each time point (0, 2, 4, 6, 8, 22 and 24 hs) were taken from the receptor chamber and replaced with the same volume of PBS. The amounts of CUR and AST permeated were analyzed by UV spectrophotometer at 424 and 492 nm, respectively.

4.2.6. Stability tests on stealth SLNs

4.2.6.1. Long-term stability

Mean particle sizes, PDI and ZP values of SLN samples were monitorated over time at intervals (zero hour, one week, two weeks, three weeks, one month, two months, three months, four mounths, five

mounths and six mounths). During storage, samples were maintained at room temperature and protected from light exposure.

4.2.6.2. Turbiscan® Technology

The stability of SLN suspensions was further evaluated by Turbiscan® Ageing Station (TAGS) (Formulaction, l'Union, France). 20 ml of each sample were placed in a cylindrical glass cell and stored in the Turbiscan for 30 days at 25°C. Turbiscan® AGS has been previously reported as a reliable technology to evaluate the occurrence of instability phenomena related to particle aggregation and/or migration [*C. Carbone et al., 2014; C. Caddeo et al., 2017; C. Puglia et al., 2020; C. Carbone et al., 2020; C. Carbone et al., 2020*]. The detection head was composed of a pulsed near-infrared light source (λ = 880 nm). Two synchronous transmission (T) and back scattering (BS) detectors receive the light which crosses the sample (at 180° from the incident beam) for the T detector, while the BS detector takes the light scattered backwards by the sample (at 45° from the incident beam). The detection head scanned the entire height of the sample cell (65 mm longitude), acquiring T and BS each 40 mm (1625 acquisitions in each scan). The Turbiscan scans at various pre-programmed times and overlays the profiles on one graph in order to show possible destabilization phenomena. In my experiments, the stability of the samples was evaluated based on the variation of backscattering (ΔBS), which is shown in ordinate, while the height of the cell is reported in abscissa.

4.2.6.3. Freeze drying of SLNs

Freeze drying, also called lyophilization, can transform colloidal suspensions into stable solid cakes for long term storage, but it is a complex process that generates stress sources itself, which can destabilize the nanoparticles formulation. For this reason, cryoprotectants have been used to decrease SLN aggregations due to the stress during this process [*W. Abdelwahed et al., 2006; L.M. Crowe et*

al., 1992; L.M. Crowe et al., 1986; G.F. Doebbler et al., 1966; Y. Bensouda et al., 1989; T. Madden et al., 1985; G. Strauss et al., 1986; M. Ausborn et al., 1992; H. Hauser et al., 1988; S. Vemuri et al., 1991; G. Strauss et al., 1984; P. Shulkin et al., 1984]. Sugars (e.g. glucose, mannitol and trehalose) are the most cryoprotectants used in freeze drying of nanoparticles [*C. Schwarz et al., 1997; W. Mehnert et al., 2001*] as they are able to immobilize them within a glassy matrix of cryoprotectant can prevent their aggregation and protect them against the mechanical stress of ice crystals. The level of stabilization afforded by sugars generally depends on their concentrations; increasing the cryoprotectant concentration to a certain level may eventually reach a limit of stabilization or even destabilize system [*W. Abdelwahed et al., 2015; M.J. Pikal et al., 1990*].

Glucose, mannitol and trehalose were tested to select the cryoprotectant and the most suitable concentration for the formulation. The SLN dispersions were added with each cryoprotectant, at different concentrations (1-3% w/w), before freezing. 2 mL of these dispersions were placed in 5 mL vials. Freezing is the first step of freeze-drying, then samples were lyophilized for 24 hs. In order to rehydrate the freeze-dried nanoparticles, the same volume of water lost during lyophilization was added. After reconstitution by manual shaking, nanoparticles size was measured by DLS. The preservation of mean nanoparticle size after freeze-drying is considered as a good indication of a successful freeze-drying cycle [*Y. Wang et al., 2012*].

4.2.7. PEG micelles preparation

Micelles of DSPE-PEG$_{2000}$ were prepared using the *thin-layer evaporation* method [*M. Kastantin et al., 2009; D. Paolino et al., 2017*]. They were prepared by dissolving the polymer in an organic solvent mixture (chloroform/methanol 1:1 v/v). Aliquots of PEG suspensions (which corresponded to 1:0.1, 1:0.25, 1:0.5, 1:0.75 and 1:1 molar ratios with respect to the lipid of SLNs) were placed in glass vials. To obtain a film, the solvents were firstly evaporated under a nitrogen stream, and then, samples were lyophilized to obtain a solvent-free film. Subsequently, the DSPE-PEG$_{2000}$ films were

hydrated using distilled water. The samples were kept at 80 °C for 1 min and vortex for 1 min, for two times and, finally, kept at 80 °C for 60 min.

4.2.8. Differential scanning calorimetry (DSC)

DSC analysis was carried out using a Mettler Toledo STAR^e system (Switzerland) equipped with a DSC-822 calorimetric cell. A MettlerTA-STAR^e software (16.00 version) was used to acquire and to analyze data. The DSC was calibrated using indium ($\geq$99.95% purity). The reference pan was filled with 120 μL of distilled water. Each sample (120 μL) was loaded into a 160 μL aluminum crucible, hermetically sealed and submitted to DSC analysis, under an atmosphere of dry nitrogen. DSC analysis was carried out using a heating scan from 5°C to 85° C (2° C/min) and a cooling scan from 85°C to 5°C (4° C/min), for at least three times [*M.G. Sarpietro et al., 2013*].

The degree of PEGylation of the CUR-pSLNs was evaluated by DSC analysis using blank and CUR-SLNs. 30 uL of each DSPE-PEG$_{2000}$ micelles was co-incubated with SLNs and submitted to DSC analysis. The scanning program consisted of a heating scan from 4°C to 85°C, an isothermal segment at 85°C for 1 h and a cooling scan from 85°C to 4°C. The analysis was repeated eight times to allow hour by hour to monitor the thermodynamic changes taking place in the SLNs.

The degree of PEGylation of AST-pSLNs was evaluated by the same technique using a heating scan rate of 2° C/min and a cooling scan rate of 4° C/min. The DSC analysis of the SLN was carried out using a heating scan rate which ranged from 5°C to 70° C and a cooling scan rate which ranged from 70°C to 5°C, respectively. All calorimetric analyses were replicated at least three times to check the reproducibility and reversibility of the thermal events.

4.2.8.1. Interaction between the SLN and MLV

The processes involved in SLN uptake by cells are very complex, and the cell membranes are very intricate structures; as a consequence the biophysical interactions between SLN and biomembranes are difficult to study and understand. I evaluated the interaction between biomembrane models, represented by multilamellar vesicles (MLVs) made of dimyristoylphosphatidylcholine (DMPC), and SLNs to achieve information on the mechanism by which SLN interact with biological membranes. As reported in literature [*L.G.M. Basso et al., 2011; L. Montenegro et al., 2012*], DMPC is widely used to study the interaction of bioactive compounds and biomembrane models because its transition temperature is about 24 °C; this allows the uptake experiments to be carried out at 37 °C, a temperature similar to the physiological one, at which the bilayers are in a disordered liquid crystalline state more favorable to interact with drug.

MLVs were synthesized using the *thin-layer evaporation* method. They were prepared by dissolving the DMPC in an organic solvent mixture (chloroform/methanol 1:1 v/v). Aliquots of DMPC suspensions (7 mg) were placed in glass vials. The solvents were firstly evaporated under a nitrogen stream, and then samples were lyophilized (Labconco, Freezone) to obtain a solvent-free lipid film. The resulting phospholipid films were hydrated using 168 μl of Tris buffer solution (50 mM, pH 7.4) and then vortex-mixed (for 1 min, three times) and heated (for 1 min, three times) at 37 °C. Finally, the samples were kept at 37 °C and stabilized for 1 h.

MLVs were prepared and incubated with SLNs and pSLNs. The interaction, occurred between MLV and the SLN, was carried out to simulate the interaction of SLN with cell membranes. The kinetic experiments allowed the evaluation of the interaction occurring between the SLN and MLV here in reported. 30 μL of SLN were put into the calorimetric pan where 90 μL of MLV were added. A heating scan rate of 2° C/min and a cooling scan rate of 4° C/min were used during the experiments. The analysis was carried out by setting up the scanning program which was run in the range from 5°C to 85°C, an cooling run from 85° to 37°, an isothermal segment at 37°C (a temperature which is very

close to the physiological temperature and at which the MLVs are in a disordered liquid crystalline state favorable to drug uptake and interaction) for 1 h and a cooling run from 37°C to 5°C. The analysis were repeated nine times to allow hour-by-hour monitoring of the thermodynamic changes taking place in the MLVs and SLN.

4.2.9. Oxygen Radical Absorbance Capacity (ORAC) Assay

Oxygen Radical Absorbance Capacity (ORAC) assay has been widely accepted as a standard *in vitro* test to measure the antioxidant activity of natural active compounds [*J.M. Awika et al., 2003; R.L. Prior et al., 2005*]. In particular, this assay measures the loss of fluorescence over time due to peroxyl-radical formation by the breakdown of AAPH (2,2'-azobis-2- methyl- propanimidamide, dihydrochloride). Trolox [6- Hydroxy-2,5,7,8- tetramethylchroman-2- carboxylic acid], a water soluble vitamin E analogue, is used as a positive control inhibiting fluorescein decay in a dose dependent manner.

Data were obtained using a VICTOR Wallac 1420 Multilabel Counters fluorimeter (Perkin Elmer, Boston, MA, USA) with a fluorescence filter (excitation 540 nm, emission 570 nm). During the ORAC assay the decay of the fluorescence of fluorescein was monitored. Fluorescein (FL) solution (12 nM) was the fluorescence probe and the target molecule for free radical attack by the peroxyl radical generator AAPH (100 mM). The assay was carried out at pH 7.0 and at 37 °C, using trolox (12.5 μM) as the control standard and phosphate buffer (pH 7.0) as the blank. Drug was solubilized in ethanol (12.5 μM), while drug-loaded pSLNs were diluted at the same concentration with phosphate buffer. After adding AAPH, the fluorescence was recorded for 24hs. All measurements were expressed in relation to the initial reading, analyzing all samples, one blank and one standard at the same time. Each measure was performed in triplicate. The ORAC value refers to the net protection area under the quenching curve of FL in the presence of an antioxidant. The results (ORAC values)

were calculated and were expressed using trolox equivalents (TE) for μM of sample (TE/μM) according to Equation 6:

$$ORAC\ units\ (TE/\mu M) = K\ (S_{sample} - S_{blank})\ /(S_{trolox} - S_{blank})$$

where K is a sample dilution factor and S is the area under the fluorescence decay curve of the sample, trolox, or blank calculated with Origin®7 (OriginLab Corporation, Northampton, MA, USA).

4.2.10. UV stability assay on AST-loaded SLNs

In order to evaluate the photoprotective effect showed by lipid nanoparticles against UVA radiation [*E. Damiani et al., 2010*], 2 mg of each sample were placed onto 5 cm^2 glass plates and left to dry at room temperature in the dark for 20 min. Subsequently, the plates were placed on a brass block embedded on ice at a distance of 20 cm from the light source. A commercial UVA sun lamp, Philips Original Home Solarium (model HB 406/A; Philips, Groningen, Holland) equipped with a 400 W ozone-free Philips HPA lamp, UV type 3 was used for irradiation. The output of UVA was measured with a UV Power Pack Radiometer (EIT Inc, Sterling, MA). The lamp was always pre-run for 10 min to allow the output stabilization. Samples were irradiated for 15 min corresponding to an incident dose of UVA of 275 kJ/m^2, i.e the dose approximately equivalent to about 90 min of sunshine [*S. Seite et al., 1998*].

For each irradiated sample, a non-irradiated sample serving as control was kept in the dark at room temperature for 30 min. All samples were collected by immersing the plates in 10 mL ethyl acetate for 30 min. From this organic solution, 50 μL were added to 2450 μL ethyl acetate in a quartz cuvette and its absorption spectra was measured on a UV Varian Cary 50 spectrophotometer (Agilent Technologies Italia S.p.A., Milan, Italy) against a blank containing ethyl acetate.

4.2.11. In vitro study on AST-loaded sSLNs

The cytotoxicity studies were carried out using different cell lines, in particular a stem cell line OECs (Olfactory Ensheathing Cells) and a cancer cell line MCF-7 have been used, in order to evaluate the different characteristics of the cell membrane.

The cell line of interest to my goal, the treatment of Alzheimer's disease, is the OECs cells. OECs are a particular glial cell type exhibiting phenotypic properties with both Schwann cells (SCs) and astrocytes [*A. Ramon-Cueto et al., 1998*]; they protect the small unmyelinated axons of olfactory receptor neurons driving them towards their correct position from the basal lamina of the epithelium to the olfactory bulb [*R. Fairless et al., 2005*]. As reported in literature [*J.P. Kesslak et al., 1988; E. Koss et al., 1987; E. Koss et al., 1988; P.J. Moberg et al., 1987; C.D. Morgan et al., 1995; S. Nordin et al., 1998; M.D. Warner et al., 1986*], losses in the ability to identify and recognize odorants are salient in the earliest phases of Alzheimer's disease (AD). Murphy [*C. Murphy et al., 1999*] suggested that olfactory tasks with memory demands could detect early changes in AD, due to the fact that areas of the brain among the first to exhibit changes with Alzheimer's are involved with either processing olfactory information or memory consolidation.

MCF-7 are a human breast cancer cell line commonly used as model cell line for cancer investigations. They have been used to compare the cytotoxic activity of SLNs on cancer cells.

Experiments were performed on 2-day old rat pups (P2, provided by Envigo RMS s.r.l. Italy, stock: C57BL6J). Animals were housed in a light and temperature-controlled room (23 $\pm$ 1°C, 50 $\pm$ 5 % RH) with tap water and standard chow provided ad libitum. Experimental animal procedures were carried out according to the Italian Guidelines for Animal Care (D.L. 116/92 and 26/2014), which are in compliance with the European Communities Council Directives (2010/63/EU) and were approved by the Ethical Committee at the University of Catania (Catania, Italy). Efforts were made to minimize the number of animals used and their suffering.

Primary OECs were isolated from rat pups (P2) olfactory bulbs as previous described (Pellitteri R et al.,2007). Briefly, pups were decapitated and the bulbs were removed. Then, they were digested by collagenase and trypsin. Trypsinization was stopped by adding DMEM supplemented with 10% heat inactivated FBS, 2 mM glutamine, streptomycin (50 μg/mL) and penicillin (50 U/mL). Cells were resuspended and plated in flasks fed with fresh complete medium. The antimitotic agent, cytosine arabinoside (10^{-5} M), was added 24 h after. To further purify, OEC cultures were processed to an additional step, transferring cells from one flask to a new one (Chuah and Au, 1993; Pellitteri et al., 2016). In the last passage, OECs were plated on 25 cm^2 flasks and cultured in DMEM/FBS supplemented with a bovine pituitary extract. Cells were then incubated at 37°C in humidified air containing 5% CO_2 with a fresh complete medium and were fed twice a week.

MCF-7 human breast cancer cell line were suspended in DMEM containing 10% (v/v) FBS, 2mM L-glutamine, 50 mg/mL, penicillin (50 U/mL), and plated in 75 cm^2 flasks at a final density of 2 x 10^6 cells or placed at the final density of 0.5 x 10^4 cells/well of a 96-multiwell plates. The cell cultures were then incubated at 37°C in humidified atmosphere. Treatment of MCF-7 cell line culture containing CO_2 (95-5%), and the medium was replaced every 2 or 3 days. When the cultures were about 80-85% confluent, cells were trypsinized by 0.05% trypsin and 0.53mM ethylenediaminetetraacetic acid (EDTA) at 37°C in humidified atmosphere containing 5% CO_2 for 7 min. After centrifugation, cells were resuspended in fresh basic complete media, plated at 1:4 density ratio in 75 cm^2 flasks and incubated at 37°C in humidified atmosphere containing CO_2 (95-5%).

The purified OECs and MCF-7 cell cultures were suspended in the specific complete culture medium and placed in 96-multiwell plates and placed for at 37° C in a humidified atmosphere and CO_2 (95-5%). Subsequently blank and AST-sSLNs (100μM) were exposed to OECs for 24 hs. The MTT (3-[4,5-dimethylthiazol-2-yl] -2,5 diphenyl tetrazolium bromide) assay is a colorimetric assay based on the conversion of MTT into insoluble formazan crystals by living cells, which determines mitochondrial activity. Since for most cell populations the total mitochondrial activity is related to

the number of viable cells, this assay is broadly used to measure the *in vitro* cytotoxic effects of drugs on cell lines.

To monitor cell viability, OECs were set up 6×10^6 cells/well of a 96 multiwell flat bottomed 200 μL microplates. Cells were incubated at 37 °C in a humidified CO_2 (95-5%) air mixture (A. *Campisi et al.,2012; A. Ramon-Cueto et al., 1998*). At the end of treatment, 20 μL of 3(4,5- dimethyl-thiazol-2-yl)2,5-diphenyl-tetrazolium bromide in Phosphate Buffer Saline (2 ml PBS/ 2 mg tetrazolium salts) were added to each multiwell. After 1 h of incubation, the supernatant was removed and replaced with 100 μL dimethyl sulfoxide (DMSO). The optical density of each well sample was measured with a microplate spectrophotometer reader (Titertek Multiskan; Flow Laboratories, Helsinki, Finland) at λ 570 nm. Results were normalized with DMSO control (0.05%) and expressed as a percentage of cell viability inhibition.

From the MTT test, it was observed that the concentration was too high and caused cell damage. Therefore, it was considered appropriate to treat cells at lower concentrations (1μM, 0.2 μM and 0.1 μM). Finally, MCF-7 cell line cultures were treated for 24 hs at different concentrations (1μM, 0.4 μM and 0.2 μM) of sSLNs.

Data were statistically analyzed using One-Way analysis of variance (ANOVA) followed by a post hoc Holm–Sidak test to estimate significant differences among groups. Data were reported as mean ± SD of four separated experiments in duplicate, and differences between groups were considered to be significant at $*p < 0.001$.

4.2.12. In vivo studies on stealth nanoparticles

4.2.12.1. Animals and treatment

The TgCRND8 (Tg) mice express two mutated human APP genes implicated in AD (Swedish, KM670/672NL and Indiana, V717F) under the regulation of Syrian hamster prion promoter gene

(Figure 18) [*M.A. Chishti et al., 2001*]. The mice were maintained on a hybrid (C57)/(C57/CH3)

background by crossing transgenic heterozygous TgCRND8 males with wild-type (wt) female mice.

The main feature of this model is a very rapid development of amyloid pathology in the brain:

amyloid β deposits start quite early since the two mutations involve both the β and γ secretase APP

cleavage sites; all mice display amyloid plaques in the cortex and hippocampus by three months of

age [*M.A. Chishti et al., 2001].* These neuropathologic manifestations are accompanied by impaired

acquisition and learning deficits.

Transgenic CRND8 mice were identified by DNA extraction from tail samples and PCR analysis

using specific primers (5'-aggactgaccactcgacca-3' and 5'-tggattttcgtagccgttc-3') for the human

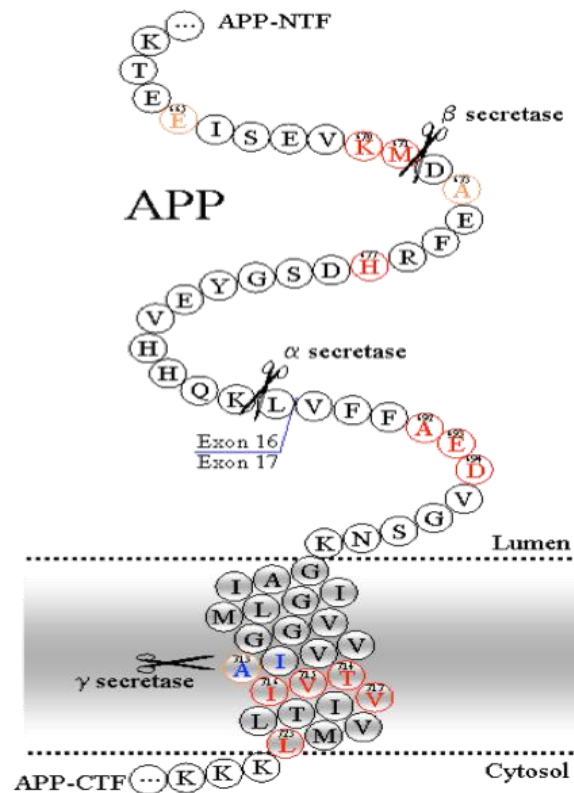mutated (KM670/672NL+V717F) cDNA insert [*A. Bellucci et al., 2006*].

Figure 18. Genetic mutations characteristic of AD.

Mice (20-30 g) were housed in a 12 h light/dark room at 21-23°C with tap water and standard chow provided ad libitum. Behavioral experiments and treatments were performed in accordance with the European (2010/63 / EC) and National (DL 26/2014) guidelines in order to minimize the suffering of animals.

4-month-old Tg mice (n = 6/group/genotype, equally divided for sex) were used for the treatment. The animal were divided into two groups: i) Tg mice treated with unloaded SLNs (n=5 mice Tg e 5 wt, 0.1 mL/10 g; untreated mice); ii) Tg mice treated with CUR-pSLN (n=5 mice Tg e 5 wt, 150 mg/kg) and AST-p80SLN (n=5 mice Tg e 5 wt, 40 mg/kg) for three consecutive weeks. All the formulations were intraperitoneally injected.

4.2.12.2. Behavioral experiments

At the end of the treatment memory performance was investigated by two widely used behavioral tests [*A.R. Bilia et al., 2019*].

- Step down inhibitory passive avoidance task

In this test, the animals learn to associate exploration of a compartment with a foot shock delivered through the floor grid. On subsequent exposure to the same environment, the mice will avoid stepping down or will increase the latency before ''stepping down'' onto the floor grid.

The term "passive avoidance" [*C.A. Netto et al., 1985*] is used to indicate *in vivo* experiments in which the animal learns to avoid a specific event, usually concerned an innate behavior, that is dangerous due to a linked punishment.

A mouse in an open field naturally spends most of the time in dark places, as near walls and corners; when the mouse is placed on an elevated-platform in the center of the field, it will try to get off the platform, to explore the environment and go near the walls. Based on this natural behavior, several

different variants of the step down inhibitory avoidance task have been used [*P. Kubanis et al., 1981; S.L. Chorover et al., 1965*].

The apparatus was an open field Plexiglas box ($50 \times 25 \times 25$ cm) with a steel rod floor and a plexiglas platform ($5 \times 8 \times 25$ cm) set on the grid floor to which intermittent electric shocks (20 mA, 50 Hz) were delivered. On day 1 (training test, TT), each rat was placed on the platform and received an electric shock for 3 s when it stepped down placing all paws on the grid floor. Responsiveness to the punishment in the TT was assessed by animal vocalization; only those rats that vocalized touching the grid (about 70% of mice) were used for retention test (RT). 24 hs after TT, each rat was placed on the platform again (RT). The latencies were compared, considering 180 s as the upper cut-off, during TT and RT: a latency longer in the RT than in TT meant the mouse learnt and could remember the punishment received the day before, otherwise the mouse showed memory impairment.

Figure 19. Step down inhibitory avoidance task.

- Object Recognition Test (ORT)

The object recognition paradigm utilized the innate tendency of mice to explore a novel object over a familiar one. The test measures spontaneous behavior, and thus requires no length training or preparation [*A. Ennaceur et al., 1988*].

Pre-training: To avoid neophobic interference a habituation phase preceded the testing. Habituation consisted in placing the mice for 5 min into a square open-field arena (60 x 50x 25 cm). During this phase the mice could explore freely the empty arena with one object inside (Figure 20).

Testing: The object recognition task was conducted 1 day after the habituation phase and comprised two trials (T1 and T2). During the T1 the animals could explore two identical objects, while in the T2 one object was replaced by a novel one. Each trial lasted 5 min, with an intertrial interval of about 60 min. All objects were made of a biologically neutral material such as plastic or metal, and animals could not move them around in the arena. Objects were not known to have any ethological significance for the mice and they never had been associated with a reinforcer. Fecal boli were removed after each tested animal.

Frequency and duration of object exploration was recorded by a video-tracking/computer-digitizing system (HVS Image, UK).

Exploration of an object was defined as directing the nose towards an object at a distance of less than a half head length and/or touching the object with the paws. Sitting on an object was not considered as exploratory behaviour. Mice without any exploration behavior towards the objects were excluded from the analysis of learning behaviour.

To analyze the object recognition test, a discrimination score was calculated: discrimination score = exploration time of the novel object (s)/total exploration time of both objects (s). A discrimination score above 0.5 indicates the ability of mice to discriminate between the familiar and novel objects while a score below or equal to 0.5, reflecting a novel object exploration time less or equal to the half

of the total time spent between the two objects, indicates memory impairment in this task. Mice with a total exploration time of less than 5 s in either the T1 or the T2 were excluded from the analysis of learning behaviour on this test day.
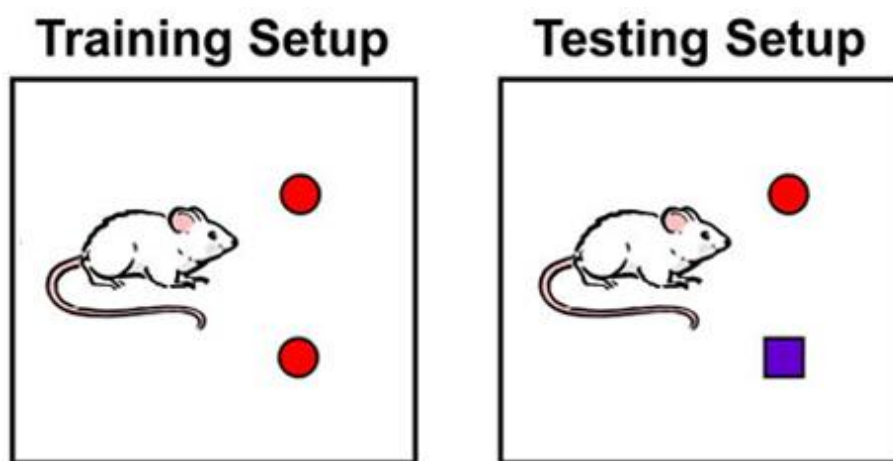
Figure 20. Object Recognition test (ORT).

One-way ANOVA followed by Bonferroni post hoc test were used to evaluate behavioral performance in the step down inhibitory avoidance and ORT.

4.3. Active natural product for the treatment of neuropathic pain

4.3.1. Preparation SLNs loaded with capsaicin

CPS-loaded SLNs were prepared by the *solvent injection* method [*M.A. Schubert et al., 2003*]. Softisan© 100 (0.2 g) and CPS (0.016 g; 0.026%) were solubilized at 35 °C in ethanol (10 mL) and then added dropwise, with continuous stirring at 500 rpm, by means of a Hei-Tec magnetic stirring hotplate (Heidolph Instruments, Schwabach, Germany), to a Tween 80 solution (50 mL) using a syringe that was equipped with a micro-needle. Stirring was continued overnight to allow for the

complete evaporation of the organic solvent. After that, the SLN dispersion was filtered and stored at 4° C. Blank SLNs were also prepared and characterized.

4.3.2. Determination of CPS Loading

The amount of CPS loaded into SLNs has been determined using a tangential ultrafiltration system (Millipore, Milan, Italy), as previously described. This system was equipped with a polyethersulfone Biomax 1000 membrane with a 1,000,000 molecular weight cut off (MWCO). The retained material was freeze-dried and after solubilization in dichloromethane and analyzed by HPLC using the method reported below. The calibration curves were performed on six solutions in the concentration range 10–100 µg/mL ($r^2 > 0.99$).

4.3.3. CPS-SLNs Characterization

The mean particle size of the formulations was determined by DLS. Analyses were performed at room temperature (25°C) using a Zetasizer Nano ZS (Malvern, UK; Laser 4 mW He–Ne, 633 nm, Laser attenuator Automatic, transmission 100–0.0003%, Detector Avalanche photodiode, Q.E. > 50% at 633 nm, T = 25 °C). The results were also expressed as intensity Distribution (Di), i.e., the size below which is placed the 10% [Di(10)], 50% [Di(50)], and 90% [Di(90)] of all the particles. All of the data are expressed as means of at least three determinations carried out for each preparation lot (three lots for each sample).

4.3.4. Atomic Force Microscopy (AFM)

The morphology of CPS-SLNs was observed by AFM (Atomic Force Microscope, Park Instruments, Sunnyvale, CA, USA) at room temperature (20–25°C) operating in air and in non-contact mode.

Triangular silicon tips were used for this analysis. The resonant frequencies of this cantilever were found to be about 190 kHz. A drop of each sample was diluted with water (about 1:100 v/v) before being applied on a small mica disk (1 cm x 1 cm); after 2 min, the excess of water was removed using paper filter. "Height image" or "topographical image" was obtained from the record of changes in Z-axis of the piezo necessary to maintain the fixed oscillation amplitude and described the morphology and the macroscopical features of the sample. The "height profile" particles, which were obtained by elaborating the "height images" and reported in x/y graphics, contributed nicely to describing the samples. The images were flattened using second-order fitting to remove sample tilt. The mean size of SLNs was carried out by processing the AFM images with the ProScan Data Acquisition software that was developed under Windows. The sizes of the nanoparticles were determined disassembling the images in arbitrary lines that cross the small vesicles. In order to obtain the dimension of each nanoparticle, two sliders were positionated. All of the data averaged measurements for each experiments.

4.3.5. Differential Scanning Calorimetry (DSC) Analysis

Calorimetric curves of samples (raw materials, blank and CPS-loaded SLNs) were carried out through Mettler DSC 12E that was equipped with a Haake thermocryostate model D8-G; each measurement was performed three times. The correlated software permitted data acquisition. The analyses were performed at a speed of 5° C/min. which ranged from 25° C to 100° C after calibration of the equipment.

4.3.6. In Vitro CPS Release Study

In order to study the release profile of CPS, free and loaded into SLNs, Franz diffusion cells (LGA, Berkeley, CA) were used. They have an exposed surface area of 0.75 cm^2 and a receiver compartment

volume of 4.5 mL. The receptor compartment was filled with a water–ethanol solution (50:50) to create the sink condition, since CPS is poorly soluble in buffer. The solution was thermostated at 32 ± 1° C, under magnetic stirring (500 rpm) during all of the experiments [*M. Siewert et al., 2003*]. The testing samples (350 µL) were placed in the donor cell maintaining a complete and intimate contact with the surface of a cellulose acetate membrane (0.2 µm pore size, 25 mm diameter, Sartorius; Göttingen, Germany). Each experiment was run in duplicate for 24 hs. At predetermined intervals, samples (200 µL) of receiving solution were withdrawn and replaced with the same volume of fresh solution. The amount of CPS permeated was quantified by High Performance Lipid Chromatography (HPLC), as described below.

4.3.7. In vivo study on CPS-SLNs

Male CD1 mice aged between eight and nine weeks were used in the present study. Experimental animal procedures were carried out according to all of the procedures (IACUC, ex art. 9 DL116-92, 9 September 2005). The animals were maintained on a 12-h light/dark cycle and allowed free access to food and water. For behavioral experiments, mice were acclimated to the experimental room one hour before testing. A researcher that was blind to the pharmacological treatment performed all of the experimental procedures and tests.

For the evaluation of spontaneous pain, 10 µL of a plain drug solution (CPS-STD) or an SLN dispersion (CPS-SLN) or the respective vehicles (VEH-STD and VEH-SLN) were administered by subcutaneous injection. CPS-STD was formulated using Tween 80 (10% w/w), ethanol (10% w/w), CPS (0.026% w/w), and distilled water (79.97% w/w). Subcutaneous injection was performed in the right hind paw (intraplantar administration, i.pl.) of the mouse immediately before the behavioral evaluation.

CD1 mice were placed in a transparent cage immediately before the i.pl. injection of the two different drug formulations (CPS-STD and CPS-SLN) or the respective vehicles (VEH-STD and VEH-SLN). The time (seconds) spent in nociceptive behavior (paw liking, lifting, and shaking) was measured for up to five min after the injection by a researcher that was blind to the treatment of the animals.

After seven days from i.pl injection, mice were sacrificed and skin biopsies that formed the site of injection were removed. Skin homogenates were obtained, following a previously described protocol [*L. Jin et al., 1997*]. Protein concentration was measured by using the Bio-Rad Dc Protein Assay kit according to the manufacturer's protocol.

In order to study the TRPV1 expression, 10 µg of total protein extracted form skin biopsies were separated by SDS-PAGE (Sodium Dodecyl Sulphate–polyacrylamide gel electrophoresis) and transferred onto nitrocellulose membranes for antibody detection (Criterion blotter; Bio-Rad Laboratories, Hercules, CA, USA). The nitrocellulose membranes were blocked at room temperature in Odyssey blocker (LI-COR Biosciences, Lincoln, NE) for 1 h, and then incubated with the following primary antibodies: anti-TRPV1 polyclonal antibody (1:1000, Santa Cruz); anti-actin monoclonal antibody (1:1000, Sigma) over night at 4°C. Secondary antibodies were: goat anti-rabbit (IRD800CW) and goat anti-mouse (Alexa 680, LI-COR, Bioscience) antibodies, being concomitantly incubated for 1 h at room temperature. The proteins were detected and quantified with the Odyssey Infrared Fluorescence Imaging System (LI-COR). The values were expressed as integrated intensity.

CPS determination was analyzed by HPLC method [*C.B. Davis et al., 2007*] slightly modified. The HPLC apparatus consisted of a Shimadzu LC10 AT Vp (Milan, Italy) that was equipped with a 20 µL loop injector and a SPD-M 10 A Vp Shimadzu photodiode array UV detector. In particular, the chromatography was performed using a Symmetry ShieldWaters C18 RP column (particle size, 5 µm; 25 cm x 4.6 mm i.d.; Waters S.P.A, Italy). The analysis was carried out using 1% acetic acid:acetonitrile (20:80) as a mobile phase at 1 mL/min. The detection was effected at 284 nm, while the CPS retention time was 8.4 min.

Statistical analysis of *in vivo* data was performed while using the one-way ANOVA, followed by two different post hoc tests: the Bonferroni's Multiple Comparison test for the determination of the spontaneous pain due to CPS i.pl. injection and the Fisher's test to determine the TRPV1 skin expression.

4.4. Active natural products for the treatment of retinal diseases

4.4.1. NLCs preparation

The formulation of the PEA-NLCs and MGN-NLCs was preceded by a preformulation study which was necessary to optimize the technological parameters of the NLC. PEA-NLCs were prepared by *high shear homogenization* coupled to *ultrasound* (HSH-US) method as described [*F. Brugè et al., 2013*] with some modifications. Briefly, 0.2 g of PEA were dissolved in an oil phase containing Miglyol (0.4 g) and Compritol 888 ATO (0.6 g) and the mixture was stirred at 80°C to obtain a dispersion. The aqueous phase consisted of Lutrol F68 (0.1 g) and distilled water (25 mL). The melted lipid phase was dispersed in the hot (80°C) aqueous phase by using a high-speed stirrer (Ultra-Turrax T25, IKA-Werke GmbH &Co. Kg, Staufen, Germany) at 13.500 rpm for 10 min, maintaining the temperature at least 10°C above the lipid melting point. The obtained pre-emulsion was ultrasonified by a Labsonic 2000 (B. Braun, Melsunen, Germany) for 8 min. The hot dispersion was then cooled by dilution in 25 mL of additional water at 4°C. Unloaded NLC were prepared by the same procedure without adding PEA.

MGN-loaded NLCs (MGN 0.1 w/v) were prepared using the same experimental protocol.

4.4.2. NLC Characterization

The average size (Z-Ave) and polidispersity index (PDI) of the nanoparticles were measured by DLS using a Zeta Sizer Nano-ZS90 (Malvern Instrument Ltd., Worcs, England), as previously described. Analyses were performed using a 90° scattering angle at 20 ± 0.2°C. Samples were prepared diluting 100 μL of NLC suspension with 900 μL of distilled water. The Zeta Potential (ZP, ξ) was measured by the same instrument. All the measurements were performed in triplicate and recorded at 25 °C. Additionally, the morphology of NLCs was investigated using Electron Microscopy (JEOL JEM-101).

4.4.3. Studies on PEA-NLCs

4.4.3.1. Determination of PEA Loading

The percentage of PEA entrapped in the lipid matrix was determined as follows: NLC dispersion was filtered by using a Pellicon XL tangential ultrafiltration system (Millipore, Milan, Italy) equipped with a polyethersulfone Biomax 10 membrane. An amount of retained material was freeze-dried, dissolved in chloroform, and analyzed by the UHPLC method described below. PEA incorporation efficiency was expressed both as encapsulation effisciency (E.E.%) and drug loading (D.L.%), calculated from equations reported below (Equations 7-8):

E.E. (%) = (Mass of PEA in nanoparticles)/(Mass of PEA fed to the system)

D.L. (%) = (Mass of PEA in nanoparticles)/(Mass of nanoparticles)

4.4.3.2.Differential scanning calorimetry (DSC)

To evaluate the fusion behavior of the lipid matrix both as a raw material and as an NLC, studies have been carried out by differential scanning calorimetry (DSC). DSC analysis was carried out using a METTLER TA89E.

Each lyophilized sample (10 mg) was loaded into a 150 μL aluminum crucible, hermetically sealed and submitted to DSC analysis, under an atmosphere of dry nitrogen. A heating scan rate of 5° C/min and a cooling scan rate of 10° C/min were used during the experiments. DSC analysis was carried out using a heating scan rate which ranged from 20° C to 150° C and a cooling scan rate which ranged from 150° C to 20° C, respectively. All calorimetric analyses were replicated at least three times to check the reproducibility and reversibility of the thermal events.

Calorimetric measurements were performed for the following samples: blank NLC, PEA-NLC, NLC with PEA out; and for the following raw materials: Lutrol F 68, Compritol 888 ATO, N-palmitoylethanolamide (PEA).

4.4.3.3.Stability Studies on PEA-NLCs

NLC's stability was evaluated by Turbiscan Ageing Station (TAGS) (Formulaction, l'Union, France), as previously described. 20 mL of each NLC were placed in a cylindrical glass cell and positioned in the Turbiscan at 25 or 35.5 ± 2°C for 14 days.

4.4.3.4. In vivo studies on PEA-NLCs

- Animals

Male Sprague-Dawley rats (175–200 g) were treated according to the ARVO (Association for Research in Vision and Ophthalmology).

Streptozocin (STZ) is used to induce experimental diabetes in rodents. After 12 hs of fasting, the animals received a single 60-mg/kg intravenous (i.v.) injection of STZ in 10 mM sodium citrate buffer, pH 4.5 (1 ml/ kg dose volume). Control (sham, non-diabetic) animals were fasted and received citrate buffer alone. After 24 hs, animals with blood glucose levels >250 mg/dl were considered diabetic, and randomly divided in groups of ten animals each. A single topically administration of PEA-NLC formulation (10 µl/eye; TID for 10 days) was carried out in the conjunctival sac. All the experiments were performed 10 days following the induction of diabetes.

- Measurements of TNF-alpha

Rat eyes were collected 10 days after STZ administration, and each retina was homogenized in 100 mL of solution consisting of 20 mM imidazole hydrochloride, 100 mM KCl, 1 mM MgCl, 1 mM ethyleneglycol-bis (b-aminoethyl ether) - N,N,N',N'-tetraacetic acid (EGTA), 1% Triton, 10 mM NaF, 1 mM sodium molybdinate, and 1 mM EDTA [*C.B.M. Platania et al., 2018*]. The solution was supplemented with a cocktail of protease inhibitors before use. Samples were cleared via centrifugation for 10 min at 10.000 x g and assessed for protein concentration with the bicinchoninic acid (BCA) assay. The TNF-α levels were estimated with the ELISA (R&D Systems, Minneapolis, MN). All measurements were performed in duplicate. The tissue sample concentration was calculated from a standard curve and corrected for protein concentration.

- Pharmacokinetics studies

Rats were treated with a single ocular topical administration (10 µl) of PEA-NLC formulation. The animals were sacrificed at 30, 60, 90 and 240 min after ocular topical administration of PEA- NLC formulation, and the eyes were enucleated and retina was collected. Tissue samples were stored at -80°C till quantitative analysis of PEA. The following pharmacokinetics parameters were determined:

peak eye tissue concentration (C_{max}), time of peak of eye tissue concentration (T_{max}), area under the curve (AUC) of eye tissue concentration of PEA [PEA] vs. time curve from 0 to 240'(AUC_{0-240}). PEA concentration values in tissues of treated animals have been normalized to PEA content in the tissues of control animals.

- Analytical methods

Frozen tissues were first lyophilized (LyoQuest-55, Telstar Technologies, Spain) for 24 hs. One mg of the lyophilized were extracted with 300 µL of ice cold acetonitrile containing 20 ng/mL of deuterated PEA (d-PEA). Samples were vortexed for 20 s and then centrifuged for 5 min at 16.000 rpm. The supernatant was filtered on a PTFE membrane (0.22 µm) and injected in the UHPLC system. UHPLC-MS/MS analysis was carried out with a Shimadzu Nexera (Shimadzu, Milan, Italy) consisting of two LC 30 AD pumps, a SIL 30AC autosampler, a CTO 20AC column oven, a CBM 20A controller, and the system was coupled online to a triple quadrupole LCMS 8050 (Shimadzu, Kyoto, Japan) by an ESI source. The separation was performed on an Ascentis Express HILIC column (Supelco, Bellefonte PA, USA) using as mobile phases: A) water containing 50 mM ammonium formate and B) acetonitrile (ACN), with a gradient starting from 99% B, 0.01 2.50 min, 85% B, 2.51-3.00 min 85-40% B, then isocratic for 1.00 min and returning to 99% B in 6 min. The flow rate was set at 0.5 mL/min. Column oven was set at 35 °C, 2 µL of extract were injected. The ESI was operated in positive ionization. Interface temperature, desolvation line temperature, heat block temperature were set, respectively at 300, 250 and 400 °C. Nebulizing gas, drying (N_2) and heating gas (air) were set, respectively, at 3, 10 and 10 L/min. PEA stock solution (1 mg/mL) was prepared in ACN and the calibration curve was obtained in a concentration range of 0.5-50 ng/mL (r^2=0.999) and Deuterated-PEA was selected as internal standard in the concentration of 20 ng/mL. Repeatability was established using repeated sample injections using different concentration gradients, but at the same

chromatographic conditions. Moreover, to eliminate any possible variable, the analyzes were checked by the same operator and on the same day.

- Draize test

In order to evaluate the tolerability and ocular toxicity of PEA-NLC, Draize Test was carried out. The Draize test was conducted by performing a topical administration on the eyes of each animal, every 30 min for 6 hs (13 treatments). Readings were performed 10 min after sample application, then after 6 hs. Methylene blue was used to evaluate the integrity of the cornea using a slit lamp. The method provided an overall scoring system for grading the severity of ocular lesions involving the cornea (opacity), iris (inflammation degree) and conjunctiva (congestion, swelling and discharge). The Draize score was determined by visual assessment of changes in these ocular structures.

4.4.4. Studies on MGN-NLCs

4.4.4.1. Antioxidant activity of MGN: ORAC assay

The antioxidant activity of MGN-NLC, MGN solution and blank NLC was measured as previously described [*C. Lucas-Abellan et al., 2011*] slightly modified. Data were obtained using an OPTIMA FLUOstar microplates reader (BMG Labtech, USA) with a fluorescence filter (excitation 485 nm, emission 520 nm). Fluorescein solution (3 μM) was prepared in 75 mM phosphate buffer (pH 7.4). The assay was carried out at 37°C, using Trolox (0.1 mM) as the control standard and phosphate buffer (pH 7.4) with fluorescein as the blank. A 96-well flat-bottomed black plate was used; the outer rows were filled with 200 μL of distilled water to avoid the evaporation due the temperature effect. Samples (MGN-NLC, MGN solution and unloaded NLC) were diluted in phosphate buffer (1:1, 1:3,

1:10, 1:20, 1:50, 1:75, 1:100 and 1:150) and then they were deposited (70 µL) in triplicate in the well of the microplate with fluorescein solution (100 µL). Moreover, eight calibration solutions using Trolox (3, 5 10, 15, 20, 30, 50 and 100 µM, in phosphate buffer) were added in triplicate (70 µL). After thermostating for 15 min at 37°C, 30 µL of AAPH solution was added and fluorescence measurement was begun. The fluorescence was recorded every 2 min for 180 min.

4.4.4.2. Ocular Tolerability: HET-CAM assay

The potential ocular irritancy and/or damaging effects of blank and MGN-loaded NLC were evaluated using the Hen's Egg Test on Chorio-Allantoic Membrane (HET-CAM) assay. It is a validated alternative to animal testing of ocular irritancy [*F. Alvarez-Rivera et al., 2019*]. The HET-CAM test was carried out using fertilized hen's eggs (50–60 g; Coren, Spain) incubated at 37 °C and a relative humidity of 60% during 9 days. The eggs were positioned in a horizontal position and rotated three times a day. On the ninth day, the eggshell was pierced at the air chamber side using a rotator saw (Dremel 300, Breda, The Netherlands) and the inner membrane was wet with 0.9% NaCl for 30 min (37°C). Afterwards, the inner egg membrane was carefully removed to avoid any damage to the fine blood vessels of the chorioallantoic membrane.

Blank and MGN-loaded NLC (100 µL) (in duplicate) were dropped on the CAM. 0.9% NaCl and 0.1 N NaOH solutions (300 µL) were used in duplicate as negative and positive controls, respectively. The vessels of CAM were observed during 5 min, under white light, for haemorrhage, vascular lysis or coagulation. The irritation score (IS) was calculated as reported below (Equation 9):

$$IS = \left(\frac{301 - \text{hemorrhage time}}{300} \times 5\right) + \left(\frac{301 - \text{lysis time}}{300} \times 7\right) + \left(\frac{301 - \text{coagulation time}}{300} \times 9\right)$$

The damage was classified by means of *IS* as non-irritant (*IS* < 1), mild irritant (1 ≤ *IS* < 5), moderately irritant (5 ≤ *IS* < 10), or severe irritant (*IS* > 10).

4.4.4.3. Hemocompatibility assay

In vitro hemolysis assays were performed for blank and MGN-NLC as previously described [*C. Chen et al., 2008*]. Hemocompatibility assay [*P.C. Caracciolo et al., 2017; M. Weber et al., 2018*] was performed using freshly drawn human whole blood (Galician Blood Transfusion Center, Santiago de Compostela, Spain). Briefly, blood samples (5 mL) were diluted with 0.9% NaCl (145 mL). Samples (100 µL; dilution 1:5) were added in diluted blood (1 mL), while positive and negative controls were incubated with Triton X-100 (4%) and phosphate buffer (PBS), respectively. After incubation (37°C) at 100 rpm for 1 h, the samples were centrifuged (Sigma 2-16P; Sigma Laboratory Centrifuges, Germany) at 10000 rpm for 30 min and released hemoglobin was monitored by measuring the absorbance of the supernatant (150 µL) at 540 nm using a microplates reader (FLUOstar Optima, BMG Labtech, USA). The percentage of hemolysis was calculated as follows (Equation 10):

$$\% \text{ Hemolysis} = \frac{(A_S - A_N)}{(A_P - A_N)} \times 100$$

Where A_S is the absorbance of sample, A_N is the absorbance of negative control and A_P is the absorbance of positive control.

4.4.4.4. Corneal permeability assay

Mangiferin corneal permeability assay was carried out, in triplicate, following a widely used protocol [*A. Varela-Garcia et al., 2020*]. Fresh bovine eyes (Compostelana de Carnes S. L:, Santiago de Compostela, Spain) were transported immersed in PBS without antibiotics, in an ice bath to the laboratory. Then, corneas were isolated leaving 2-3 mm of surrounding sclera with the help of scalpel

and tongs, washed with PBS and mounted on vertical diffusion Franz cells. Donor and receptor (6 mL) chambers were filled with a propylene glycol:water (40:60) solution and placed in a bath at 37 °C, under magnetic stirring, in order to equilibrate the ocular tissues. After 1h, the donor chambers were completely emptied and filled with 2 mL of MGN-NLC formulation. The area available for permeation was 0.785 cm^2. The chambers were covered with parafilm to prevent evaporation and all the system was protected from light to avoid mangiferin degradation. One mL of sample was taken from the receptor chamber every 30 min for 6 hs and replaced with the same volume of propylene glycol:water (40:60), taking care of removing any bubble from the diffusion cells.

The amount of MGN permeated was quantified using a JASCO (Tokyo, Japan) HPLC (AS-4140 Autosampler, PU-4180 Pump, LC-NetII/ADC Interface Box, CO-4060 Column Oven, MD-4010 Photodiode Array Detector), fitted with a C18 column (Waters Symmetry C18, 5 µm, 4.6 × 250 mm) and operated with ChromNAV software (ver. 2, JASCO, Tokyo, Japan). The analysis was carried out by isocatric elution using 0.1% formic acid:acetonitrile (87:13) as a mobile phase at 1.5 ml/min and 26°C. The injection volume was 100 µL and the UV detector was set at 254 nm (retention time 12 min) [*P. Naveen et al., 2017*]. The standard solutions were 0.075-1 µg/mL of mangiferin in ethanol:propylenglycol:water (10:40:50). MNG content in the samples was calculated from a validated calibration curve.

After 6 hs of test, aliquots of the donor chambers were collected to quantify the amount of residual MNG and the corneas, after being visually inspected to verify that none of them had cracks or modified their appearance, were placed in Falcon tubes with 2 mL acetonitrile for 24 hs at 37 °C to extract the amount of MGN. Then, they were sonicated during 99 min at 37 °C, centrifuged (1000 rpm, 5 min, 25 °C), and the supernant was filtered (Scharlau® Syringe Filter, 0.22 µm 13 mm PTFE hydrophilic), centrifuged again (14,000 rpm, 20 min, 25 °C), and filtered again to be measured in HPLC as reported above.

The steady state flux (J) and the lag time (t_{lag}) were obtained from the slope and the x-intercept respectively, of the linear regression obtained after the representation of the cumulative amounts of MGN permeated per area versus time [*A. Varela-Garcia et al., 2018*].

Chapter 5

5.1. Active natural products for the treatment of CNS disorders

5.1.1. Screening of lipid matrix

The choice of the most suitable lipid matrix to formulate stealth systems loaded with CUR and AST was carried out by MTT assay. As previously mentioned, this test was able to determine the potential cytotoxic effects of the excipients on neuronal cell line (DPSC). The research was conducted on a neuronal cell line in order to evaluate the effect of CUR and AST in the treatment of important CNS pathologies involving a deficit of antioxidant defense (i.e. Alzheimer's disease). This lipid screening was done by preparing the blank SLNs using different lipid matrices such as stearic acid, cetyl palmitate, Compritol 888 ATO and Precirol 5 ATO. Subsequently, the effect of these formulations were investigated on cell viability of neuronal cell line DPSC, because these stem cells possess protective effects against models of neurodegenerative diseases including Alzheimer's disease [*S. Grontos et al., 2000; G. Bonaventura et al., 2019; T. Ueda et al., 2020*].

The stealth system (s-SLNs) loaded with CUR were formulated using two different strategies using polyethylene glycol (pSLNs) and polysorbate 80 (p80SLNs).

Curcumin-loaded SLNs using the PEGylation strategy were formulated using Compritol® 888 ATO (glycerol behenate) as lipid phase and Lutrol F68® (Poloxamer 188) as surfactant.

As reported in figure 21, no significant changes in the percentage of cell viability in the cell cultures exposed to stearic acid and Compritol 888 ATO were observed with respect to the control (untreated cells), while Precirol 5 ATO induced a cytotoxic effect in DPSC cell cultures. Although Compritol 888 ATO and stearic acid showed a similar effect, CUR-pSLNs were formulated using Compritol 888 ATO as lipid matrix due to the interesting results of DLS characterization of blank SLNs.
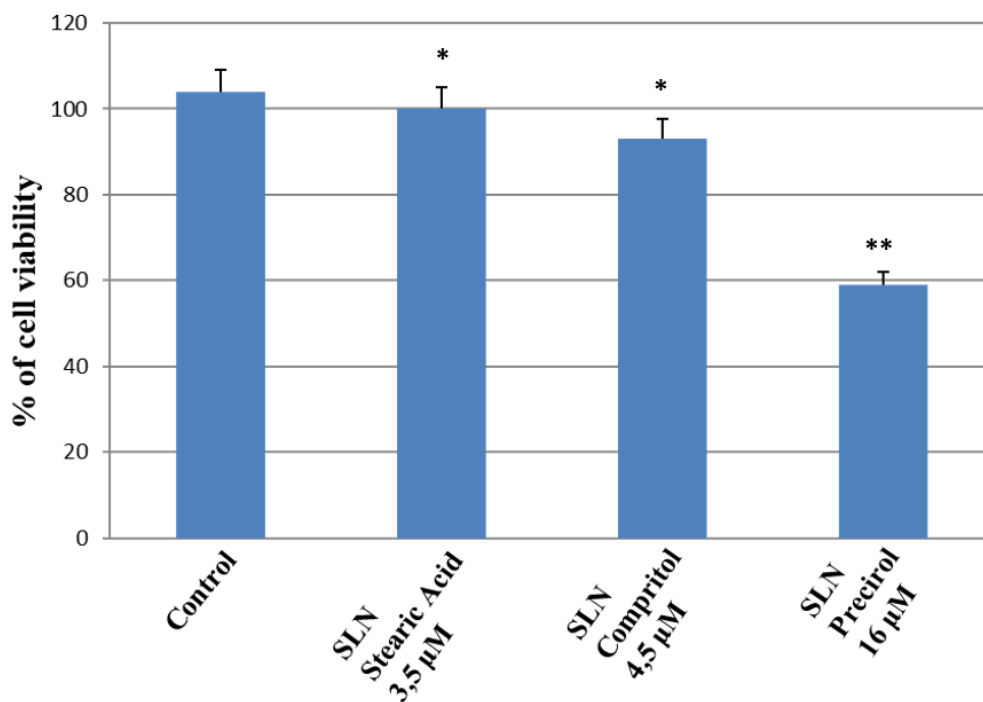
Figure 21. Percentage of viability of primary human DPSC cell cultures exposed to stearic acid (3,5 μM), Compritol (4,5 μM) 888 ATO and Precirol (16 μM) 5 ATO for 24 h. Results are expressed as the mean ± S.D. of the values of five separated experiments performed in triplicate. **indicate p< 0.05 significant differences vs control, and * represents p>0.05 vs control (untreated cells).

As regard the modification strategy with polysorbate 80, CUR-p80SLNs were prepared using different lipid matrices (Compritol 888 ATO, stearic acid, cetyl palmitate). No lipid matrix was able to obtain interesting results of DLS characterization (data not shown). Therefore, the latter strategy was discarded by the study and the PEGylation was chosen as best modification to obtain a valid stealth system.

Stealth systems loaded with AST were formulated using stearic acid as lipid matrix. As previously mentioned in the *in vitro* assay performed on the neuronal cell line (DPSC), this lipid was selected as no significant change in the percentage of cell viability was observed with respect to the untreated cells. Furthermore, this lipid matrix is the most suitable for the encapsulation of AST [*P.C. Bhatt et al., 2015*].

5.1.2. PEGylated SLNs characterization

CUR-pSLNs were formulated following a valid and highly reproducible method, using Compritol®
888 ATO (glycerol behenate) as lipid phase and Lutrol F68® (Poloxamer 188) as surfactant. As
reported in Table 1, DLS data showed good technological parameters with a mean diameter ranging
from 130 to 180 nm, polydispersity index (PDI) values around 0.24-0.26 and zeta potential (ZP)
values were in the range of -31 to -24 mV, predicting a good long-term stability. The slight difference
in terms of mean particle size (10-20 nm) between SLNs and pSLNs was probably due to the PEG
chains which fitted into the surface of the nanoparticle giving it an umbrella structure [*Z. Dong et al.,
2017*].

Moreover, the encapsulation efficiencies of CUR-SLNs and CUR-pSLNs were determined throught
tangential ultrafiltration system and they were approximately of 82%.

Formulation	Z-Ave [nm ± SD]	PDI [-] ± SD	ZP [mV ± SD]
Blank SLN	161.8 ± 0.1	0.24 ± 0.1	-31.4 ± 0.3
Blank pSLN	176.0 ± 0.2	0.26 ± 0.1	-29.0 ± 0.1
CUR-SLN	132.0 ± 0.1	0.25 ± 0.0	-24.3 ± 0.2
CUR-pSLN	153.3 ± 0.2	0.26 ± 0.2	-23.9 ± 0.1

Table 1. The values of Z-Ave, PDI and Z-potential for blank SLNs, blank pSLNs, CUR-SLNs and CUR-pSLNs recorded at 25°C.

AST-pSLNs were formulated by *solvent-diffusion* technique using stearic acid as lipid phase and
Lutrol F68® (Poloxamer 188) as surfactant. As reported in Table 2, nanoparticles showed a mean
diameter around 110-170 nm and a good homogeneity, while Z potenzial values pointed out a good
stability of the nanodispersions.

Therefore, both formulations showed good technological parameters suitable for parenteral
administration.

Formulation	Z-Ave [nm ± SD]	PDI [-] ± SD	ZP [mV ± SD]
Blank SLN	136.0 ± 0.2	0.27 ± 0.1	-20.4 ± 0.2
AST-SLN	111.1 ± 0.2	0.33 ± 0.2	-16.2 ± 0.2
Blank pSLN	168.7 ± 0.2	0.23 ± 0.3	-21.7 ± 0.1
AST-pSLN	123.5 ± 0.2	0.24 ± 0.2	-18.3 ± 0.1

Table 2. Mean particle size (Z-Ave), polydispersity index (PDI) and zeta potential (ZP) of SLN and pSLN unloaded and loaded with AST.

The morphology of formulations was determined using TEM (Figure 22). TEM images showed that the lipid nanoparticles had a spherical appearance having a particle size below 200 nm. This particle size was in agreement with DLS data.
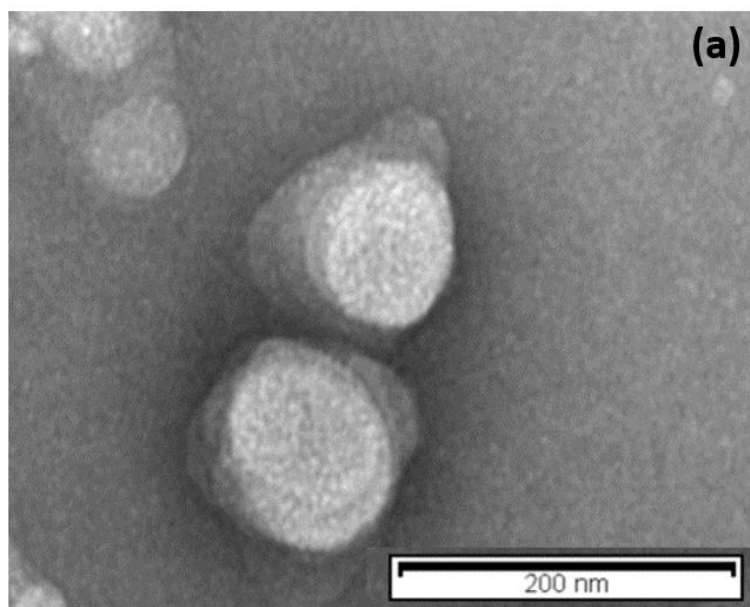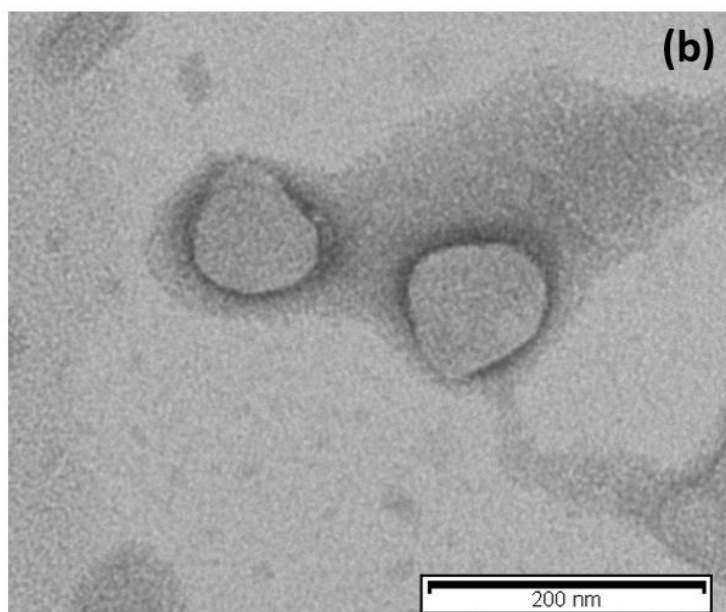
Figure 22. Transmission electron microscopy images of (a)CUR-pSLNs and (b) AST-pSLNs. The scale bar

represents 200 nm.

5.1.3. In vitro release of CUR and AST

The *in vitro* release profile of CUR and AST from lipid nanoparticles, as shown in figure 23, follows a "two-step drug release" related to distribution of active compound in SLN matrix. In the first phase, the spreaded drug on the nanoparticle surface is released immediately, while in the second phase the drug is released slowly; this could be due to the slow release of the drug from the lipid core. Therefore, the encapsulation of drug into SLN could be an effective way to supply drug continuously in the body.

In this last phase, approximately 70% of encapsulated drug is released and both formulations showed a similar behavior.
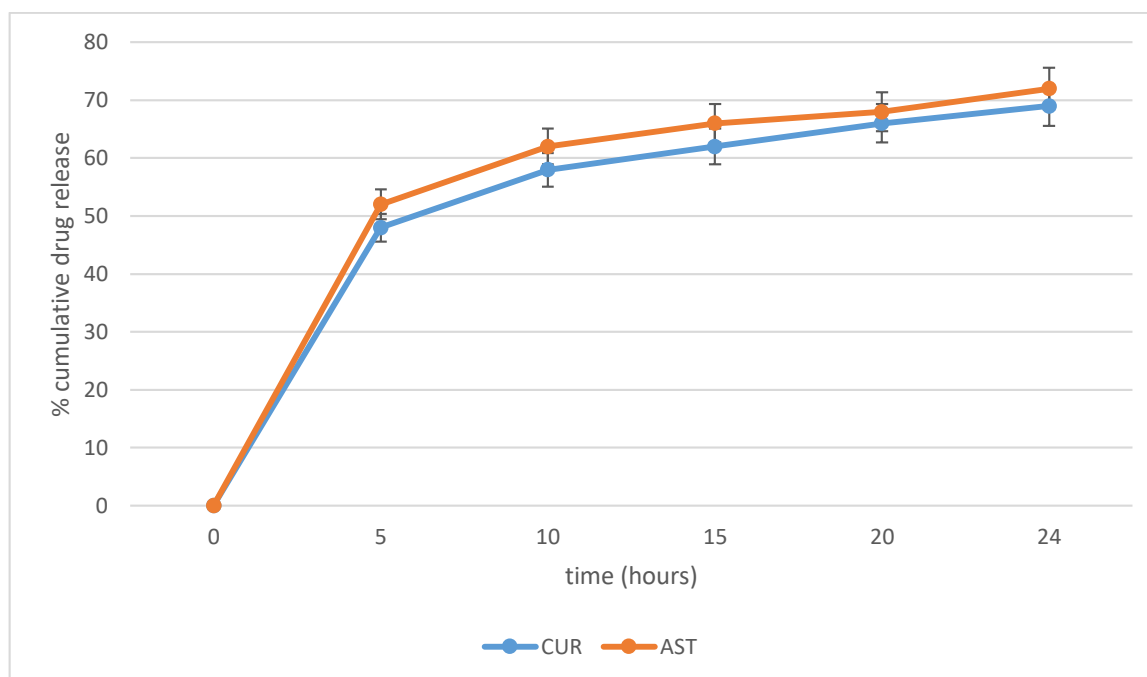
Figure 23. In vitro release profile of CUR and AST from SLN. Each point represents the mean value ± S.D. (n=3).

5.1.4. Stability studies on PEGylated nanoparticles

5.1.4.1. Long-term stability

Stability of PEGylated nanoparticles was monitored for six months during storage at room temperature. The data showed that nanoparticle size of CUR-pSLNs did not undergone any significant variation (Figure 24). A similar trend has been observed of PDI and ZP values, thus dimostrating a good long-term stability after six months of storage. On the contrary, AST-pSLNs showed instability phenomena after two months due to the aggregation of the nanoparticles (Figure 25). In both cases, PEGylated systems loaded with CUR and AST have greater stability than blank nanoparticles due to the preservative action of natural compounds.
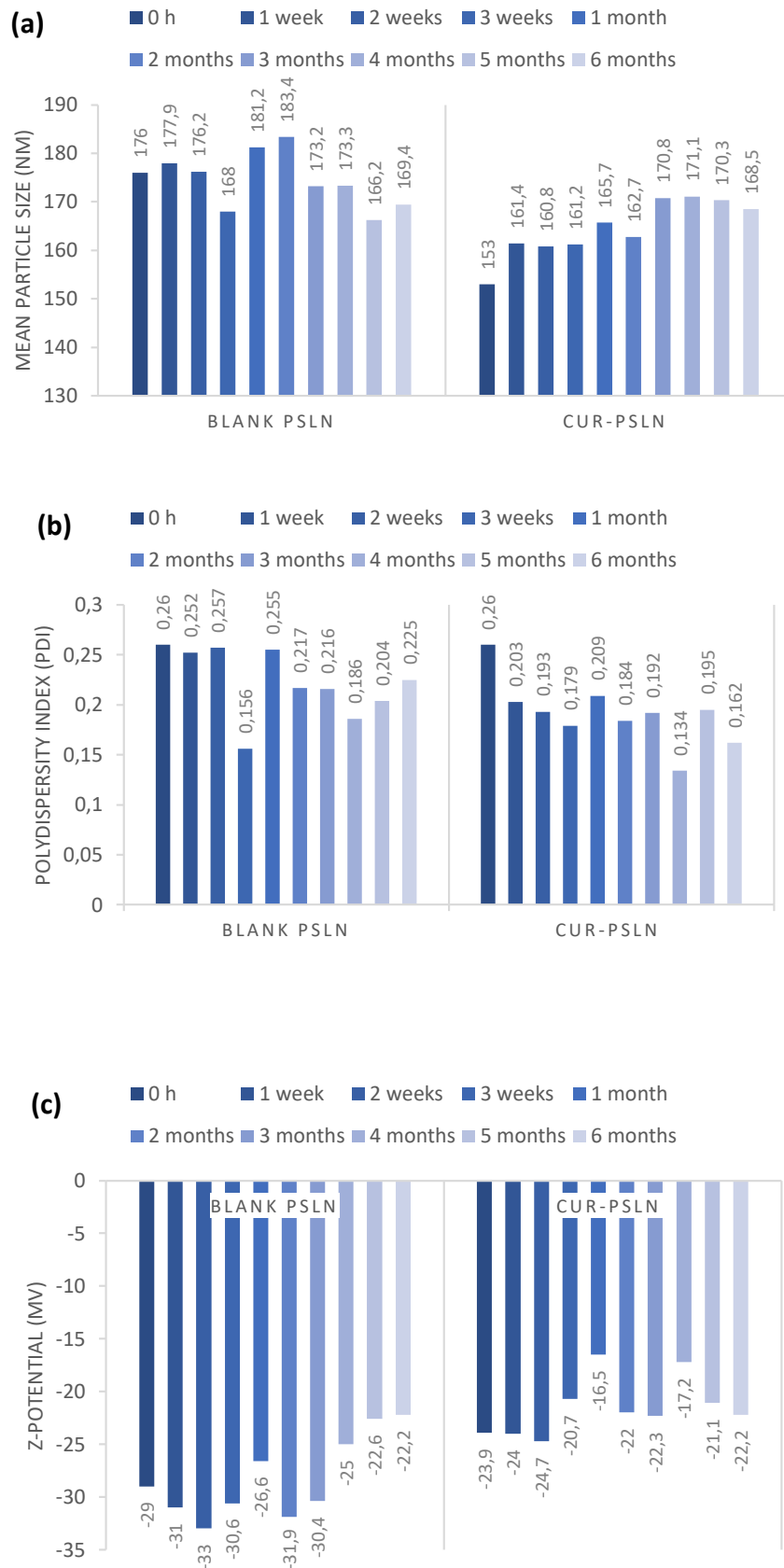
Figure 24. (a) Particle size, (b) polydispersity index (PDI) and (c) Z-potential of blank pSLNs and CUR-pSLNs during storage at room temperature for six months.
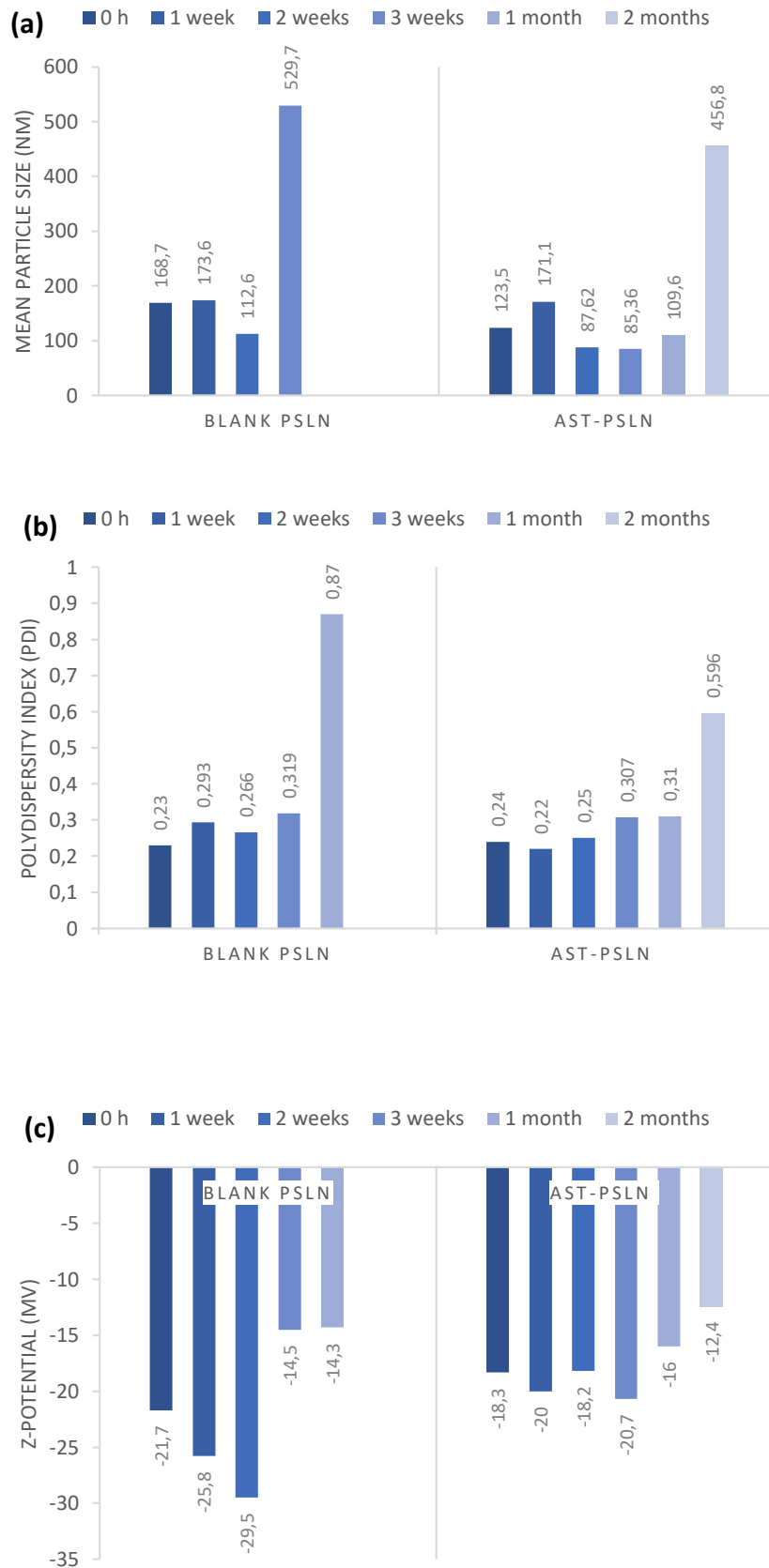
Figure 25. (a) Particle size, (b) polydispersity index (PDI) and (c) Z-potential of blank pSLNs and AST-pSLNs during storage at room temperature for two months.

5.1.4.2. Turbiscan Techonology

The physical stability of the nanoparticles was further investigated by Turbiscan Technology. All the formulations were stored at 25°C for 30 days in Turbiscan® station, to evaluate the occurrence of physical instability phenomena. Important variation in ΔT signal at the bottom or the top of the spectra indicates particles migration phenomena (clarification, sedimentation or creaming), while variations in the middle are related to particle size changes. The transmission profile of blank and CUR-pSLNs are reported in figure 26. The linearity of the transmission profiles (ΔT < 10%) clearly demonstrates the great physical stability during storage, without the occurrence of particles aggregation or migration at the top or at the bottom of the cuvette. The great physical stability could be related to the zeta potential values of the samples (around -30 mV). Destabilization kinetics reported as TSI unit (Figure 27), clearly showed that both samples were highly stable, since they did not show significant modification of the TSI value until 30 days of storage. Moreover, the loading of CUR slightly increases the physical stability of the colloidal dispersion.
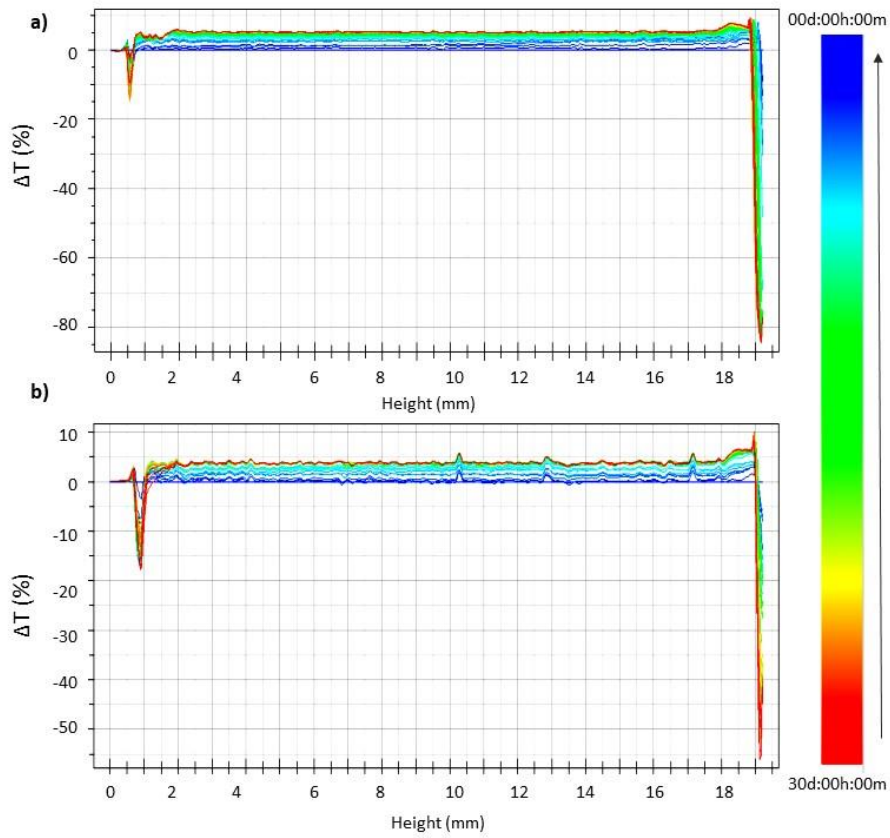
Figure 26. Turbiscan® ΔT profiles of blank (a) and CUR (b) pSLNs stored for 30 days at 25°C.
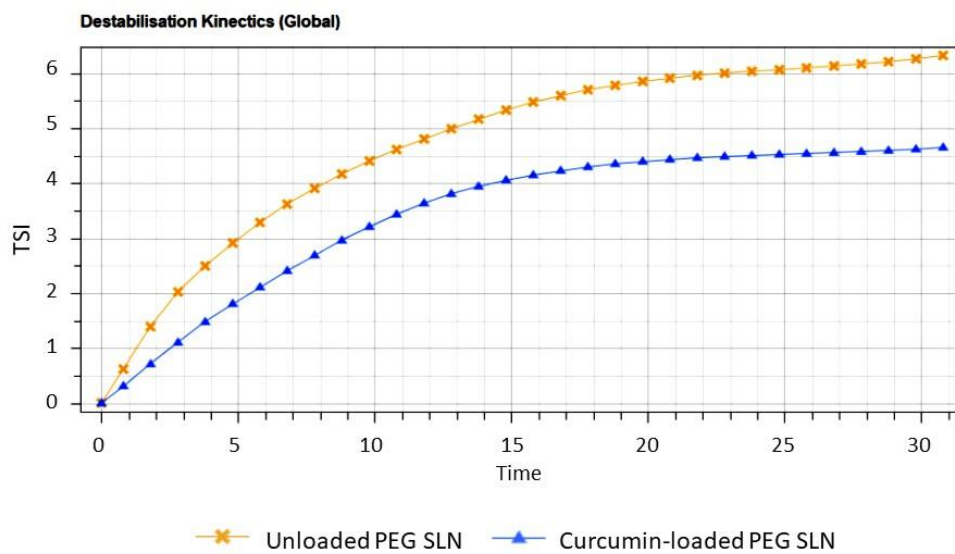

Figure 27. Destabilization kinetics in terms of Evolution of Turbiscan® Stability Index (TSI) of blank and CUR-pSLNs stored for 30 days in TAGS at 25 °C.

The transmission profiles of unloaded and AST-pSLNs clearly highlight the occurrence of significant (T>20%) instability phenomena related to both aggregation and migration of the particles to the bottom and top of the cuvette (Figure 28).
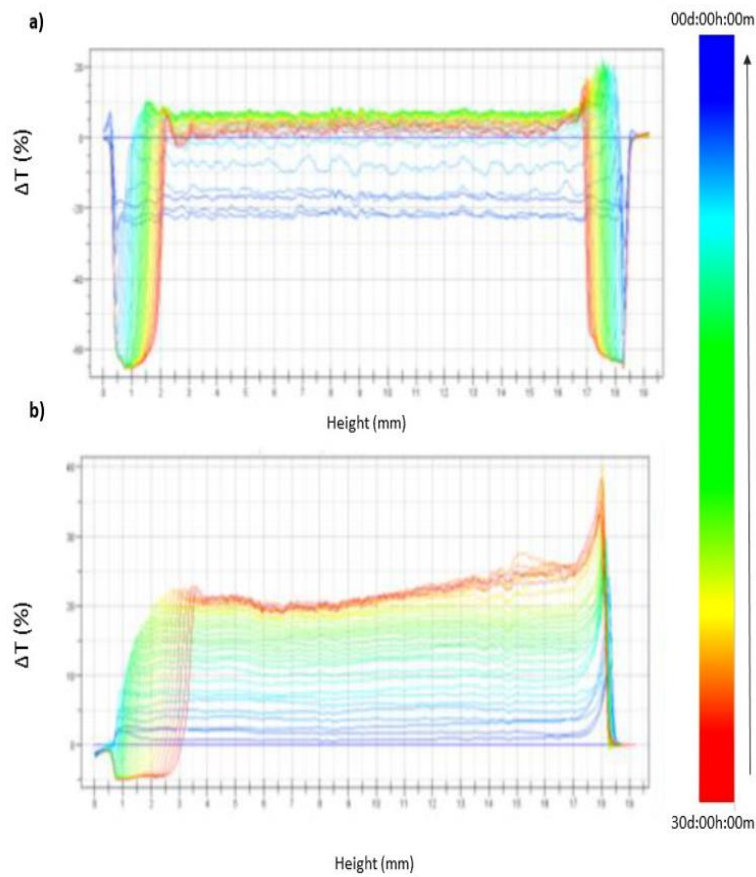

Figure 28. Turbiscan ΔT profiles of (a) blank and (b) AST-loaded p-SLN of samples stored for 30 days at 25°C.

Moreover, destabilization kinetics reported as TSI unit (Figure 29), clearly showed that blank and AST-pSLN were unstable as shown by the changes in the TSI value.
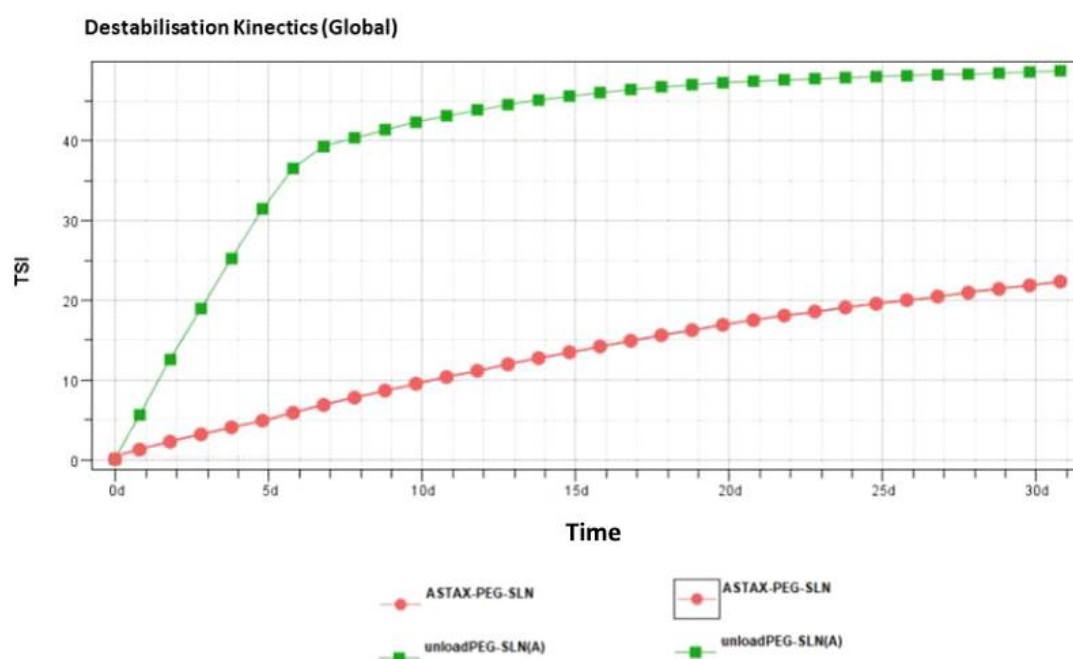
Figure 29. Destabilization kinetics in terms of Evolution of Turbiscan Stability Index (TSI) of unloaded and AST-pSLNs stored for 30 days in TAGS at 25 °C.

5.1.4.3. Freeze-drying study

Since SLNs are suspensions in aqueous medium, their storage for long periods is compromised due to their physical (aggregation / fusion of particles) and / or chemical (drug loss, microbiological contamination) stability problems [*C. Freitas et al., 1995; C. Freitas et al., 1999*].

In order to overcome this problem, it is highly desirable to have a freeze-dried SLNs formulation. Therefore, in a pre-formulation study I screened the ideal cryoprotectant between glucose, mannitol and trehalose, following the evidences reported in literature which identified these compounds as the most effective in protecting nanoparticles during the freeze-dring process [*C. Schwarz et al., 1997; W. Mehnert et al., 2001; W. Abdelwahed, 2015*]. The obtained results demonstrated that trehalose and mannitol in different concentrations (1-3% w/w) were not effective as cryoprotectants. In fact, all the samples dispersed after lyophilization, showed a significative increase in both mean particle size, ranging from 5119 nm to 8081 nm, and PDI values that were around 1.000. On the contrary, very

promising results were obtained using glucose as cryoprotectant at the same tested concentrations. As reported in figure 30, data demonstrated that 2% (w/w) of glucose is the best percentage obtain a cryoprotectant effect for blank pSLNs during lyophilization. Similar results were observed for CUR p-SLNs (data not shown).
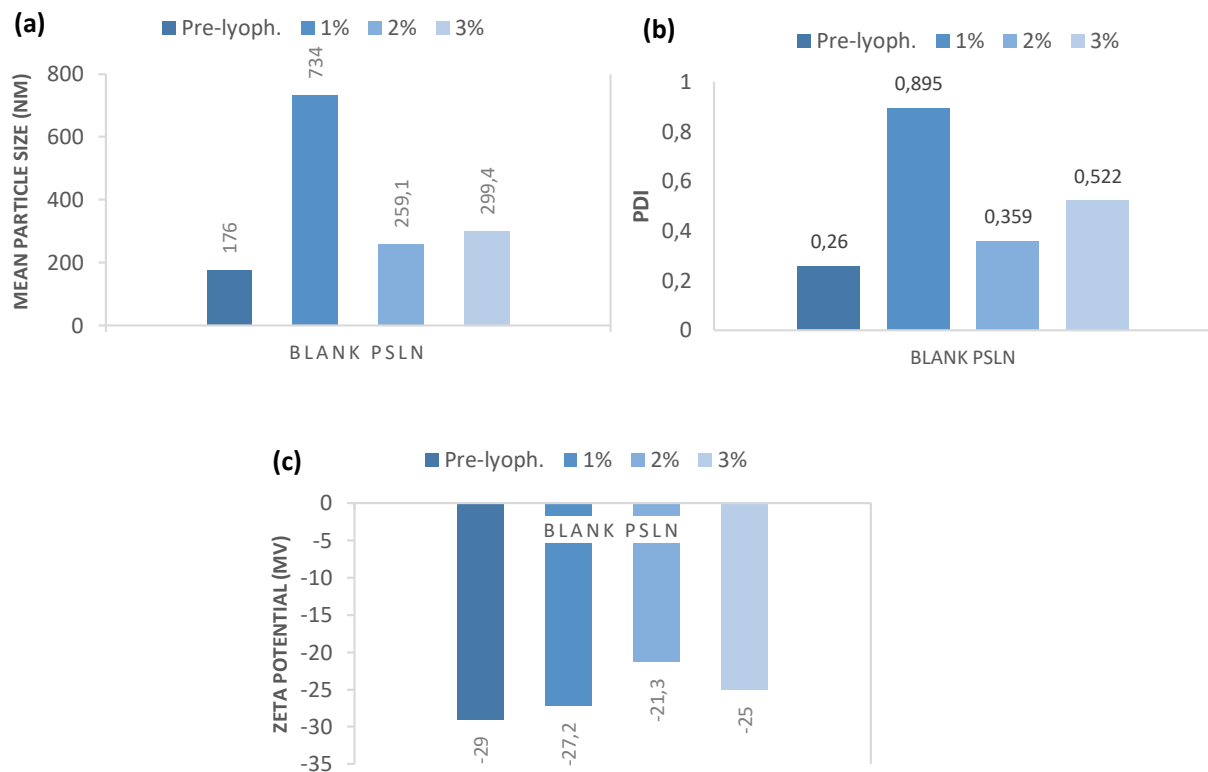

Figure 30. (a)Mean particle size (Z-Ave), (b) polydispersity index (PDI) and (c) zeta potential of blank pSLNs using increasing concentrations of glucose.

Although several cryoprotectants (glucose, trehalose and mannitol) were tested at different concentrations (1-3% w/w), these studies on AST-pSLNs showed unsatisfactory results (data not shown).

5.1.5. Differential scanning calorimetry (DSC) studies on PEGylated nanoparticles

5.1.5.1. DSC Analysis of the interaction between SLN and PEG

DSC studies were conducted in order to evaluate the degree of the PEGylation on the pSLN surface. In order to obtain information among the interaction between PEG (free compound or PEG micelles) and SLNs, kinetic experiments were run at different SLN/PEG molar ratios (1:0.1; 1:0.25; 1:0.5; 1:0.75; 1:1).

Free PEG at different molar ratios was weighted in the bottom of the DSC calorimetric pan, SLNs were added and the samples were submitted to calorimetric analysis. The calorimetric curves (referring to the molar ratio 1: 0.5, the other molar ratios gave similar results) are shown in figure 31. In these conditions PEG did not exert a remarkable effect on SLNs leaving almost unaffected the calorimetric curve; just a broadening of the main peak was visible. This result is a clear evidence that free PEG does not interact with SLNs.
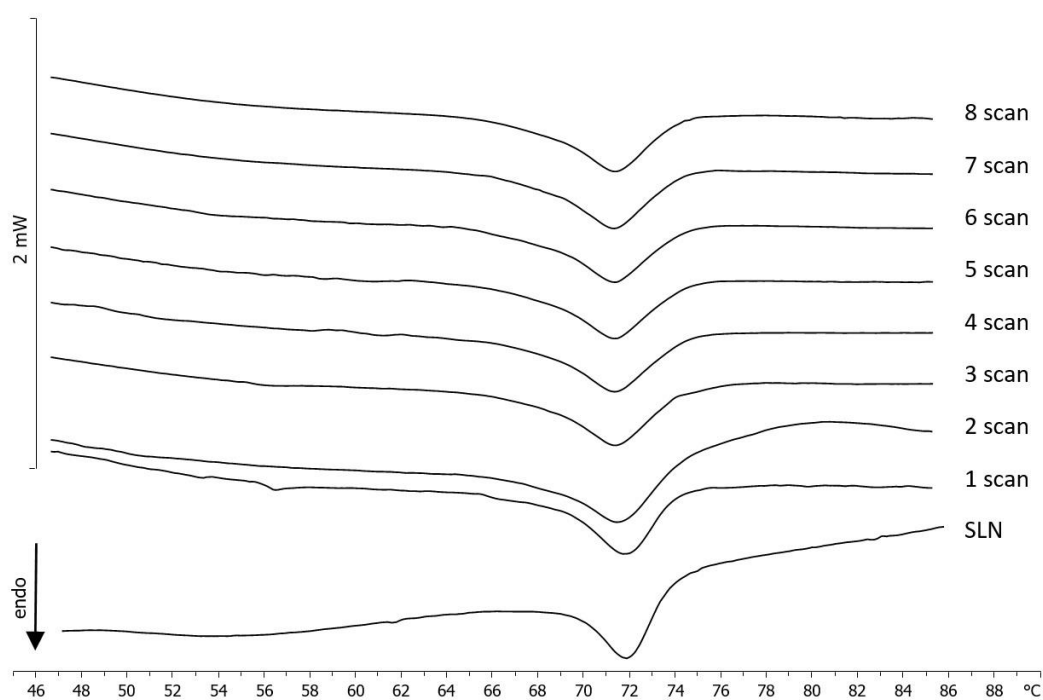

Figure 31. Calorimetric curves, in heating mode, of SLNs left in contact with PEG (1:0.5), at increasing time of incubation.

Moreover, blank SLNs were put in the calorimetric pan and PEG micelles were added at different molar ratios. In figure 32, the calorimetric curve of blank SLNs are compared with the calorimetric curves of SLNs put in contact with PEG micelles at different time of incubation (scan) (only the most representative calorimetric curves corresponding to 1:0.1, 1:0.5 and 1:1 molar ratio are shown). It was clearly evident that PEG affects the SLNs calorimetric curve in different ways depending on the molar ratio. SLNs show a main peak at about 72.5 °C. At 1:0.1 SLN/PEG molar ratio, the main peak is still present; however, a shoulder at about 69 °C is also visible. At 1:0.25 molar ratio the main peak decreases and the shoulder increases. These results indicate that PEG interacts with the SLN and localizes on the outer layer of the SLN; in particular, the stearoyl moieties of the DSPE could be inserted on the SLN; whereas the PEG moiety could protrude on the SLN surface. The presence of two peaks at some amount of PEG micelles, indicate that in the outer layer of the SLN two different regions coexist: PEG rich regions and PEG poor regions. In particular, the signal at lower temperature is related to the PEG rich regions whereas the signal at higher temperature is related to the PEG poor regions. On increasing the amount of PEG micelles, I observed that the peak at higher temperature decreased in favor of the peak at lower temperature and hence, in the SLN outer layer, the PEG poor regions decreased whereas the PEG rich regions increased. At 1:1 molar ratio, the presence of a single peak at lower temperature suggests that PEG could be omogeneously present in the SLN outer layer; this could promote the drug release in the case of CUR-SLNs or AST-SLNs.
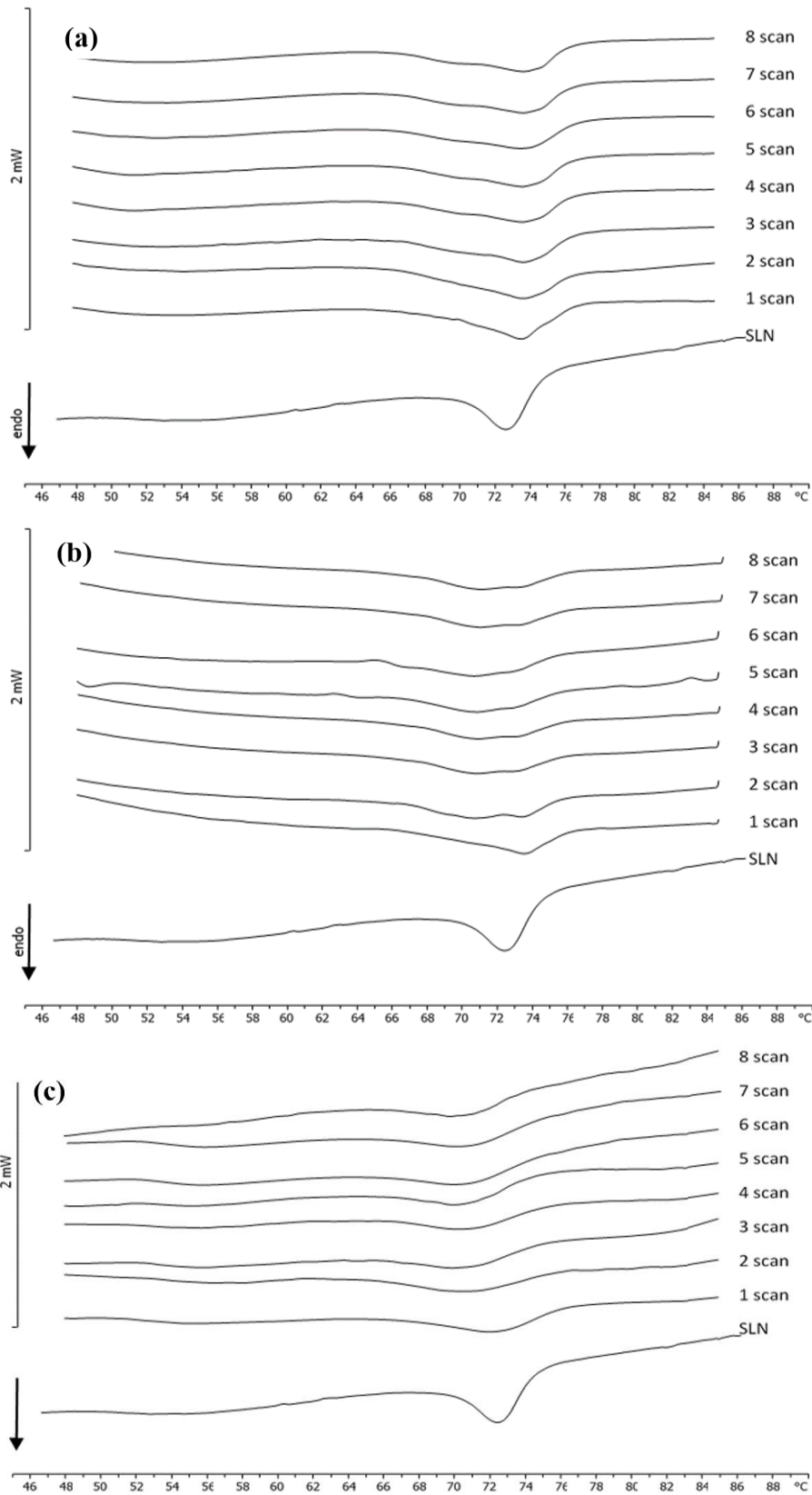
Figure 32. Calorimetric curves, in heating mode, of SLNs left in contact with PEG micelles (a)1:0.1, (b) 1:0.5 and (c) 1:1 at increasing time of incubation.

5.1.5.2. DSC studies on CUR-loaded nanoparticles

In figure 33 the calorimetric curves of blank SLNs, CUR-SLNs, blank pSLNs and CUR-pSLNs are reported. PEG exerted a remarkable effect on blank SLNs; in fact, the large shoulder almost vanished and the sharp peak moved to lower temperature and decreased in intensity. In CUR-SLNs the sharp peak appeared at temperature lower than that of blank SLNs and the shoulder decreased. CUR-pSLNs showed a smaller shoulder and a main peak to a lower temperature than other SLNs; while the peak intensity was lower than blank SLNs. These results indicated that CUR and PEG showed a similar effect on SLNs; both lowered the fluidity of the SLN structure and decreased the cooperativity of the molecules in the system as indicated by the lower temperature and the decreased intensity of the peak. It might suggest that both are localized among the SLN molecules.
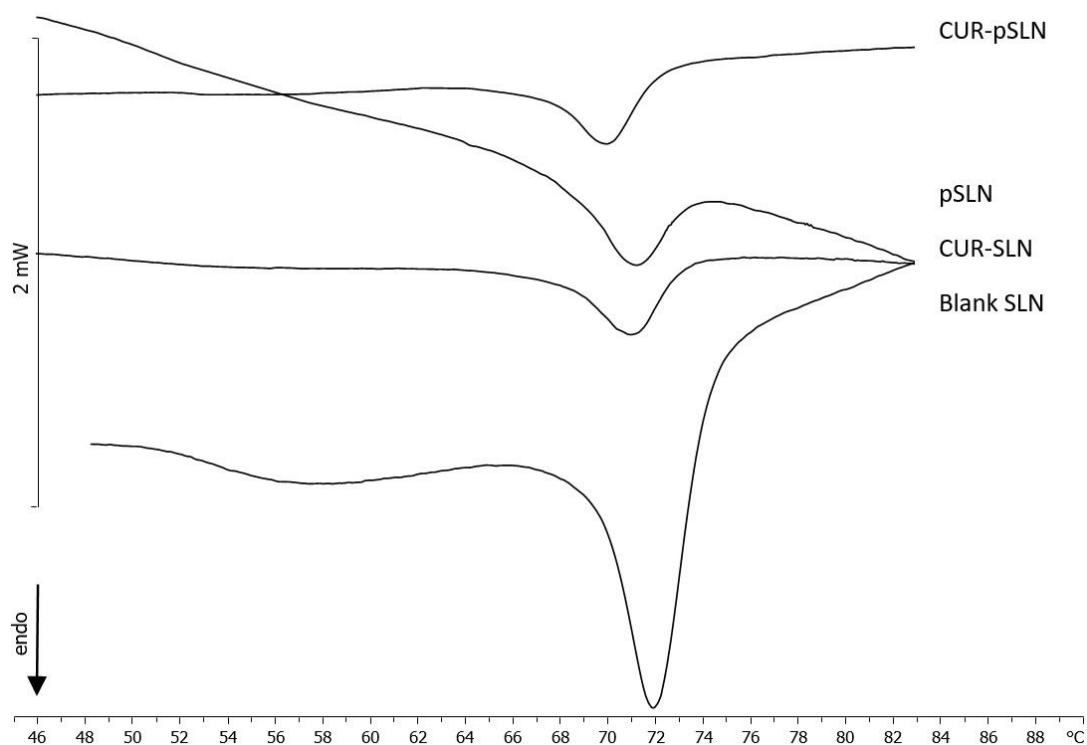

Figure 33. Calorimetric curves, in heating mode, of blank SLNs, CUR-SLNs, blank pSLNs and CUR-pSLNs.

5.1.5.3. DSC studies on AST-loaded nanoparticles

Calorimetric curve of blank SLNs is characterized by a mean peak at about 67.5°C. In figure 34 the calorimetric curves of blank SLN, AST SLN, blank pSLN and AST-pSLN are reported. In the pSLN the peak shifts to higher temperature; this behavior indicates a stabilization of the SLN structure in the presence of PEG. Moreover, the presence of AST in the pSLN causes deep variation in the SLN calorimetric curve: the sharp peak at about 67.5 °C shifts to higher temperature; in addition, its intensity increases. These results indicate that AST and PEG show a synergistic effect on SLN.
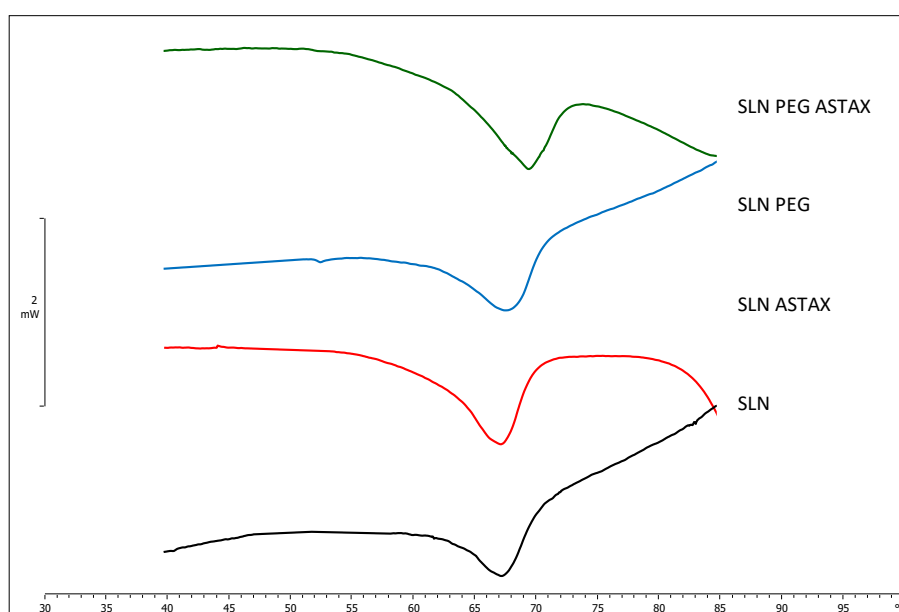
Figure 34. Calorimetric curves, in heating mode, of blank and AST-loaded SLNs and pSLNs.

5.1.5.4. DSC Analysis of the interaction between SLN and MLV

It was evaluated the ability of SLN to act as carrier for AST and to permit its entry into the cells, studying the interaction of SLN and pSLN with biomembrane models (MLV). In particular, SLNs were put in contact with MLV at 37 °C and the samples were analyzed immediately after the contact and at hourly intervals. The interaction between SLN and MLV was assessed through the changes of SLN and MLV thermograms.

In the MLV calorimetric thermogram, two signals exist which are associated with two phase transitions: the pretransition, at about 16 °C, and the main transition, at about 25 °C. The transitions separate three distinct phases: lamellar gel, rippled gel, and liquid crystalline phase.

With regard to the experiment with SLNs (Figure 35), the first thermogram (recorded immediately after the contact) shows a small peak at about 16 °C, related to the MLV pretransition, a main peak at about 25 °C, related to the MLV transition, a shoulder at about 65°C related to SLN (it is visible in detail in figure 36). In the second scan thermogram, the pretransition disappears and the main peak of MLV shifts to lower temperature. It is clear evidence of the entry of the SLN into the MLV. The peak related to SLN remains unchanged, suggesting that SLN maintain their structure, but in the third scan thermogram it disappears. It indicates that SLN goes into the MLV and that, as the incubation time increases, SLN moves from the outer bilayers to the inner bilayers of MLV.
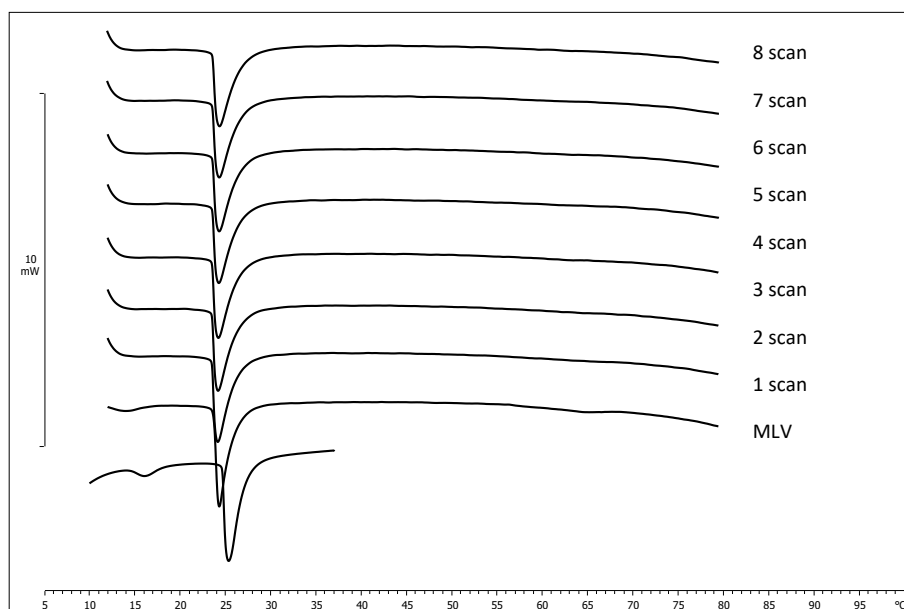

Figure 35. Calorimetric curves, in heating mode, of MLV put in contact with SLNs.
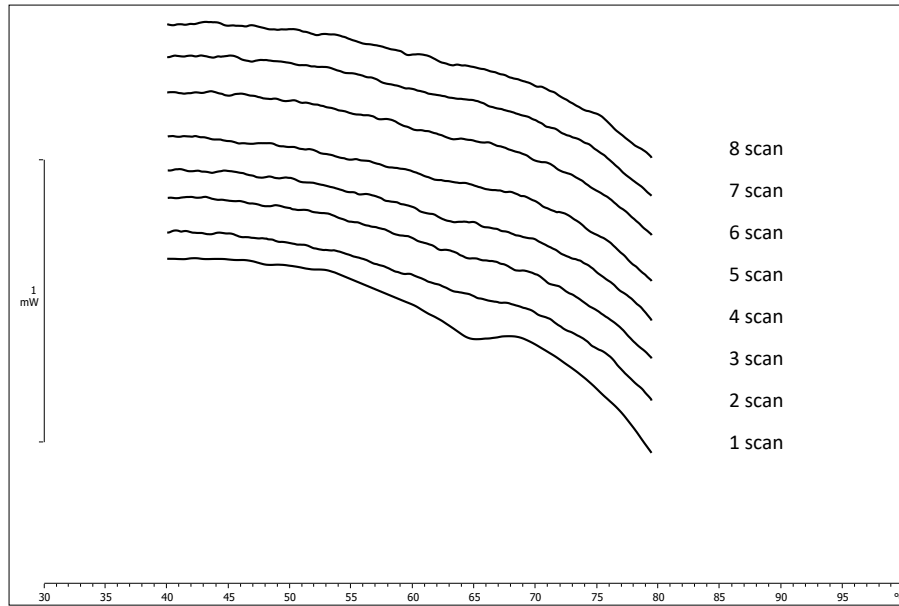
Figure 36. Detail related to the SLN.

Therefore, it was analyzed the interaction between MLV and pSLN, and the resulting thermograms were compared with those of MLV, blank pSLN (Figures 37-38) and AST-pSLN (Figures 39-40). A similar behavior was observed for MLV and pSLN: the MLV pretransition peak disappears, the MLV main peak shifts to lower temperature and the signal related to SLN disapperars from the third scan thermogram. The results on the interactions between AST-pSLN and a biological membrane model pointed out that SLN could be able to penetrate into the biomembrane, thus facilitating AST permeation into the biomembrane itself. The same results were obtained with the CUR-pSLNs (data not shown).

Figure 37. Calorimetric curves, in heating mode, of MLV put in contact with pSLN.

Figure 38. Detail related to the PEG SLN.

Figure 39. Calorimetric curves, in heating mode, of MLV put in contact with AST loaded PEGylated SLN.

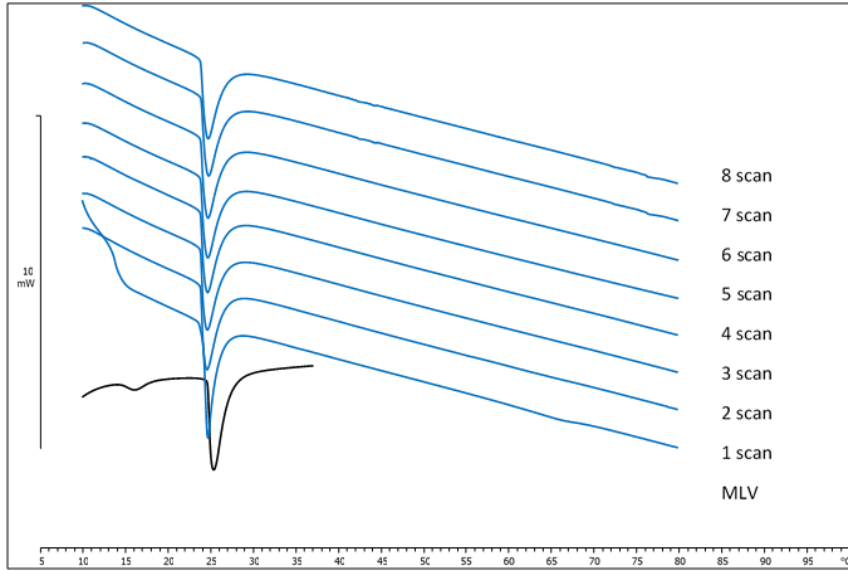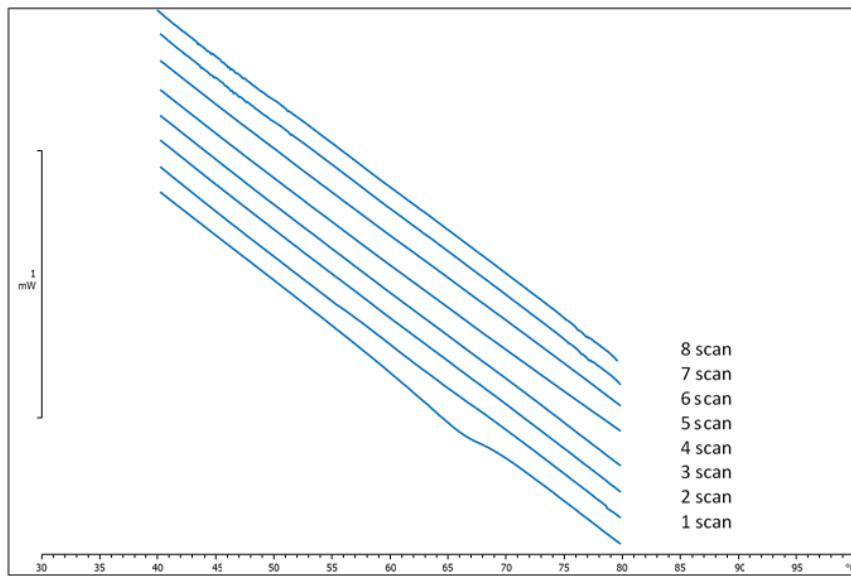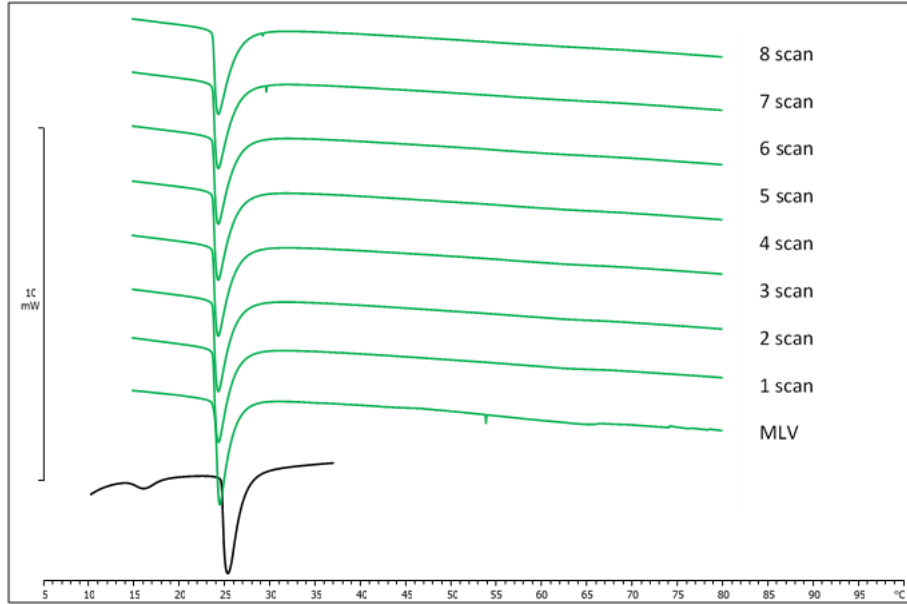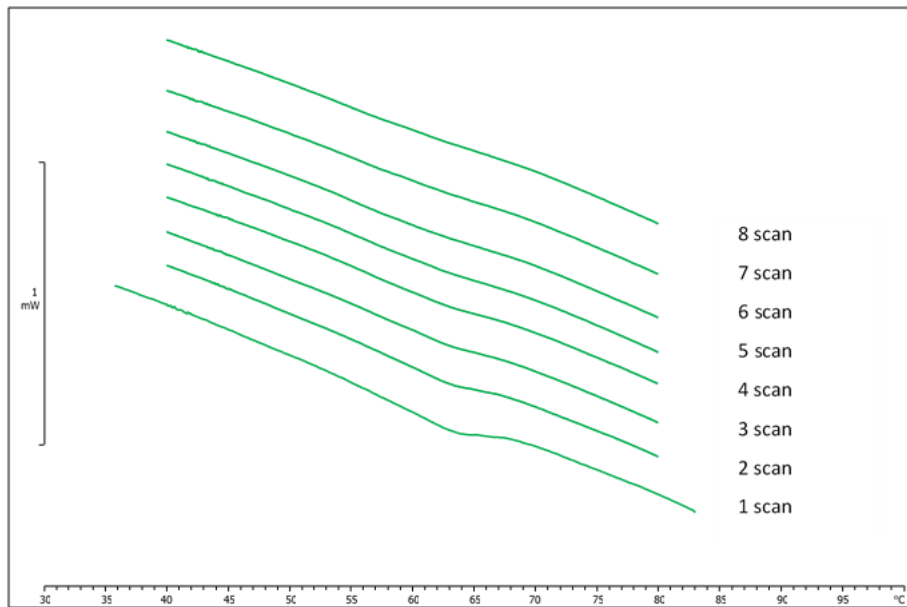*Figure 40. Detail related to the AST PEG SLN.*

5.1.6. MTT Bioassay on PEGylated systems

The MTT assay is important to assess cell viability and it can be used to indirectly measure cytotoxicity. As previously mentioned, the cytotoxicity study was carried out using two different cell lines: stem cell line OECs and a cancer cell line MCF-7. AST has been chosen as the reference substance for this study, as CUR has already been extensively investigated in a previous research project.

A preliminary study was carried out on OECs cells to establish the concentration of pSLN which did not produce toxic effect. Figure 41 shows the percentage of cell viability performed by the MTT test in OECs cultures exposed to blank and AST-pSLN for 24 h to 100 μM, when compared with the control (PBS).
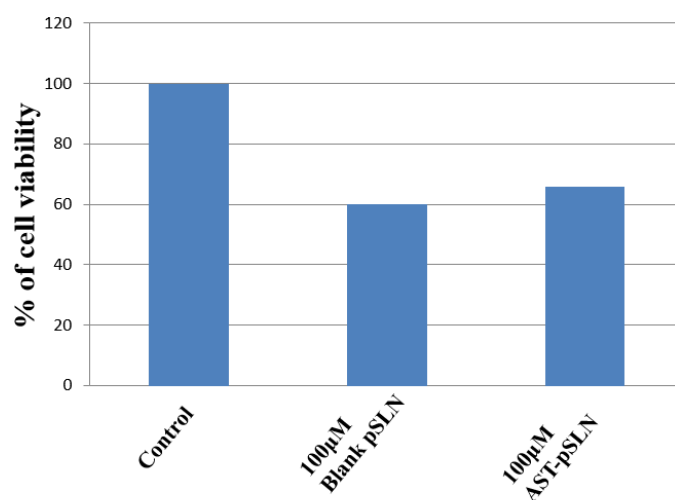
Figure 41. Percentage of viability cells in control, blank pSLNs 100μM and AST-pSLNs 100 μM. Results are expressed as a percentage of the control. Data were statistically analysed using One-Way analysis of variance (ANOVA) followed by a post hoc Holm–Sidak test to estimate significant differences among groups.

It was found that the treatment of OECs with pSLN at 100 μM produced significantly toxic effects. This is due to high concentration of pSLN (100 μM) that caused a harmful effect on the cells with a mortality around 40%. In the case of AST-pSLN, mortality is lower than blank pSLN due to AST activity.

Based on the results obtained from the preliminary experiment, it was decided to treat the cells using lower SLN concentrations, such as 1 µM, 0.2 µM and 0.1 µM (Figure 42).
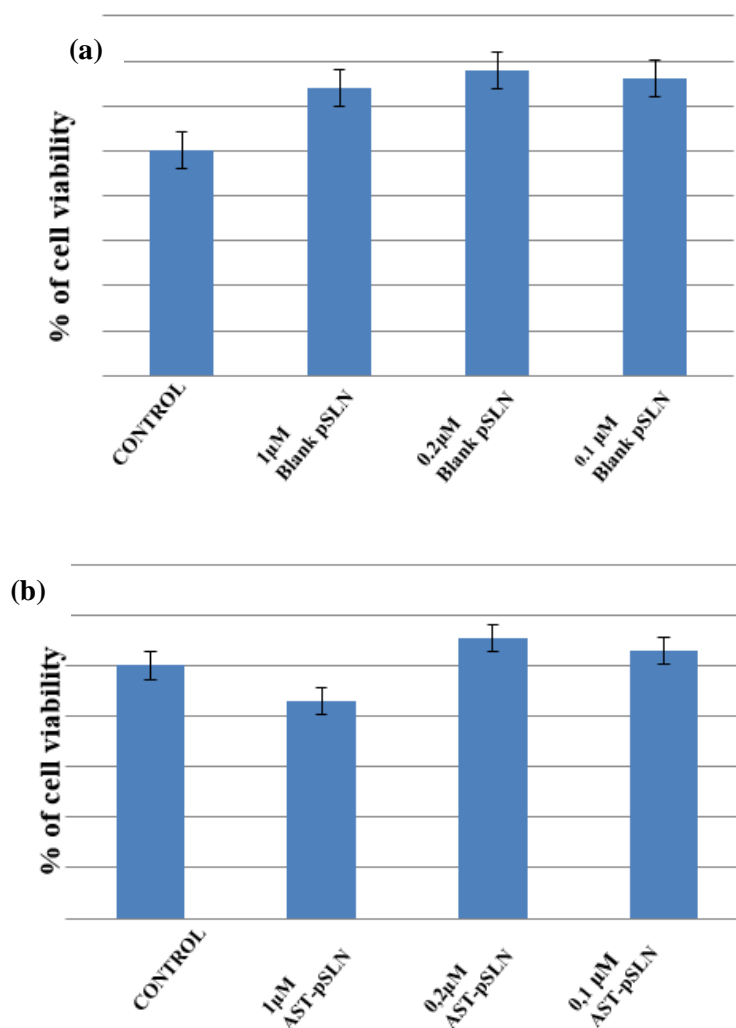
*Figure 42. Percentage of cell viability in OECs exposed to different concentrations of (a) blank and (b) AST-pSLN (1 µM, 0.2 µM, 0.1µM) for 24 hs. All the values shown represent the average ± S.D. of 3 experiments carried out separately. * p <0.05 vs the respective control.*

The results obtained by the MTT test showed that the optimal SLN concentration was between 1 µM and 0.2 µM. Therefore, subsequent experiments were conducted by treating the cancer cells culture MCF-7 at SLN concentrations between 1 µM and 0.2 µM. In particular, it was evalutated the treatment of MCF-7 with pSLN at 1µM, 0.4 µM and 0.2µM for 24 hs.
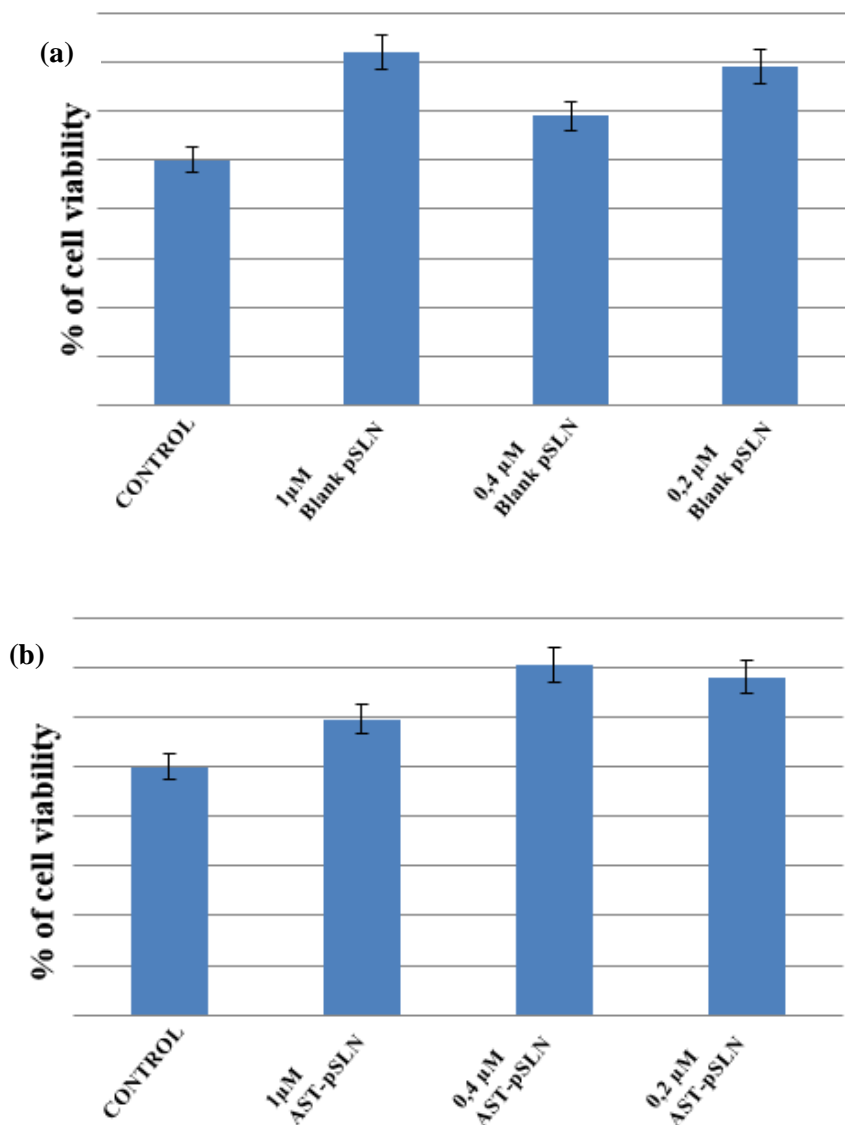
*Figure 43. Percentage of cell viability in MCF-7 exposed to different concentrations of (a) blank and (b) AST-loaded pSLN 1 μM, 0.4 μM, 0.2 μM for 24 hs. All the values shown represent the average ± S.D. of 3 experiments carried out separately. *p <0.05 vs the respective control.*

Figure 43 shows that the best concentration for PEGylated systems was 0.2 μM, in fact at this concentration the cells exhibit the same cell viability as the control.

5.1.7. *In vitro antioxidant activity of CUR and AST*

The antioxidant activity of CUR and AST, free or loaded into pSLNs, was assessed *in vitro* using the ORAC assay, according to the procedure previously described [*G. Cao et al., 1993; B. Ou et al., 2001*].

The obtained results highlighted the effect of encapsulation on CUR antioxidant activity (Figure 44). In particular, at t_0 hs, free CUR showed a remarkable antioxidant activity with respect to encapsulated CUR. After 24 hs of monitoring, free CUR antioxidant activity decreased, while the activity of CUR encapsulated in pSLNs significantly increased. These results confirm the evidences reported in literature regarding the key role of SLN encapsulation in preserving the antioxidant capacity of active antioxidant compounds for a longer time, with a mechanism probably related to the preservation of the compound stability [*C. Puglia et al., 2019*]. On the contrary, AST-pSLNs were unable to preserve and increase the molecules activity, in fact only free AST showed an antioxidant activity (Figure 45).
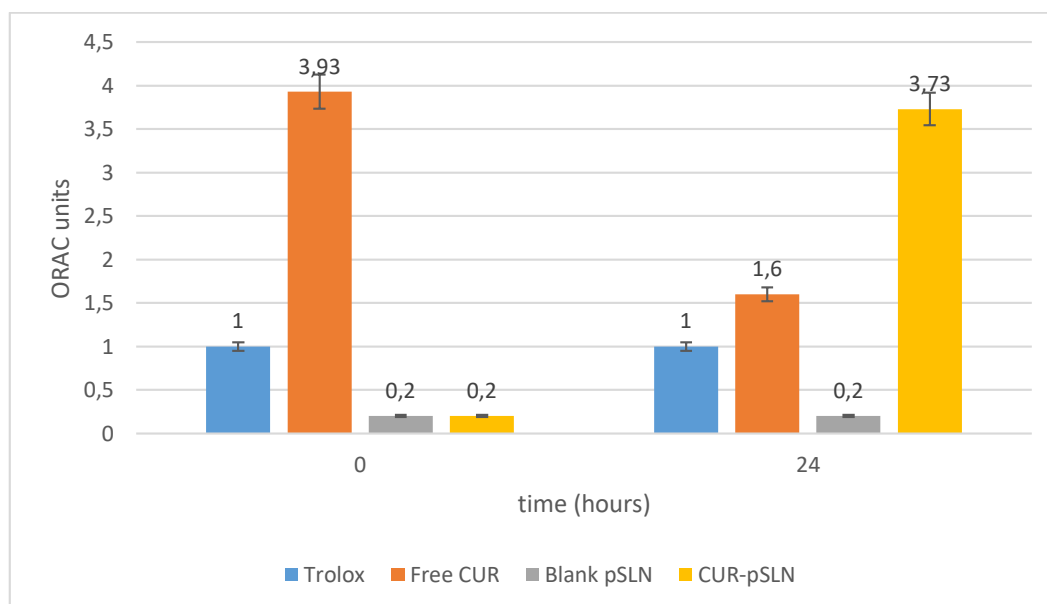
Figure 44. Oxygen radical absorbance capacity (ORAC) activity of Trolox, curcumin, blank pSLNs and CUR-pSLNs. Trolox = 1 Units ORAC.
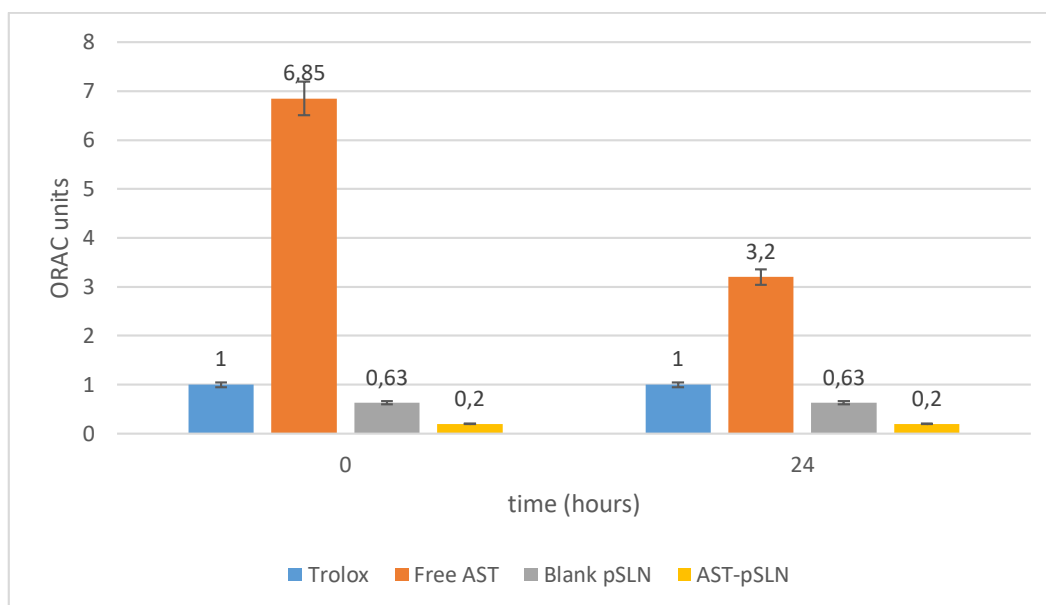
Figure 45. Oxygen radical absorbance capacity (ORAC) activity of Trolox, astaxanthin, blank pSLNs and AST-pSLNs. Trolox = 1 Units ORAC.

5.1.8. Stealth lipid nanoparticles with polysorbate 80

5.1.8.1. Characterization of p80SLNs

Based on the unsatisfactory results obtained for the encapsulation of AST by the PEGylation strategy, it was decided to realize "stealth" systems by coating the SLN surface with polysorbate 80 (p80). The method used to prepare AST-p80SLNs has proven to be valid and reproducible despite the instability of the AST. The obtained results are interesting as confirmed by DLS data and drug loading determination (DR%). AST-p80SLNs showed a mean diameter of 110 nm, a PDI value around 0.32 and a ZP value around -13 mV (Table 3). As regards to DR%, the encapsulation efficiency of AST was above 90%.

Formulation	Z-Ave [nm ± SD]	PDI [-] ± SD	ZP [mV ± SD]
Blank SLN	136.0 ± 0.2	0.27 ± 0.1	-20.4 ± 0.2
AST-SLN	111.1 ± 0.2	0.33 ± 0.2	-16.2 ± 0.2
Blank p80SLN	154.2 ± 0.3	0.29 ± 0.2	-18.2 ± 0.3
AST-p80SLN	130.8 ± 0.2	0.32 ± 0.3	-13.0 ± 0.4

Table 3. Mean particle size (Z-Ave), polydispersity index (PDI) and zeta potential (ZP) of SLN and p80SLN unloaded and loaded with AST.

5.1.8.2. Stability studies on p80SLNs

In addition, the long-term stability of blank and AST-p80SLNs were monitorated for six months during storage at room temperature (Figure 46). The data showed that nanoparticles had an acceptable long-term stability after six months of storage compared to the PEGylated systems. Furthermore, AST-p80SLNs had greater stability than blank p80SLNs due to the preservative action of AST.
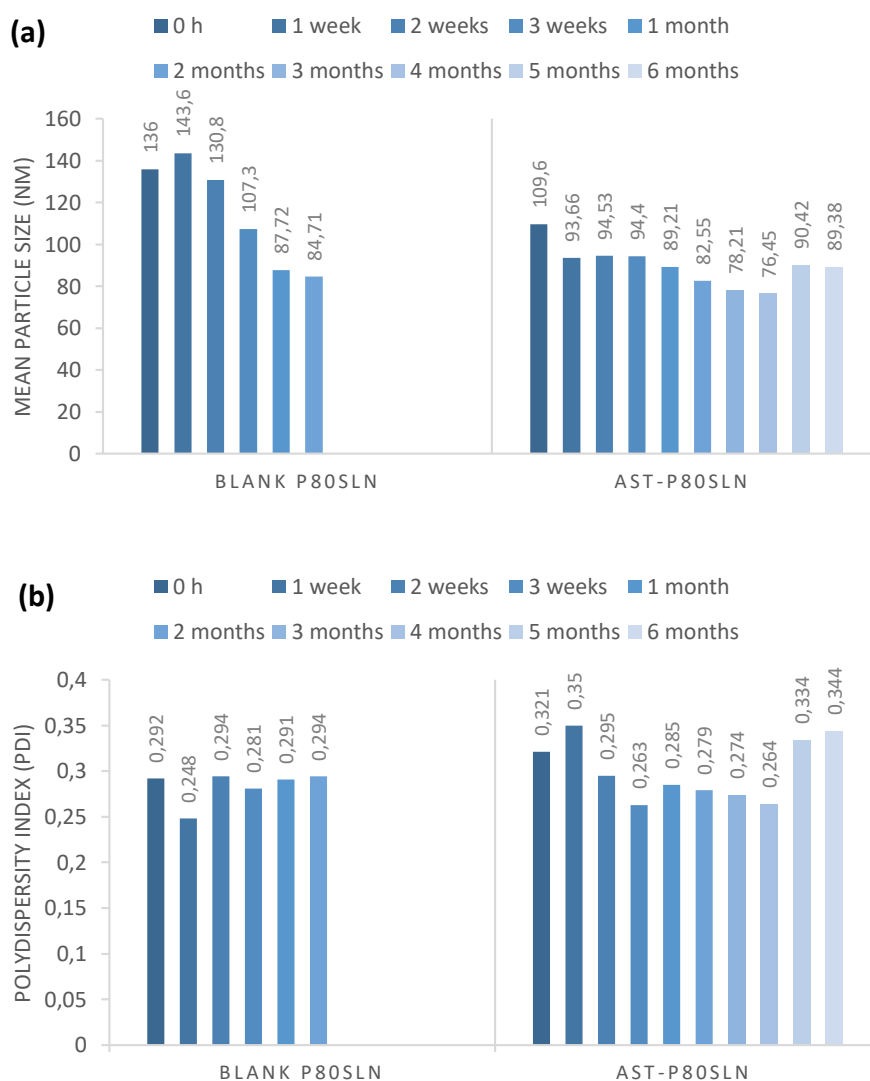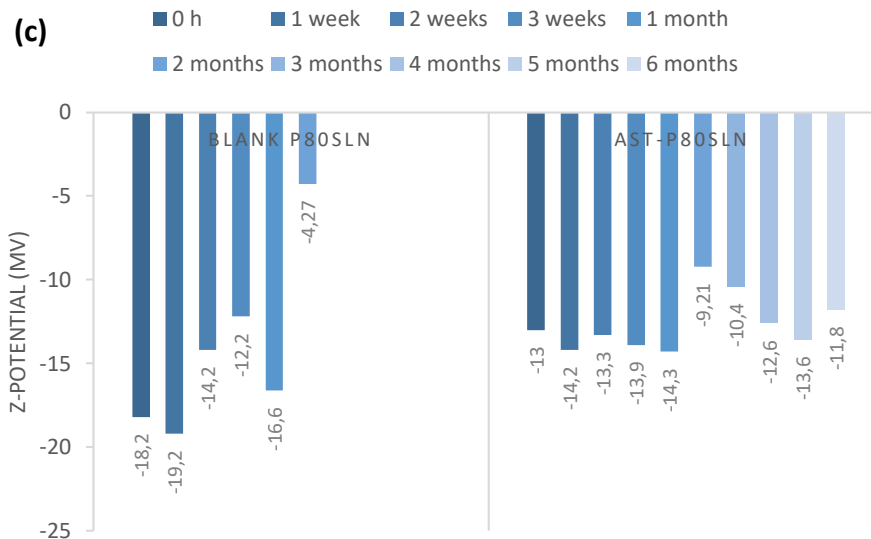
Figure 46. (a) Particle size, (b) polydispersity index (PDI) and (c) Z-potential of blank and AST-p80SLN during storage at room temperature for six months.

Lyophilization studies on p80SLNs showed unsatisfactory results as previously seen on PEGylated systems (data not shown).

5.2.8.3.In vitro assay on p80SLNs

In order to evaluate the toxic effects of blank and AST-loaded p80-SLN, MTT assay was carried out following the same procedure performed on the PEGylated systems. A preliminary test was performed on OECs cells using a p80SLN concentration of 100 µM (Figure 47).
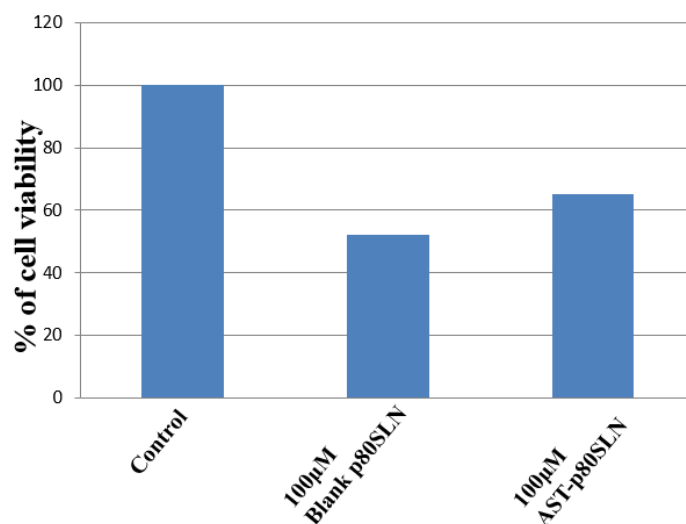
Figure 47. Percentage of viability cells in control, blank p80SLNs 100μM and AST-p80SLNs 100 μM. Results are expressed as a percentage of the control. Data were statistically analysed using One-Way analysis of variance (ANOVA) followed by a post hoc Holm–Sidak test to estimate significant differences among groups.

Since the treatment produced significantly toxic effects, the p80SLN concentration was reduced to 1 μM, 0.2 μM and 0.1 μM (Figure 48).

(b)
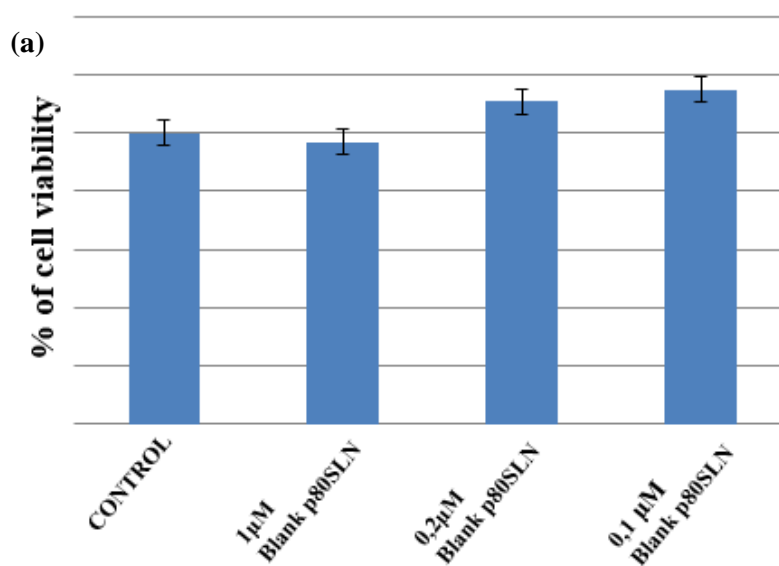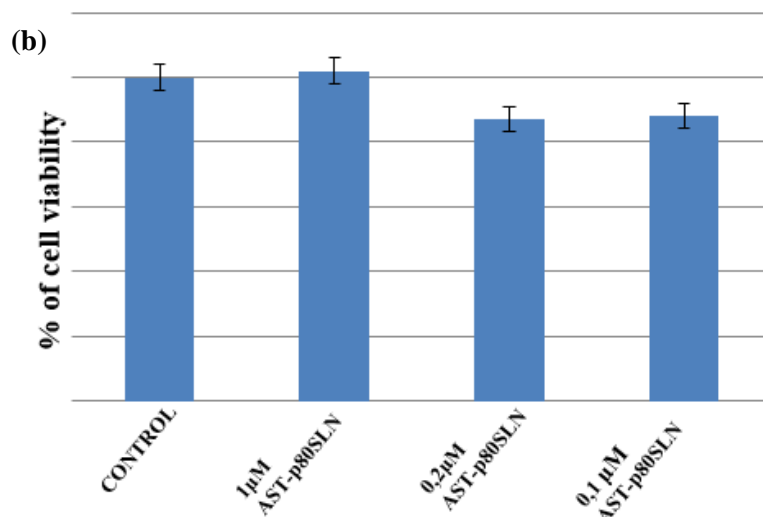
*Figure 48. Percentage of cell viability in OECs exposed to different concentrations of (a) blank and (b) AST-p80SLN (1 µM, 0.2 µM, 0.1µM) for 24 hs. All the values shown represent the average ± S.D. of 3 experiments carried out separately. * p <0.05 vs the respective control.*

The same results were obtained as those performed on pSLN showing that the optimal concentration range was approximately 1 µM- 0.2 µM. Therefore, the subsequent study was conducted by treating the cancer cells culture MCF-7 at SLN concentrations of 1µM, 0.4 µM and 0.2µM for 24 hs (Figure 49).

As reported in Figure 49, the best p80 SLN concentration was 0.2 µM.

(a)
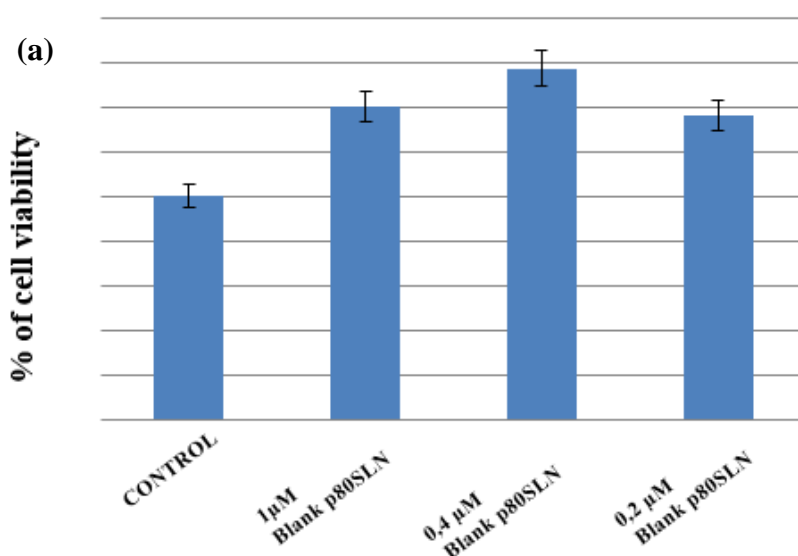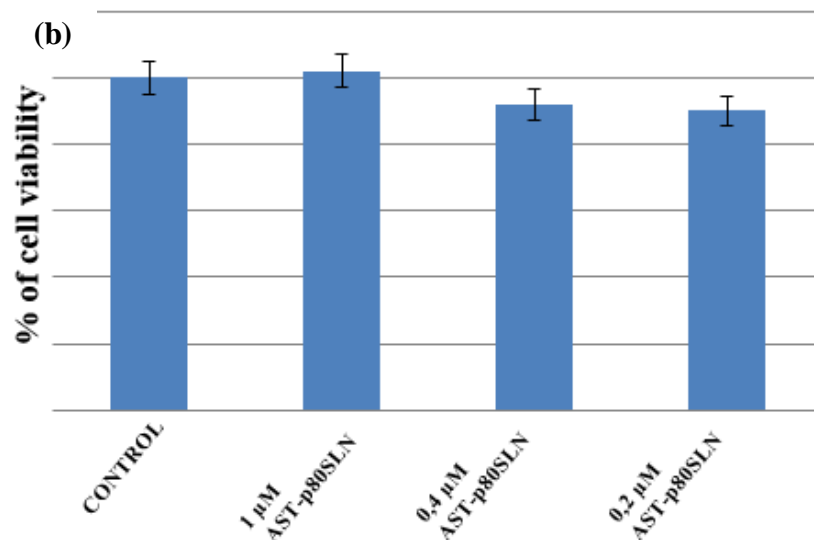
*Figure 49. Percentage of cell viability in MCF-7 exposed to different concentrations of (a) blank and (b) AST-loaded pSLN 1 µM, 0.4 µM, 0.2 µM for 24 hs. All the values shown represent the average ± S.D. of 3 experiments carried out separately. *p <0.05 vs the respective control.*

5.2.8.4. ORAC assay on AST-p80SLNs

The antioxidant activity of AST, free and encapsulated into p80SLNs, was evaluated through ORAC assay (Figure 50). The obtained values showed that at 4 hs, blank and AST-loaded p80SLNs had a high fluorescence value respect to untreated control (FL with AAPH). This showed a protective effect of all the tested samples, as they preserve fluorescein from the degradation of peroxyl radicals. At 12 hs, AST-p80SLN had a much higher fluorescence value (6770 nm) than free AST (620 nm) and blank p80SLN (810 nm). These results suggest that the encapsulating of AST into stealth lipid nanoparticles (p80SLNs) preserved the antioxidant capacity of AST for a longer time (24 hs) and probably maintains its stability.
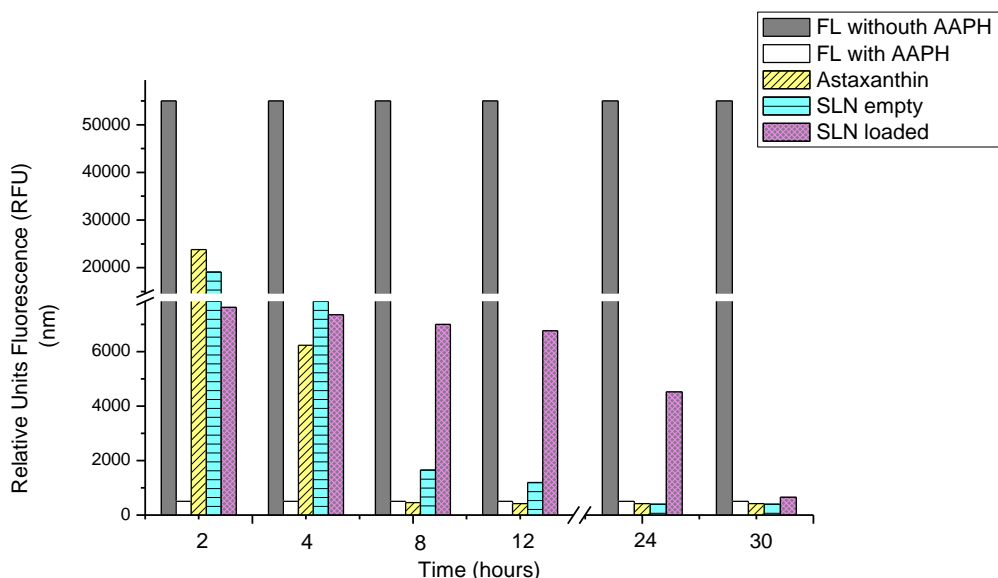
Figure 50. ORAC assay of free AST, blank and AST-loaded p80SLN. FL = fluorescein; FL+AAPH = fluorescein solution containing AAPH.

5.2.8.5.UV stability assay

The photoprotective effect showed by lipid nanoparticles against UVA radiation was evaluated by UV stability assay. Also in this case, AST has been chosen as the reference substance for this study as CUR has already been extensively investigated in a previous research project.

As reported in figure 51, AST alone and once loaded in p80SLN showed the same spectral profile with absorbance changes after UVA exposure. In particular, an increase in absorbance was observed in the spectral profile of AST-p80SLN; this evidence confirms that the lipid shell of SLN protects AST from photodegradation. On the contrary, free AST showed a decrease in absorbance without changes in the spectral profile was observed after UVA exposure. This is attributable to the cis-trans photo-isomerization of AST.
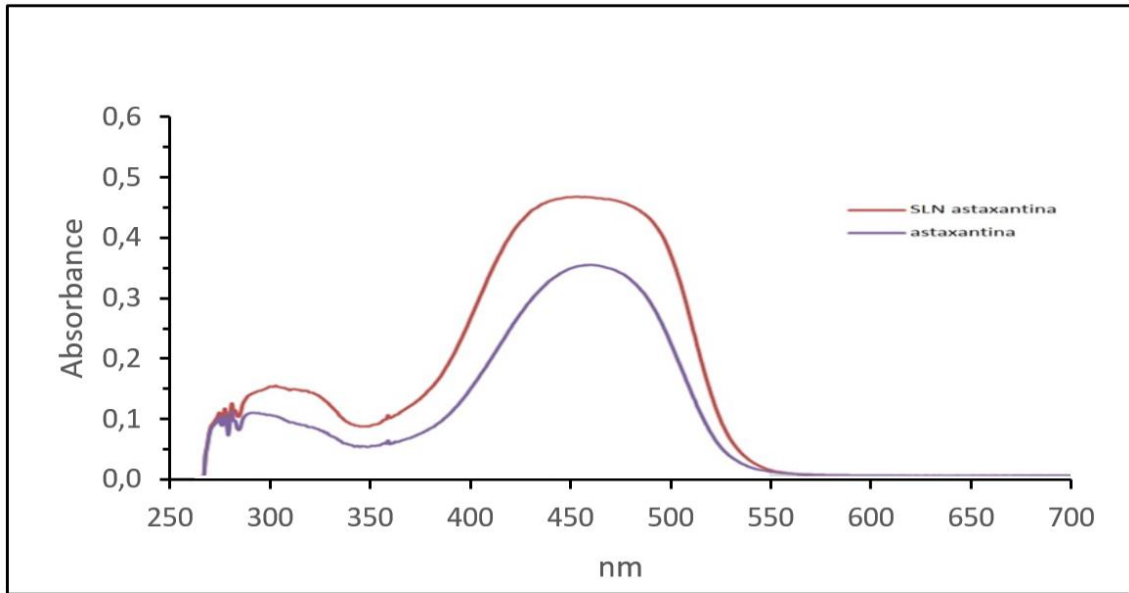
Figure 51. UV-absorption spectra of AST alone and once loaded in p80SLN after UVA exposure.

Moreover, figure 52 shows the spectra of AST-p80SLNs before and after UVA exposure. Both spectral absorbances were equal, thus further confirming that lipid nanoparticle systems protect AST from UVA-induced photodegradation.
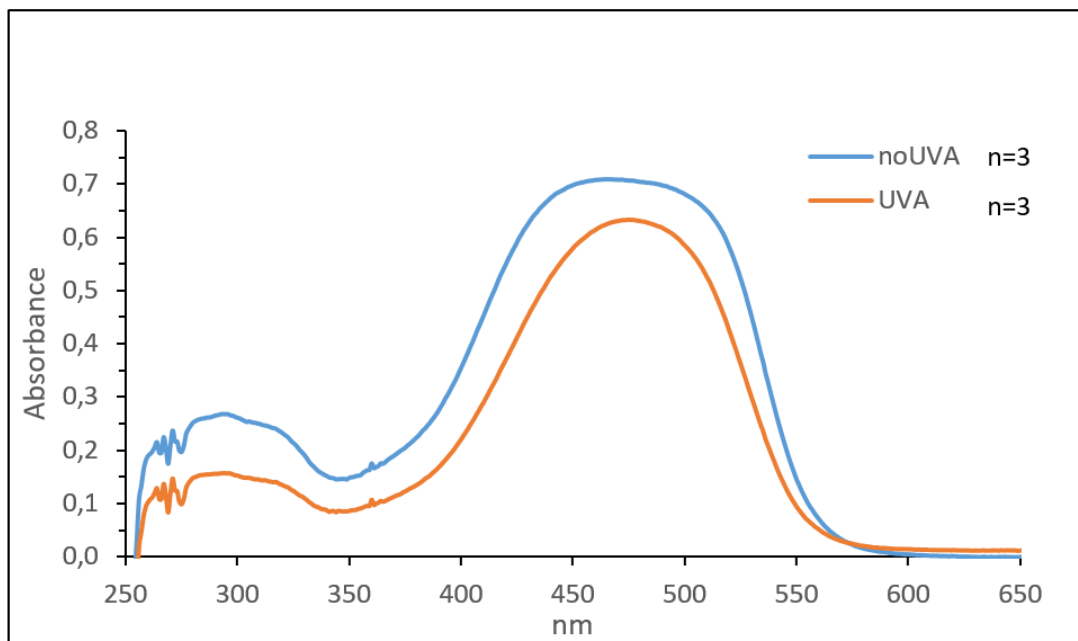
Figure 52. UV-absorption spectra of AST-p80SLNs before and after UVA exposure.

5.1.9. Behavioral experiments

TgCRND8 mice were treated for 3 weeks with CUR-pSLN (150 mg/kg) and AST-p80SLN (40 mg/kg). Cognitive performance was assessed using Step-Down and ORT tests.

Memory performance, investigated in the step down inhibitory avoidance task, showed no significant differences during the training test (TT) between the animals treated with CUR-pSLN (Tg CU) and AST-p80SLN (Tg AS) or Tg mice treated with blank SLN (untreated Tg). However, in the 24 hs retention test (RT) step-down, the latencies recorded for Tg mice were significantly reduced ($P < 0.05$) with respect to wt mice and not significantly different from training latency ($P > 0.05$), indicating that the Tg mice did not memorize the punishment. The administration of drug-loaded SLN significantly improved the performance of Tg mice to a higher level than wt mice (Figure 53).
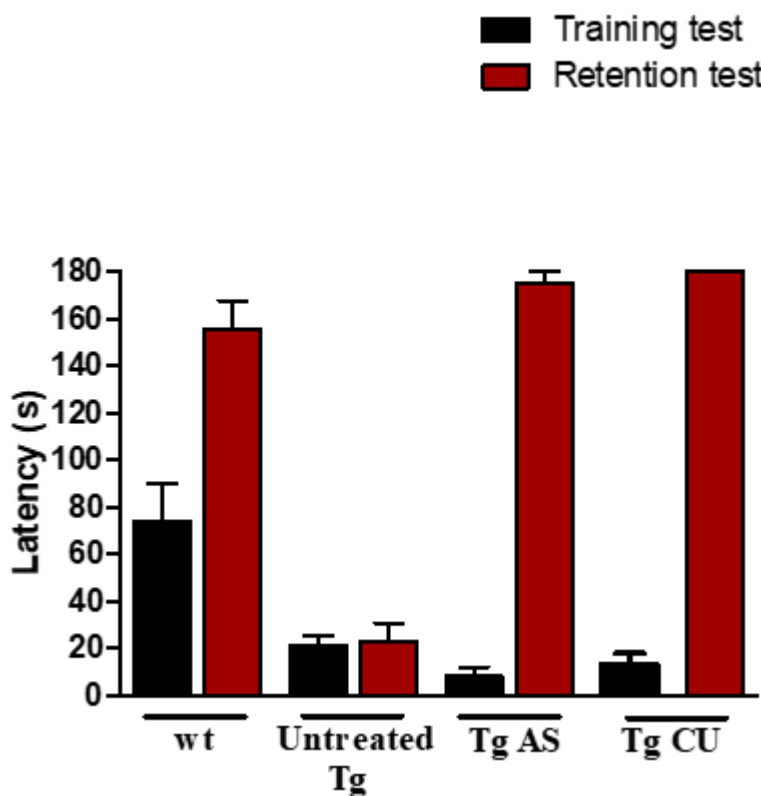
Figure 53. Step down test.

Moreover, ORT results showed that the Tg mice treated with CUR-pSLN and AST-p80SLN had recovered the ability to discriminate a new object from a familiar one. These results demonstrate that, in the TgCRND8 model, the cognitive deficit is completely recovered by the administration of the tested formulations.

5.2. Active natural product for the treatment of neuropathic pain

5.2.1. CPS-SLN: Formulation and Characterization

CPS-SLNs were prepared by *solvent injection* method using Softisan©100 (Hydrogenated Coco-Glycerides) as lipid and Tween 80 as surfactant. A pre-formulation study was effected to establish the lipid matrix most suitable for the encapsulation of CPS. Softisan 100 has been selected as it showed the best characteristics in terms of solubility and affinity towards CPS. This evidence justifies the high encapsulation efficiency found for CPS-SLN formulation (97.3 ± 2.53%). As reported in Table 4, unloaded and CPS-SLNs showed a mean diameters ranging about 250–300 nm and a polydispersity index (PDI) of about 0.3.

Sample	Z-Ave [nm ± SD]	PDI [-] ± SD	Di (10) [nm ± SD]	Di (50) [nm ± SD]	Di (90) [nm ± SD]
Blank SLN	296 ± 26	0.282 ± 0.0071	64 ± 23	330 ± 43	1112 ± 58
CPS-SLN	287 ± 86	0.410 ± 0.004	112 ± 32	342 ± 72	780 ± 68

Table 4. Particle size, intensity distribution (Di), and polydispersity index (PDI) of SLN based formulations.

Regarding the PDI values, which correctly describe the size distribution of the samples, CPS-SLNs showed the same median diameter D (50) of blank SLN (about 340 nm) but a greater presence of aggregates (D90> 1 μm).

These results were confirmed by AFM analysis on mica, reported in figure 54. All samples presented nanoparticles with a spherical shape and well-defined contours. AFM "height images" (scansion of

about 8 micron) described the major heterogeneity of CPS-SLNs if compared to blank SLNs, even if particles sizing from 200 to 400 nm remained representative of this sample.
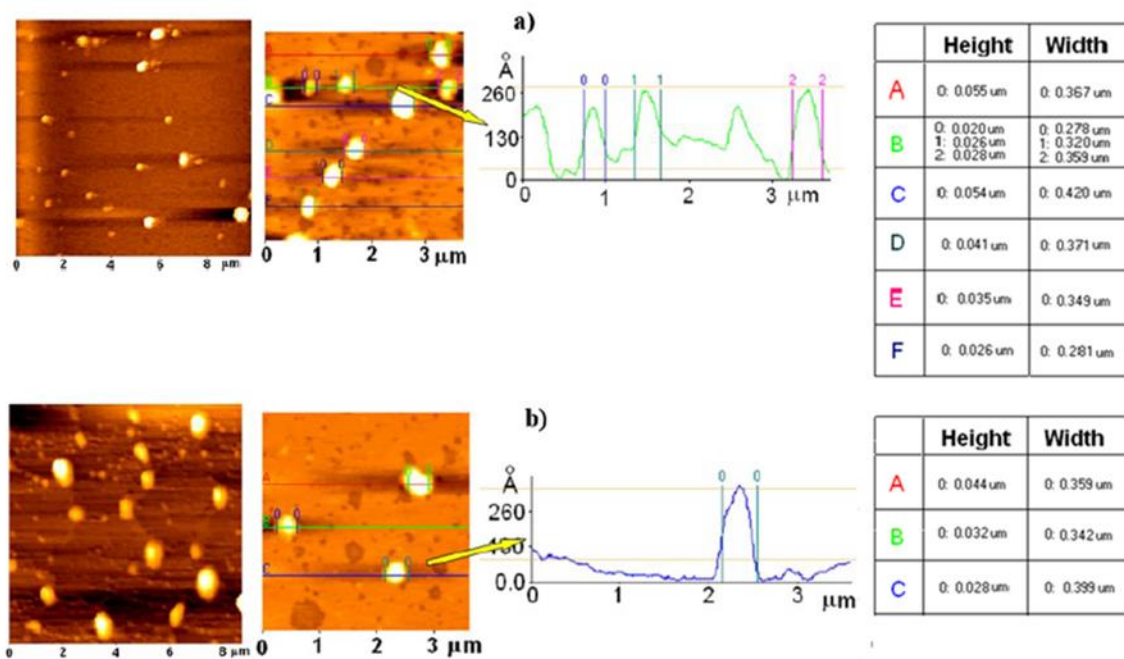
Figure 54. Atomic Force Microscopy (AFM) images, height profile and elaboration of (a) blank SLN and (b) CPS-loaded nanocarriers (CPS-SLN).

The xy graphics describing the "height" profile of SLN (Figure 54a) nicely contributed to describing the regular shape (symmetry) of the SLN, also after CPS encapsulation (Figure 54b). Moreover, the SLN can be described as flattened-platelet shaped carriers since the diameters of SLN were higher than the related heights with a height (H)/width (W) ratio close to 1/10 [*E. Vighi et al., 2007*]. As reported in literature, the difference between width and height could be partially due to the interaction between the sample and the substrate, as well as to the continuous movement of the cantilever probe of the AFM that, by pushing and warming the particles, might determinate a deformation of their original morphology [*B. Ruozi et al., 2005*]. The physical state of lipids affects the permeability and the stability of the SLN.

5.2.2. DSC studies on CPS-SLNs

Figure 55 shows the DSC thermograms of the component of unloaded and CPS-loaded SLN. The calorimetric curves of raw materials showed a melting point of 39 °C for Softisan© 100 and 65 °C for CPS, respectively. Blank SLNs and CPS-SLNs showed a slight decrease of melting point correlated to lipid constituent (36.2 °C for SLN and 36.5 for CPS-SLN) and a modification of the endothermic peak that appeared broader. The depression of endothermic peak is often observed when the bulk lipid is transformed into SLN. These data explain that the crystalline structure of the Softisan 100 was modified by the SLN formulation as the lipid matrix interacted with the other components of the system. Moreover, the heating curve of the CPS-SLN differs from that of the raw CPS: this confirms that CPS has interacted with the lipid nanoparticles.
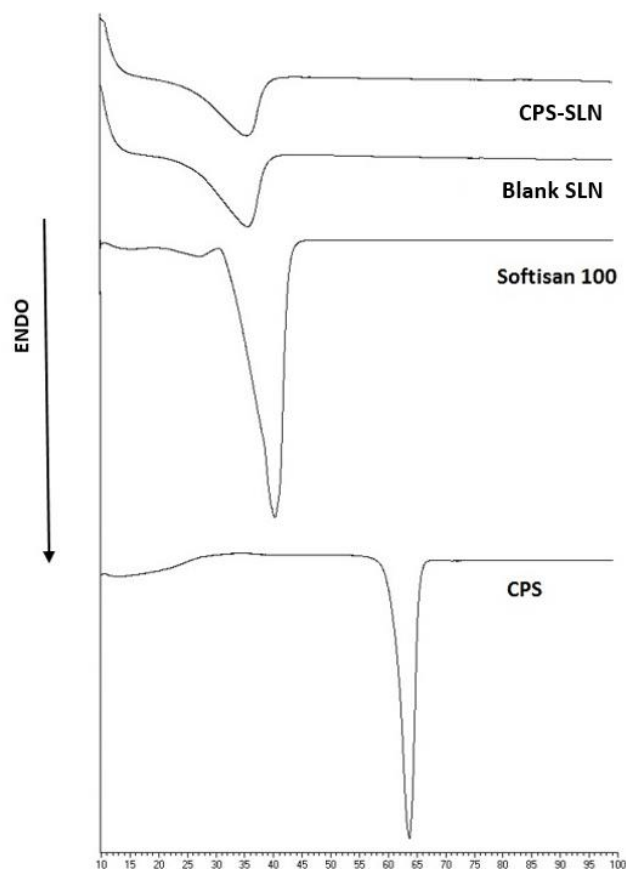
Figure 55. Differential Scanning Calorimetry (DSC) thermogram scans of components, blank and CPS-SLN.

5.2.3. In vitro Release Study

The *in vitro* release profile of CPS from SLN (Figure 56) follows a "two-step drug release" related to distribution of active compound in SLN matrix [*M. Geszke-Moritz et al., 2016*]. CPS-SLNs exhibit a minimum burst effect within the first 2–3 hs. In this first phase, the CPS spread on the surface and the drug is released immediately because of a wide diffusion in concentration gradient represents the burst release. In the second step, CPS-SLNs continued to release its content until 24 hs, at which it released 70% of encapsulated drug.

Therefore, it could be concluded that drug incorporation into the CPS-SLNs can prolong drug release due to the slow release of the drug from the lipid matrix. This result is consistent with the findings of other researchers regarding drug release from lipid nanoparticles [*C. Puglia et al., 2008; E. Esposito et al., 2013; L.G. Souza et al., 2011*].
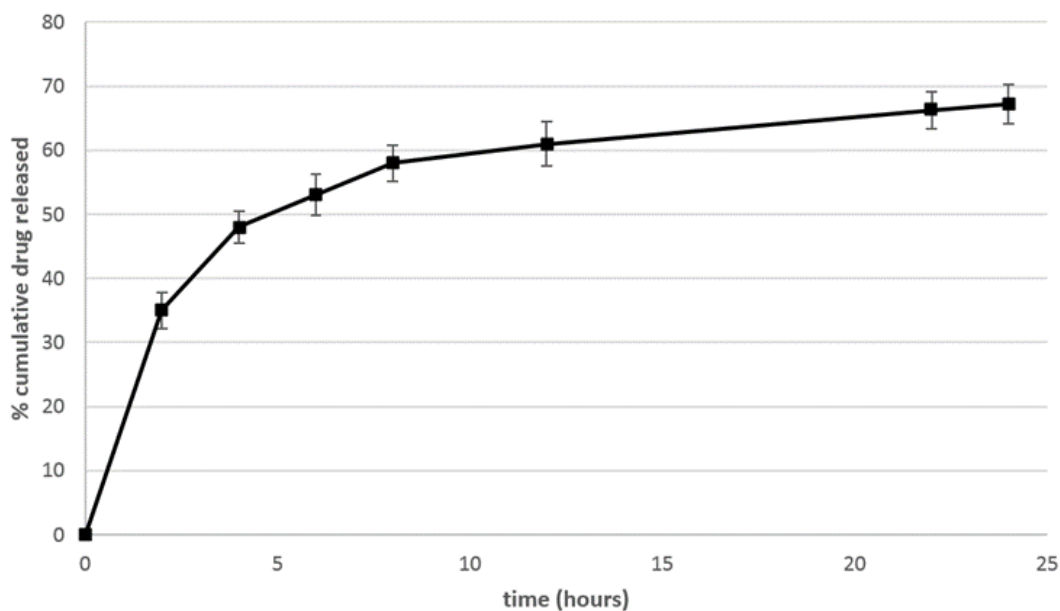
Figure 56. Percentage of cumulative CPS released from free CPS and CPS-SLN. Each point represents the mean value ± S.D. (n = 3).

5.2.4. In Vivo Study on CPS-SLNs

The acute activation of TRPV1 receptors by CPS is known to lower pain threshold [*M.J. Caterina et al., 2000*]. In this experiment, CPS was locally administrated in the plantar surface or the right hind-paw. The intradermal injection was selected to rapidly deposit a precise amount of CPS directly into the site of injection. This procedure is known to produce a sensation of intense pain at the site of injection [*D.A. Simone et al., 1987*]. Spontaneous pain induced by the injection of CPS was assessed in mice for 5 min after administration and measured as liking, lifting, and shaking behavior of the injected paw (Figure 57). As expected, the activation of TRPV1 receptors by both CPS formulations tested induces spontaneous pain. The inclusion of CPS into SLN induced a lower pain response when compared to drug dissolved in a standard vehicle (CPS-STD), according to western blot results. No differences in pain behavior after VEH-STD and VEH-SLN administration were observed (Figure 57), showing that neither the standard vehicle nor the blank SLN induce a pain response in itself. Thus, the nociceptive behavior observed in CPS-STD and CPS-SLN groups has to be related to the presence of CPS that is able to activate TRPV1 receptors. Moreover, no pain response was observed in the contralateral uninjected paw (data not shown), thus excluding the systemic effect of the drug.
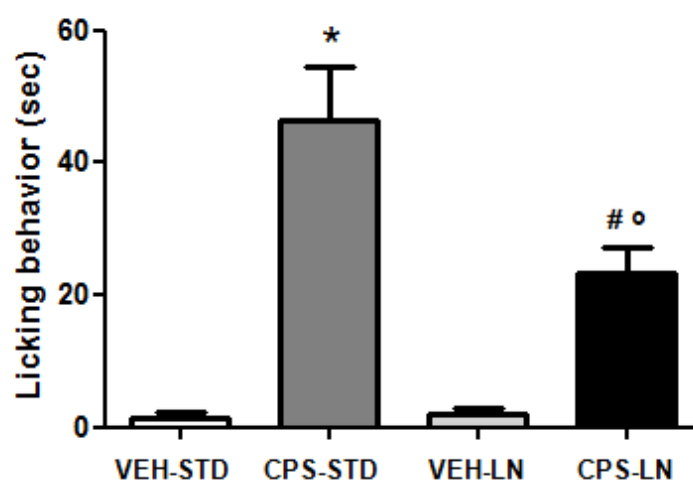
Figure 57. Intraplantar (i.pl.) injection of CPS induces spontaneous pain. The nocifensive response to i.pl. injection of CPS (0.125%/10 μl) dissolved in standard vehicle or included in LN in naïve mice is shown. Data are means ± S.E.M of 6 mice, and refer to the number of sec spent in licking behavior in the first 5 min

following injection. *p < 0.05 vs. mice injected with vehicle, #p < 0.05 vs. mice injected with LN, op < 0.05 vs. mice injected with capsaicin (one-way ANOVA followed by "Bonferroni's Multiple Comparison Test").

5.2.5. TRPV1 Skin Expression

Prolonged exposure to CPS can desensitize the TRPV1 receptor or induce its internalization and degradation. In agreement with the literature, the local i.pl. injection of CPS-STD induced a significant reduction of TRPV1 expression in the mouse skin at the site of injection, as shown in Figure 58 [*P. Holzer, 2008; K.R. Bley et al., 2010*]. In addition, CPS once loaded into SLN prevented from TRPV1 down-regulation in the skin, an effect that is probably due to a slow release of the drug, thus preventing TRPV1 internalization and degradation. Agonist-induced defunctionalization of TRPV1 receptors is the underlying mechanism for long-term nociceptors desensitization. CPS-induced down regulation of membrane TRPV1 levels has been used as a strategy for pain treatment [*N. Ellison et al., 1997; C.P. Watson et al., 1988*]. However, different functions of TRPV1 receptors other that pain perceptions have emerged. For example, a number of studies indicate a role for TRPV1 receptors in carcinogenesis [*M. Lazzeri et al., 2005; N. Prevarskaya et al., 2007; C. Amantini et al., 2007*].

Some studies indicate that TRPV1 receptor antagonist promote skin carcinogenesis through the EGFR, thus a role for TRPV1 receptors as tumor suppressors have been proposed [*A.M. Bode et al., 2009*].
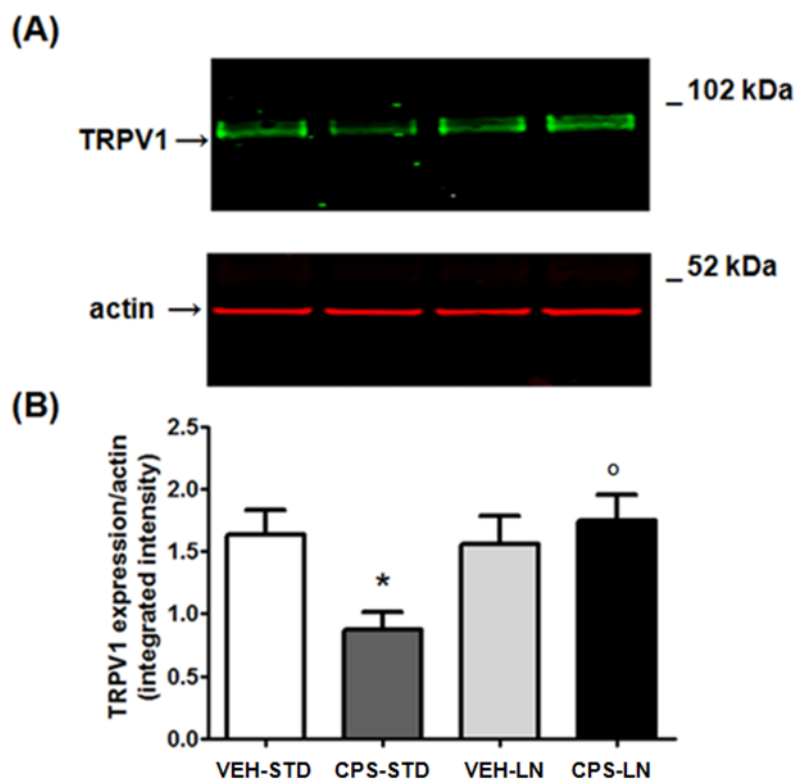
*Figure 58. Expression of TRPV1 receptor in the skin of CD1 mice after 7 days from the i.pl. injection of CPS included in standard vehicle or LN. I.pl. injection of CPS induces a significative downregulation of TRPV1 receptors that is blocked by LN inclusion. A representative immunoblot of TRPV1 in the skin of naïve mice and mice injected with capsaicin (0.125% /10 μl) in the absence or presence of LN is shown in (A). Densitometric analysis is shown in (B), where values are means + S.E.M. of four determinations. *p < 0.05 vs. vehicle mice; ᵒp < 0.05 vs. mice injected with capsaicin (one-way ANOVA followed by Fisher's post hoc test).*

Therefore, CPS-SLN could be a valid alternative to obtain a controlled release of CPS avoiding the TRPV1 defunctionalization.

5.3. Active natural products for the treatment of retinal diseases

5.3.1. NLCs preparation and characterization

Blank NLCs were formulated using two different preparation strategies in order to select the best method to obtain lipid-based nanocarriers suitable for ocular administration. Two well-known

techniques, such as the high shear homogenization technique (HSH) and the method based on a combination of HSH technique and ultrasound (HSH / US) [*F. Brugè et al., 2013; C. Puglia et al., 2016*], were evaluated. The obtained formulations (NLC1 for HSH/US and NLC2 for HSH techniques, respectively) were fully characterized in order to obtain information about the nanoparticles characteristics. DLS data proved that the NLC1 formulation (NLC1) showed better technological parameters than NLC2 (Table 5), as confirmed in literature [*C. Puglia et al., 2013*].

Formulation	Z-Ave [nm ± SD]	PDI [-] ± SD	ZP [mV ± SD]
NLC1	264.5 ± 0.19	0.200 ± 0.035	-37.1 ± 0.02
NLC2	731.2 ± 0.21	0.269 ± 0.038	-41.4 ± 0.01

Table 5. Mean particle size (Z-Ave), polydispersity index (PDI) and zeta potential (ZP) ± standard deviation of NLC1 and NLC2. Values are the mean of at least 3 measures.

These results demonstrate the important role of US in controlling the final particle size. Therefore, this formulation strategy was selected to deliver PEA and MGN (Table 6).

Both formulations were prepared by high shear homogenization coupled to ultrasound (HSH-US) method. These nanocarriers were formulated using Compritol® 888 ATO (glycerol behenate) and Miglyol 812® (mixture of medium chain triglycerides) as lipid phase and Lutrol F68® (Poloxamer 188) as surfactant. NLC systems were characterized by good homogeneity, as demonstrated by the PDI value, and by a remarkable stability over time. This last indication is a function of the value of the zeta potential [*R.H. Muller et al., 2002*]. This could be due to presence of Poloxamer on particle surface, thereby creating a stabilizer layer [*I. Ghosh et al., 2011; A.A.M. Shimojo et al., 2019; C. Puglia et al., 2018*]. The choice of surfactant is very important because it controls the particle size and the stability, preventing their aggregation during storage [*M. Mohammadi et al., 2017; M. Trotta et al., 2003*].

Formulation	Z-Ave [nm ± SD]	PDI [-] ± SD	ZP [mV ± SD]
Unloaded NLC	123.1 ± 0.10	0.180 ± 0.024	-28.6 ± 0.01
PEA-NLC	234.7 ± 0.14	0.186 ± 0.03	-20.0 ± 0.03
PEA OUT NLC	102.1 ± 0.04	0.389 ± 0.05	-35.4 ± 0.02
MGN-NLC	148.9 ± 0.10	0.210 ± 0.04	-23.5 ± 0.20

Table 6. Mean particle size (Z-Ave), polydispersity index (PDI) and zeta potential (ZP) ± standard deviation of unloaded NLC and NLC loaded with PEA. Values are the mean of at least 3 measures.

Furthermore, the HSH/US method used to formulate NLC1, was useful to increase the E.E.% (from 20.6% to 82.3%) and D.L.% (from 0.08% to 0.32%) in comparison with NLC2, which is formulated by the HSH technique.

The morphology of formulations was determined using TEM confirming that particle size was in agreement with DLS data (Figures 59-61). In accordance with DLS data, TEM images of PEA-NLC and MGN-NLC showed that the lipid nanoparticles had a particle size below 200 nm having a spherical appearance.

Furthermore, TEM images showed that the particle internal structure at high magnification (140.000X) evidenced the presence of low-electrondense compartments within the matrix. The presence of low-electrondense spherical objects and their coalescence can be ascribed to the occurrence of oily nano-compartments dispersed in the solid lipid matrix, as previously hypothesized by Muller and coworkers [*R.H. Muller et al., 2002*]. In fact, the relative high oil content and the reduced miscibility during particle solidification cause the separation of the oil, leading to formation nano-compartments within the solid matrix.

These low-electrondense compartments had the tendency to merge together during sample heating by the microscope electron beam (Figure 59). This behavior shows that the internal structure is made up of lipid droplets, on the contrary, if it were gas or water the collapse of the nanoparticles would occur.

Additionally, Figure 60 shows one fractured particle where it is possible to observe oil nano-compartments (red arrows).
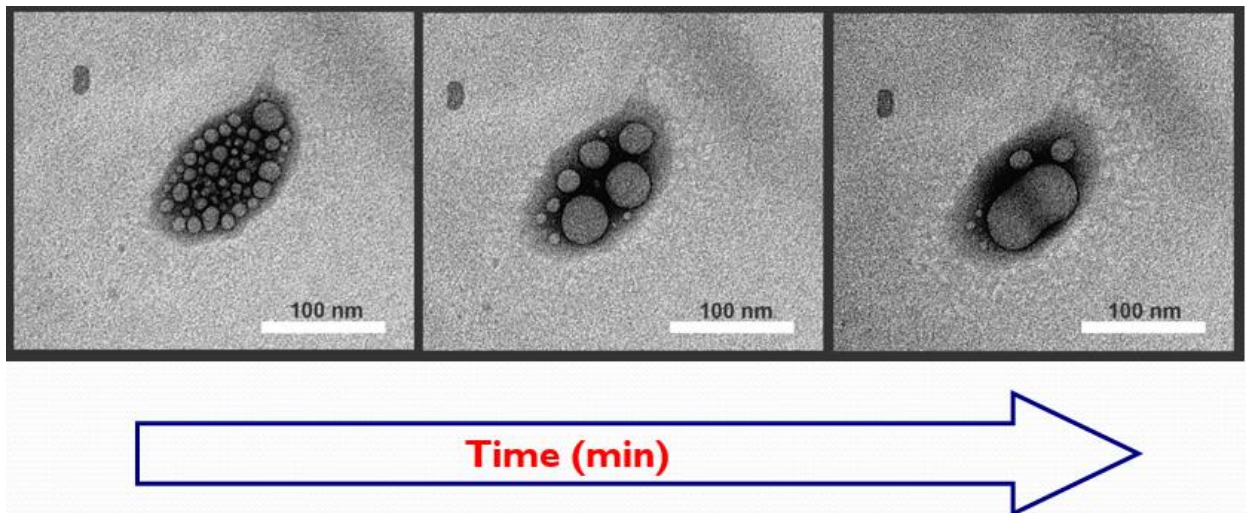
Figure 59. Transmission electron microscopy (TEM) photographs of PEA-NLC during heating.
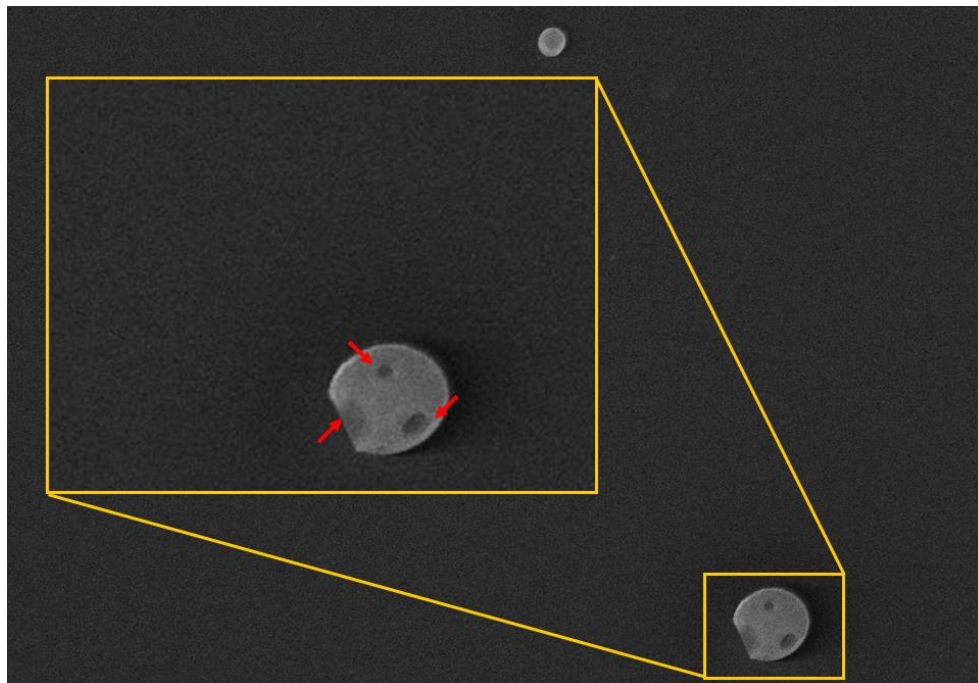
Figure 60. Field emission-scanning electron microscopy (SEM) photographs of a fractured particle (PEA-NLC). Insert: enlargement of the fractured particle. Red arrows indicate the nano-compartments.

121
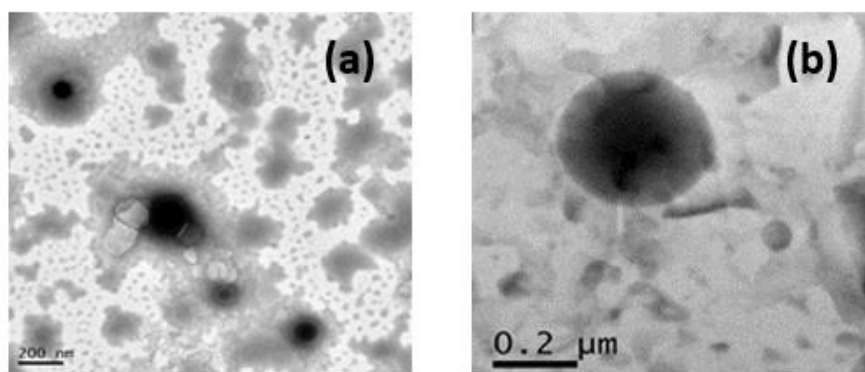
Figure 61. (Figures a-b) Transmission electron microscopy images of MGN-NLC. The scale bar represents 200 nm.

5.3.2. Stability studies on NLCs

The two different methods used to formulate NLCs (NLC1 and NLC2) were further investigated in term of stability.

The physical stability of both formulations was evaluated by Turbiscan, a well-known technology described in literature to achieve objective information about the physical stability of colloidal suspensions in terms of particle migration or aggregation [*C. Carbone et al., 2014; C. Caddeo et al., 2017*]. As clearly shown in the destabilization kinetics reported in figure 62, NLC1 was very stable at both 25 and 35.5°C, since no significant variation in the Turbiscan Stability Index (TSI) was shown after 14 days of storage, while the occurrence of instability phenomena was observed in sample NLC2, even after 1 day of storage.
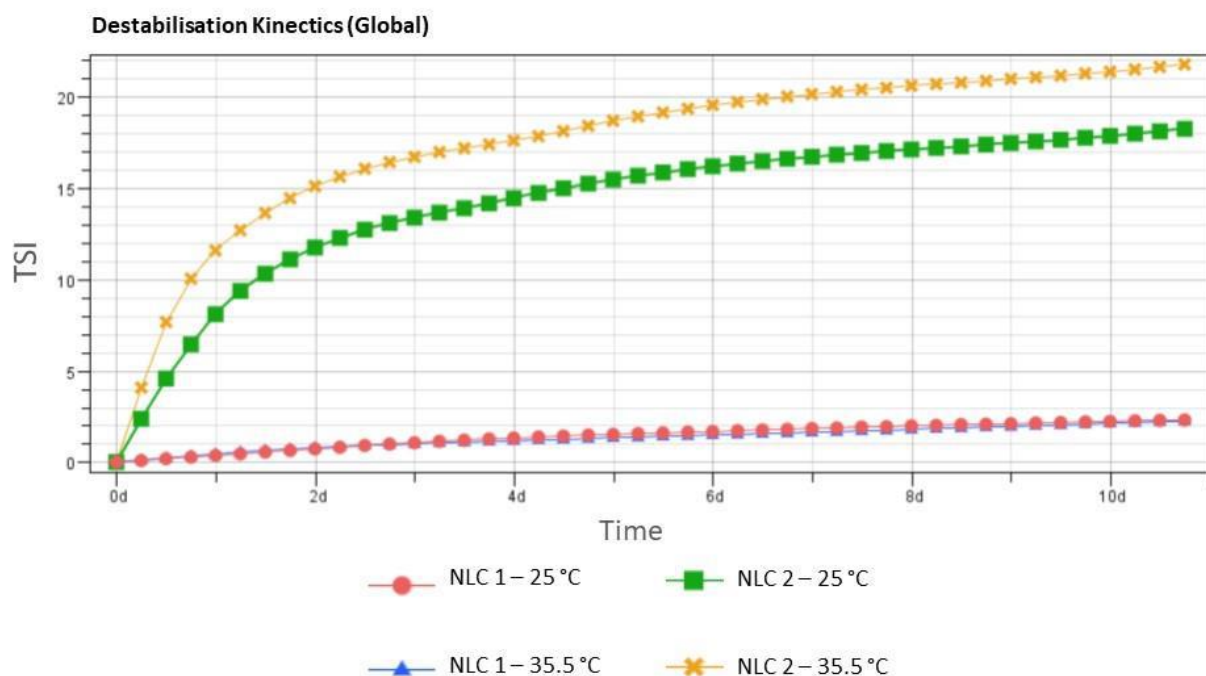
Figure 62. Destabilization kinetics represented in terms of evolution of Turbiscan Stability Index (TSI) of NLC 1 and NLC 2 stored 14 days at 25 and 35.5 °C.

In order to deepen the instability phenomena, I evaluated the backscattering profiles of the formulations stored at 25°C and 35.5°C (Figures 63-64). Interestingly, I observed a linear profile for NLC1, related to high stability at both temperatures, that clearly reveals the absence of particle aggregation and only a slight particle migration toward the bottom of the cuvette, which can be considered not significant ($\Delta BS \ll 10\%$). On the other hand, the backscattering profiles of NLC2 highlight the occurrence of important instability phenomena at both the tested temperatures, which are mainly related to particle aggregation, as clearly shown by the ΔBS values $\geq 20\%$. These results are in accordance with previous findings, demonstrating the greater physical stability of NLC1.
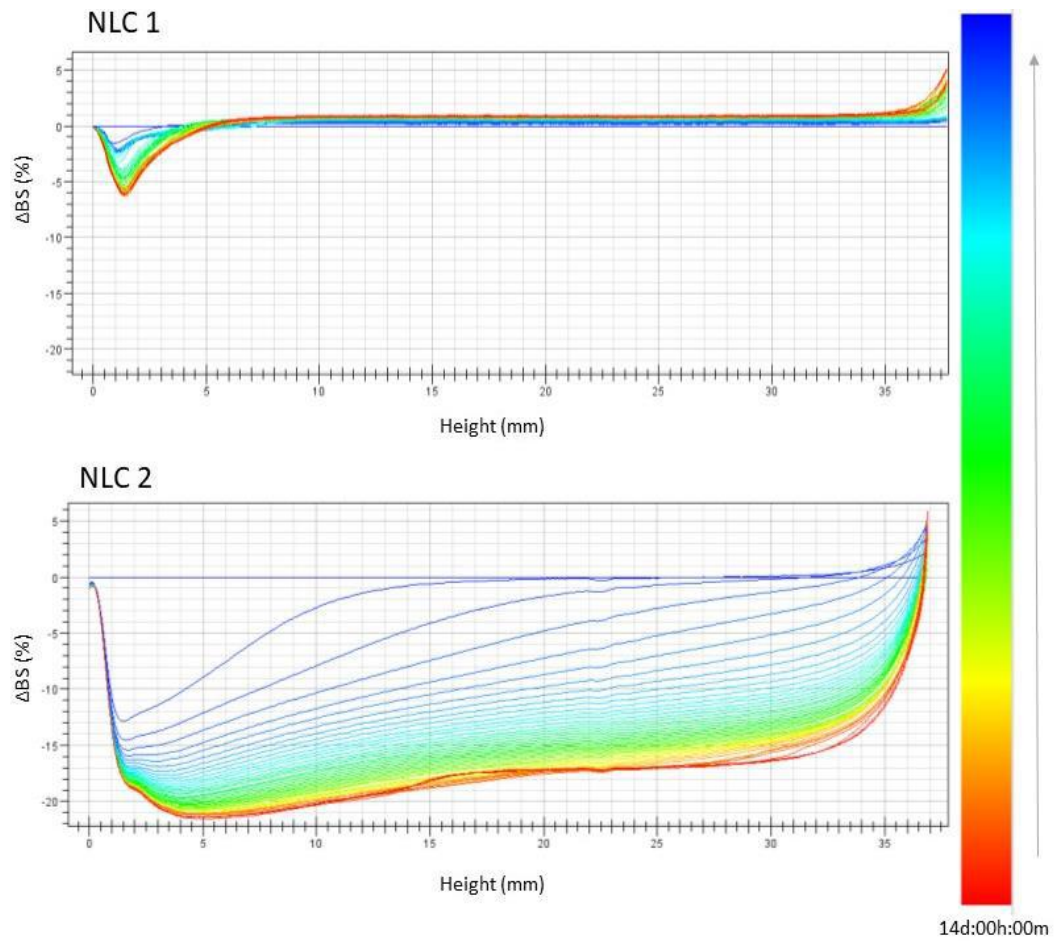
Figure 63. Backscattering profiles (ΔBS) of NLC 1 and NLC 2 stored in Turbiscan at 25.0 ± 1.0 °C. Data are represented as a function of time (0–14 days) of sample height (0–20 mm); the sense of analysis time is indicated by the arrow.
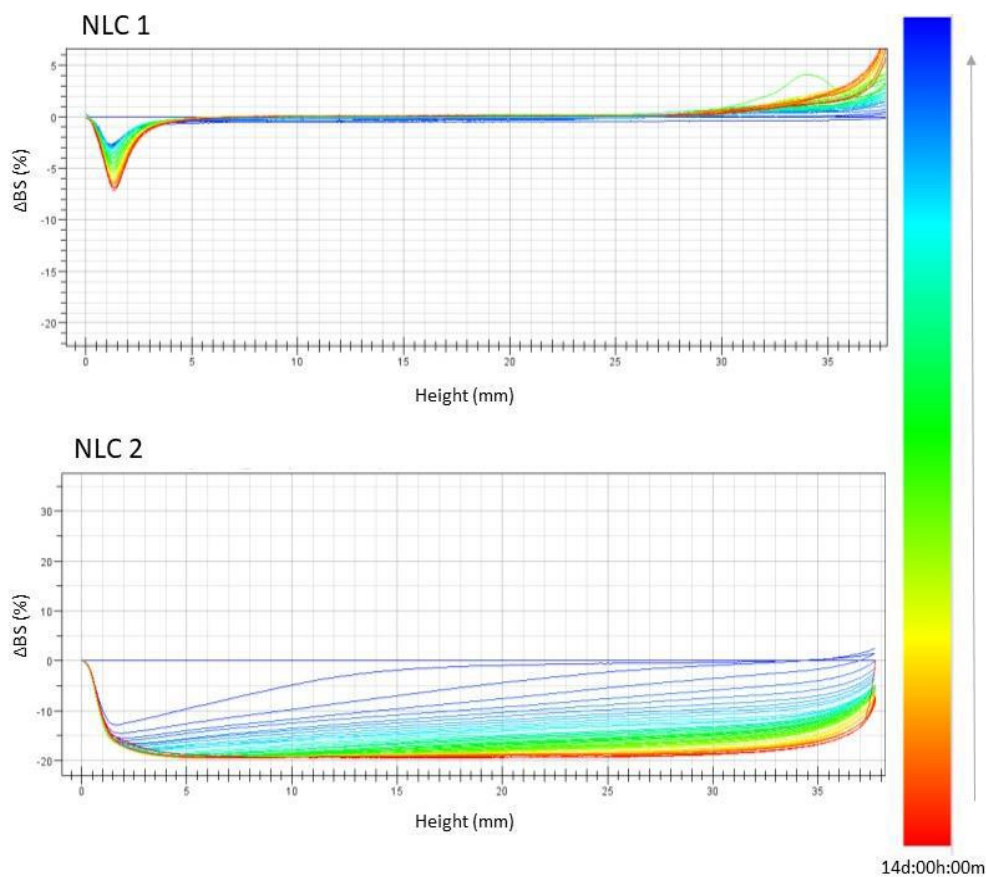
Figure 64. Backscattering profiles (ΔBS) of NLC 1 and NLC 2 stored in Turbiscan at 35.5 ± 1.0 °C. Data are represented as a function of time (0–14 days) of sample height (0–20 mm); the sense of analysis time is indicated by the arrow.

5.3.3. Studies on PEA-NLCs

5.3.3.1. Differential scanning calorimetry (DSC)

As shown in the DSC thermogram (Figure 65), the raw lipid has a melting point of around 75 °C. The heating curves of the blank NLC, PEA-NLC and NLC PEA OUT differ considerably from those of raw lipid and raw surfactant. These data explain that the crystalline structure of the Compritol 888 ATO was modified by the NLC formulation [*A. Sharma et al., 2010*]. This is due to the interaction of the lipid with the other components of the system.
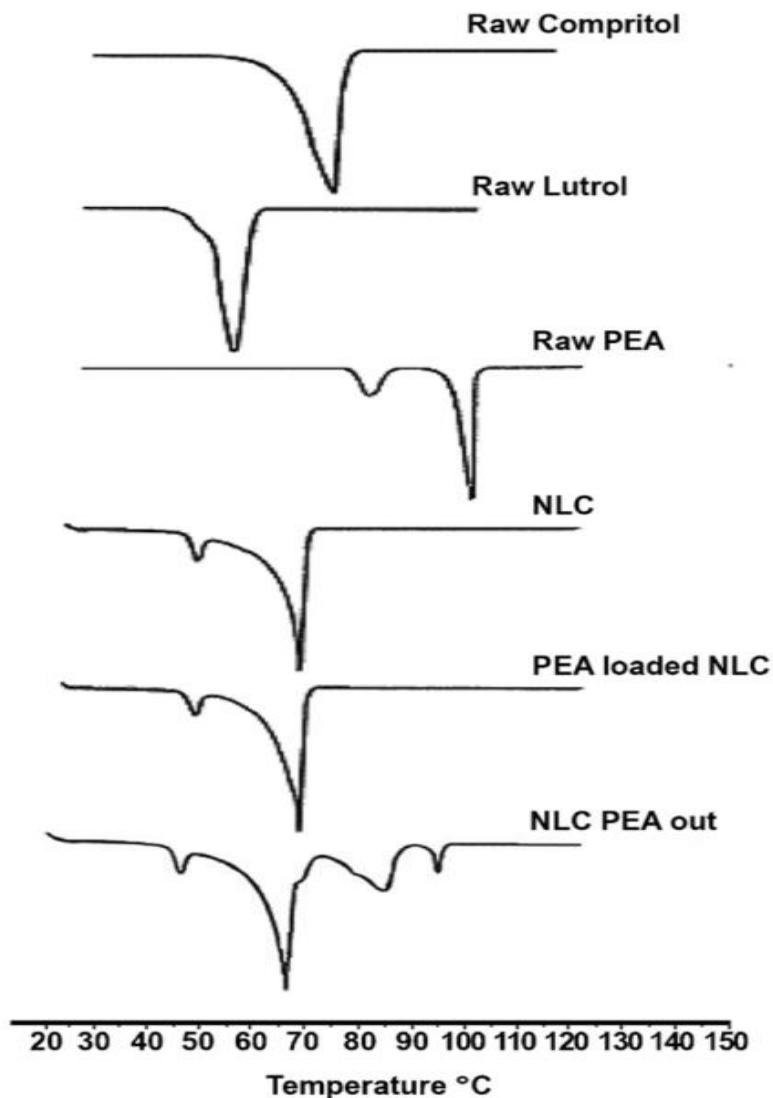
Figure 65. DSC thermogram of raw materials, NLC PEA, NLC PEA out and unloaded NLC.

The melting point of the raw PEA is 103 °C. The heating curve of the PEA-NLC differs from that of the raw PEA: in this case too, a melting point shift has occurred. This confirms that PEA has interacted with the lipid nanoparticles. Further confirmation of the inclusion of PEA into the nanoparticles is provided by the comparison of calorimetric curves between the system loaded with PEA (PEA-NLC) and that in which the compound is outside (NLC PEA OUT). The peak of the raw PEA is not present in the PEA-NLC curve, since it was incorporated into the system.

5.3.3.2. In vivo studies

- Measurements of TNF-alpha

TNF-α represents an inflammatory cytokine, among others, that trigger inflammatory process in the eye and it is the major contributor to the blood–retinal barrier breakdown (BRB) during DR. The induction of TNF-α could be attributed to various mediators that operate during the course of diabetes, such as hyperglycemia and oxidative stress, which signal via NF-κB. The obtained results demonstrated that PEA once loaded in NLC was able to reduce the amount of TNF-α in retinal tissues collected 10 days after STZ injection (Figure 66).
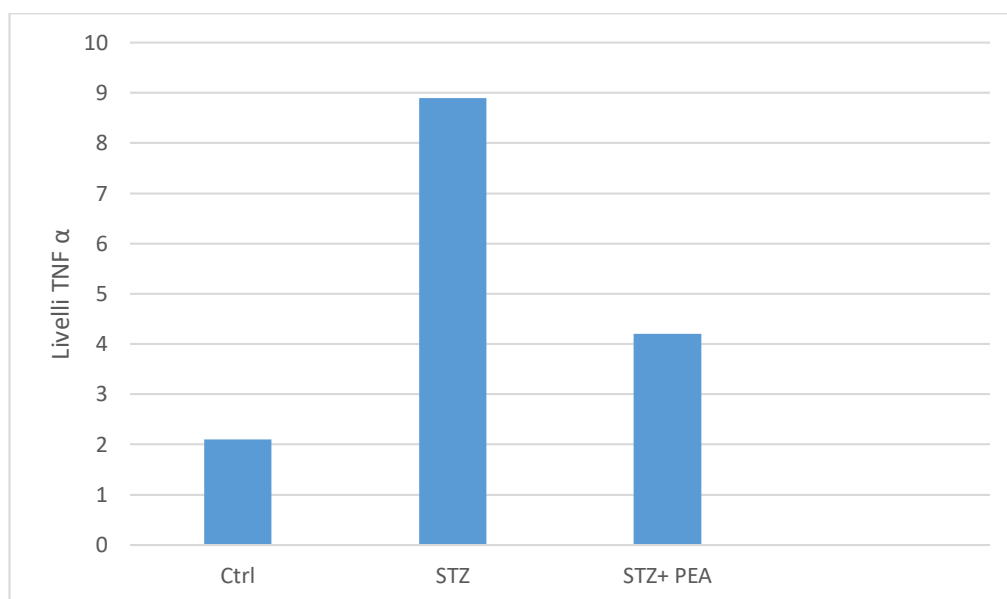
Figure 66. TNF-α levels in retinal tissue 10 days after STZ injection with and without PEA treatment.

These results confirm the evidences observed by Bucolo and coworkers [*C. Bucolo et al., 2013*] regarding the remarkable increase of retinal TNF-α in STZinduced diabetic rats.

Moreover, it was demonstrated the protective effect of PEA on DR [*I. Paterniti et al., 2015*]; this emphasized the importance of a drug targeting strategy in order to maximize PEA pharmacological activity.

- Pharmacokinetic studies and Analytical methods

The pharmacokinetic profile of a single dose (10 µl) of PEA-NLC formulation was compared to the same dose of PEA aqueous suspension (PEA suspension). PEA, administered as an aqueous suspension, did not reach detectable levels in the retina. On the contrary, PEA encapsulated into nanoparticles (PEA-NLC) reached a maximum concentration of 8.3 ng / g after 4 hs from instillation (240 min) via a transscleral route (Figure 67).
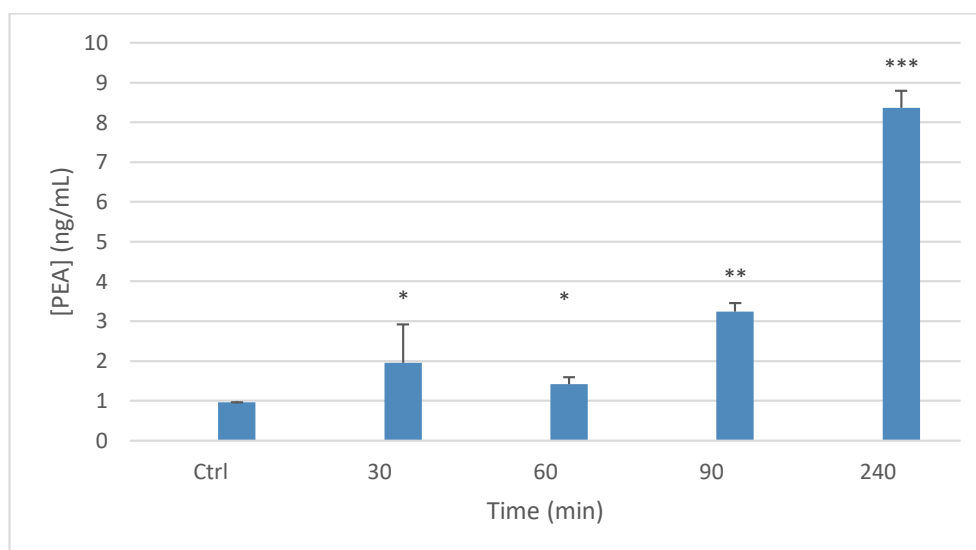
Figure 67. Retinal PEA accumulation during time-course experiments
* p< 0.05 vs control; ** p< 0.01 vs control; ***p< 0.005 vs control.

These results confirmed that PEA, once encapsulated in NLC, was able to reach the posterior eye segment, guaranteeing a prolonged release over time.

- Draize test

Ocular tolerability of blank NLC and PEA-NLC was assessed in rat eye. Both formulations were well tolerated since all the scores of the Draize test were equal to 0 (Table 7).

Formulation	Conjunctiva			Iris (*inflammation degree*)	Cornea (*opacity*)
	Congestion	*Swelling*	*Discharge*		
Blank NLC (10 min)	0	0	0	0	0
Blank NLC (6 h)	0	0	0	0	0
PEA - NLC (10 min)	0	0	0	0	0
PEA - NLC (6 h)	0	0	0	0	0

Table 7. Ocular tolerability

These results suggest that PEA-NLCs could be a new promising strategy for the treatment of DR through topical administration.

5.3.4. Studies on MGN-NLC

5.3.4.1.HET-CAM assay

Ocular tolerability of MGN-NLC was evaluated by HET CAM test. It is an *in vitro* assay highly sensitive for predicting the ocular irritation effect [*F. Alvarez-Rivera et al., 2019*]. This test is an alternative of Draize test and provides information on the potential ocular irritancy of the formulations. Potential ocular irritation effects of MGN-NLC and blank NLC were determined on the chorioallantoic membrane (CAM) of fertilized hen eggs. No damage to the blood vessels on the CAM surface after a 5 min period of contact with MGN-NLC was detected, as reported in figure 68. The IS was 0.0, as occurred with the negative control (0.9% NaCl), while the IS of the positive control was about 18.82. Thus, MGN-NLC can be classified as non-irritant (IS < 1), since no hemorrhage, lysis or coagulation was observed. The slight white halo observed in figures 68C and 68D was due to the milky appearance of the formulations tested.

Therefore, in terms of safety all the components used for the formulation of nanoparticles are safe [*J, Araújo et al., 2011; C. Puglia et al., 2018; E.H. Gökçe et al., 2009; A. Leonardi et al., 2014*], as confirmed by HET CAM test.
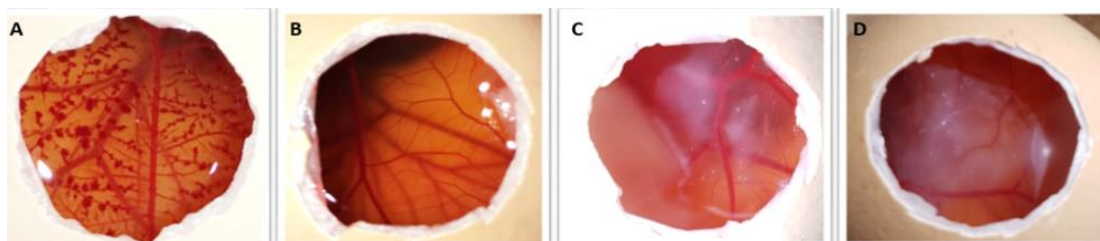
Figure 68. Pictures of chorioallantoic membrane (CAM) after application of: (A) 0.1 M sodium hydroxide (NaOH) solution (positive control), (B) 0.9 wt% saline solution (negative control), (C) blank NLC and (D) MGN-NLC.

5.3.4.2. Hemocompatibility assay

This test is used to evaluate the index of hemocompatibility of materials intended for biological applications. A high hemolysis ratios indicate a damage to the erythrocyte cells.

During the hemolysis, they release the adenosine diphosphate increasing the assembly and adhesion of platelets to the scaffolds, thus accelerating the formation of thrombus. Investigation of the hemocompatibility profiles of tested formulations revealed that they had hemolysis effects about of 10%. Percentage of hemolysis for blank NLC and MGN-NLC were $11.16 \pm 3.12\%$ and $8.10 \pm 0.95\%$, respectively. According to ISO 10993-4, materials showing hemolysis values below 5% are safe [*P.C. Caracciolo et al., 2017]*, therefore, the formulations may cause some damage to the erythrocyte cells.

5.3.4.3. Antioxidant activity of MGN

During the ORAC assay the decay of the fluorescence of fluorescein was monitored. A calibration curve was obtained by plotting the area under the curve (AUC) against trolox concentration ($r^2 = 0.9913$). The ORAC assay was applied to determine the antioxidant activity of the MGN-NLC (0.002

M) using blank NLC, as a control, and MGN solution (free compound, 0.002 M), reaching values of 6494 ± 186, 769 ± 52 and 3521 ± 271 µM TE/g, respectively (Table 8). The values obtained showed that the antioxidant activity of MGN-NLC was higher than that of the free compound (MGN solution). This confirmed that the encapsulation of the drug was able to preserve and increase its activity. These results are in accordance with the findings reported in scientific literature regarding the important role that nanocarriers play in protecting and preserving the drug once encapsulated [*C. Puglia et al., 2019*]. Therefore, the antioxidant activity against radicals ranked in the order MGN-NLC > MGN solution > blank NLC (control).

Formulation	Trolox-equivs. (µM TE/g)
Unloaded NLC (1:50)	769 ± 52
MGN-NLC (1:75)	6494 ± 186
MGN solution (1:50)	3521 ± 271

Table 8. The antioxidant activity of unloaded, MGN-NLC and MGN solution. Results are presented as the mean ± S.D., n=3.

5.3.4.4. Corneal permeability assay

Bovine corneal permeability test for MGN in MGN-NLC formulation was carried out with a view to ascertaining the capability of MGN to permeate through the cornea towards the receptor medium mimicking the aqueous humor. The amounts of MGN that remained in the donor chamber, permeated into the cornea and diffused to the receptor chamber were monitored. Propylene glycol: water (40:60) was used as receptor medium instead of the carbonate buffer pH 7.2 recommended in the BCOP test protocol [*F. Alvarez-Rivera et al., 2016*] due to the low solubility of MGN in aqueous solutions [*J. Acosta et al., 2016*]. The accumulative amount of MGN permeated per area after 6 hs was 2.75 (s.d. 1.18) µg/cm^2, as reported in figure 69, and 1.86 (s.d. 0.51) µg/cm^2 of MGN were held in the cornea. 48.94 (s.d. 4.0) µg/mL of MGN were remained in the donor chamber. This concentration value along

with the steady state flux (J) which was estimated to be 0.73 µg/cm^2/h were used to calculate the permeability coefficient (P_{app}) to be 4.14 x 10^{-6} cm s^{-1}. Furthermore, the t_{lag} was estimated to be 1.69 h. A lag time of ca. 2 hs was observed in agreement with reports for other drugs [*B. Lorenzo-Veiga et al., 2019; A. Varela-Garcia et al., 2018*], which is understandable considering the compact layered structure of the cornea. After 6 hs contact, a relevant amount of MGN accumulated in the cornea, 1.86 (s.d. 0.51) µg/cm^2, and a larger amount permeated, 2.75 (s.d. 1.18) µg/cm^2 The permeability coefficient (P_{app}) obtained (4.14 x 10^{-6} cm s^{-1}) was in the range of those recorded for other NCLs [*R. Liu et al., 2012*] and for other hydrophobic molecules formulated as micelles [*A. Varela-Garcia et al.,2020; F. Alvarez-Rivera et al., 2016*].
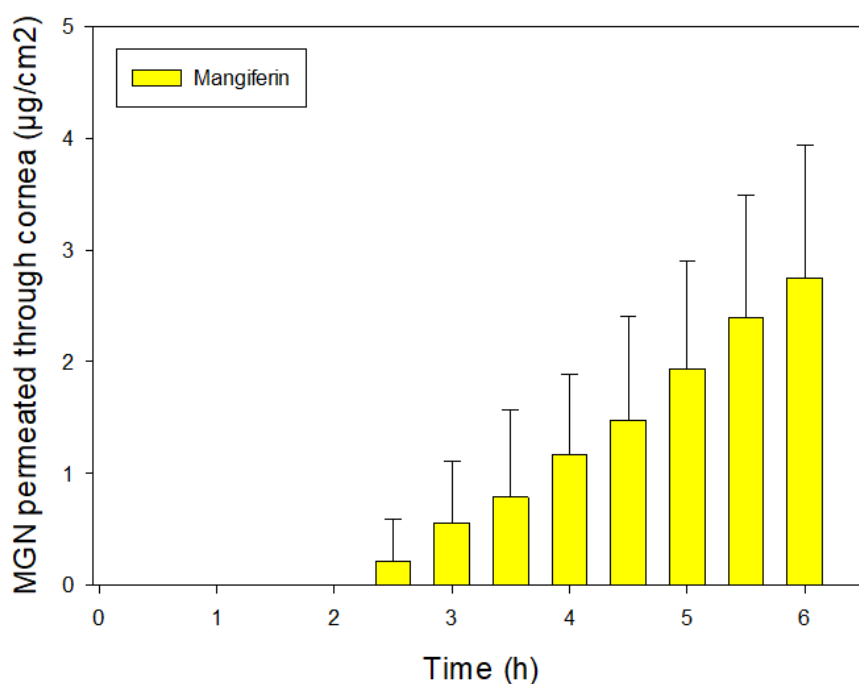
Figure 69. Accumulated amounts of MGN permeated through bovine cornea for 6 hs.

Therefore, NLC system is a promising approach for ocular delivery of MGN.

Chapter 6

6.   Conclusions

The nervous system is the most complex system of our body. It is divided into peripheral (PNS) and central nervous system (CNS), the latter being composed of the brain and spinal cord that constitute the control center of all functions body.

The brain microenvironment, essential for its normal function, is ensured by the blood–brain barrier (BBB), a physical physiological barrier that represents the major obstacle to reach CNS. Due to this complex anatomy, most of the current therapeutic strategies remain ineffective for the CNS treatment.

Nowadays, the incidence of CNS disorders has greatly increased and they represent a serious problem, not only concerning the high costs of treatment, but in addition, the quality of life of the patient. Among these, Alzheimer's disease (AD) is a neurodegenerative disorder of which the main cause is a marked oxidative stress at the level of the encephalic cells. Recent studies indicate that the normalization of antioxidant capacity could represent a very promising therapeutic for the treatment of AD. Moreover, research has made a significant effort to develop innovative therapies based on natural compounds, as old synthetic drugs cause numerous side effects.

CUR and AST are two natural antioxidants that possess therapeutic properties for the treatment of AD, although they show poor biovailability due to their high lipophilicity. In order to overcome these limits that compromise their therapeutic use, the researchers' attention is focused on the development of innovative and efficient stealth carriers (sSLN) loaded with these antioxidants, capable of avoiding the defense line represented by the macrophages and improving the drug stability, in order to achieve good bioavailability in the brain.

The best strategies to realize sSLN, suitable for parenteral administration, were to coat the CUR-SLN surface with hydrophilic polymer PEG (CUR-pSLNs), while the AST-SLN with surfactant polysorbate 80 (AST-p80SLNs).

CUR-pSLNs were prepared by the *solvent evaporation* method obtaining spherical nanoparticles having a particle size suitable for parenteral administration (<200 nm). Nanoparticles showed a good stability for six months at room temperature, as confirmed by Turbiscan Technology. Furthermore, the obtained data showed that the freeze-drying of CUR-pSLNs under optimized conditions lead to a lyophilized sample with good reconstitution properties, thus protecting the drug.

Finally, CUR-pSLNs showed greater antioxidant activity over time than free CUR, confirming the key role of encapsulation in preserving and therefore increasing the antioxidant activity of powerful active compounds.

Regarding AST, AST-p80SLNs were prepared by *solvent-diffusion* technique showing a good mean particle size suitable for parenteral administration (<200 nm), as confirmed by TEM. In term of stability, AST-p80SLN showed an acceptable stability during six months of storage. Moreover, the formulation did not produce toxic effects on the cell cultures. In addition, AST-p80SLNs showed greater antioxidant activity over time than free AST. The protective effect of SLN was further demonstrated by UV stability assay confirming that the lipid shell protected AST from photodegradation.

In conclusion, the pharmacological activity of CUR-pSLNs and AST-p80SLNs have been evaluated by *in vivo* assay using transgenic mice TgCRND8. The obtained results showed that the cognitive deficit was completely recovered. Therefore, CUR-pSLNs and AST-p80SLNs could be regarded as a promising carriers for the treatment of CNS disorders, through systemic administration.

An injury to the nerves of the PNS or the structures of the CNS causes a chronic painful sensation called neuropathic pain. The perception of pain involves nociceptors, of which TRPV1 receptor is the most studied.

Capsaicin is a natural agonist highly selective of TRPV1 that allows used for the treatment of thermal hyperalgesia in chronic pain conditions. Since prolonged exposure to CPS induces TRPV1

defunctionalization, CPS loaded lipid nanocarriers (CPS-SLNs) were formulated in order to optimize CPS release, thus preventing TRPV1 internalization and degradation. CPS-SLNs were prepared by using the *solvent injection* method showing a good homogeneity and a high encapsulation efficiency. AFM study revealed a regular shape of the SLN. *In vivo* study pointed out that CPS inclusion into SLN induced a lower pain response compared to drug dissolved in a standard vehicle (CPS-STD). Therefore, CPS-SLNs were able to provide a long term activation of TRPV1 receptors without the unwanted reduction of TRPV1 receptor expression.

In conclusion, SLNs could be useful as a valid alternative to conventional vehicles when a controlled release of CPS is required to prevent TRPV1 defunctionalization after a prolonged activation of the receptor.

Retina is defined the "window to the brain" as it considered integral parts of the CNS. It is the site of many ocular diseases. The conventional therapies (eye drop, ocular injection or ocular implant) show many disadvantages such as low bioavailability, high costs and low patient compliance.

Recently, the development of lipid-based nanocarriers, in particular the NLC, has made it possible to overcome these problems and improve the ocular bioavailability of natural ophthalmic drugs.

PEA is a molecule that has numerous therapeutic properties, in fact it can be considered a good candidate for the treatment of retinal pathologies, such as diabetic retinopathy. It has never been formulated as eye drops due to its high lipophilicity. This obstacle has been overcome by encapsulating this compound in the NLCs, as they are able to deliver PEA in the posterior eye segment and to improve the ocular bioavailability of drug.

NLCs have been formulated using two well-known techniques, such as the high shear homogenization technique (HSH) and the method based on a combination of HSH technique and ultrasound (HSH / US), to obtain NLC suitable for ocular administration.

NLC1 formulated following the *HSH/US* method provided better results in terms of mean particle size (Z-Ave), population homogeneity (PDI), and ZP with respect to NLC2 formulated by HSH technique. This result outlines the important role of US in controlling the final dimension of a lipid nanoparticle dispersion. Stability studies by Turbiscan®AGS demonstrated that NLC1 have a greater physical stability compared to NLC2 due to the higher energy applied in the emulsification process used in the HSH/US method. Therefore, it was proved that sonication represents a key intermediate step for the formation of colloidal suspensions of small homogeneously dispersed nanoparticles with very high stability without the occurrence of particle migration/aggregation phenomena during storage.

As demonstrated by the Draize test, PEA-NLC formulation has high tolerability and stability.

In *vivo* studies showed that the drug reaches the target site, the retinal tissue, through a transscleral route. This is demonstrable as no significant drug concentrations were found at the level of the inner segments of the eye. Furthermore, a progressive increase of the PEA concentration at the retinal level has been observed; the maximal concentration was about 4 hs after instillation. Therefore, the results demonstrated that PEA-NLC formulation for ophthalmic application, has a unique pharmacological profile both in terms of retinal distribution and inhibition of inflammation.

MGN is another potential natural compound for the potential treatment of eye diseases. Although it has a wide range of pharmacological properties, including anti-inflammatory and antioxidant activities, its use in ophthalmology is compromised due to its high lipophilicity. This obstacle has been overcome by encapsulating this compound in the NLC. MGN-NLCs, formulated by *HSH/US* method, showed an appropriate particle size, good stability, high ophthalmic tolerability and adequate corneal permeability. Furthermore, the antioxidant activity of MGN-NLC was higher than free compound. This demonstrated that the carrier preserved the drug.

In conclusion, these findings suggest that the NLC system is a potential strategy to improve ocular bioavailability of lipophilic drugs.

Bibliography

Abdelwahed W. Lyophilization of solid lipid nanoparticles for brain targeting. Int. J. Pharm. Pharm. Sci. 2015, 7, 381–385.

Abdelwahed W., Degobert G., Stainmesse S., Fessi H. Freeze- drying of nanoparticles: formulation, process and storage consideration. Adv Drug Deliv Rev 2006, 58, 1688-1713.

Acosta J., Sevilla I., Salomón S., Nuevas L., Romero A., Amaro D. Determination of mangiferin solubility in solvents used in the biopharmaceutical industry. J Pharm Pharmacogn Res 2016, 4, 49-53.

Aftab N., Vieira A. Antioxidant Activities of Curcumin and Combinations of This Curcuminoid With Other Phytochemicals. Phytother Res 2010 Apr;24(4):500-2. doi: 10.1002/ptr.2960.

Aggarwal B.B., Harikumar K.B. Potential therapeutic effects of curcumin, the anti-inflammatory agent, against neurodegenerative, cardiovascular, pulmonary, metabolic, autoimmune and neoplastic diseases. Int J Biochem Cell Biol 2009, 41, 40-59.

Aiello L.P., Northrup J.M., Keyt B.A., Takagi H., Iwamoto M. A. "Hypoxic regulation of vascular endothelial growth factor in retinal cells," Archives of Ophthalmology, vol. 113, no. 12, pp. 1538–1544, 1995.

Allèmann E., Gurny R., Doelker E. Drug loaded nanoparticles- preparation methods and drug targeting issues. Eur J Pharm Biopharm 1993, 39: 173-191.

Alvarez-Rivera F., Fernández-Villanueva D., Concheiro A., Alvarez-Lorenzo C. α-Lipoic Acid in Soluplus (®) Polymeric Nanomicelles for Ocular Treatment of Diabetes-Associated Corneal Diseases. J Pharm Sci 2016, 105, 2855-2863. DOI: 10.1016/j.xphs.2016.03.006

Alvarez-Rivera F., Serro A.P., Silva D., Concheiro A., Alvarez-Lorenzo C. Hydrogels for diabetic eyes: Naltrexone loading, release profiles and cornea Penetration. Mater Sci Eng C 2019, 105:110092. DOI: 10.1016/j.msec.2019.110092

Amantini C., Mosca M., Nabissi M., Lucciarini R., Caprodossi S., Arcella A., Giangaspero F., Santoni G. Capsaicin-induced apoptosis of glioma cells is mediated by TRPV1 vanilloid receptor and requires p38 MAPK activation. J. Neurochem. 2007, 102, 977–990.

Ambruosi A., Yamamoto H., Kreuter J. Body distribution of polysorbate80 and doxorubicin-loaded [14C]poly(butyl cyanoacrylate) nanoparticles after i.v. administration in rats. J. Drug Target 13, 535–542 (2005)

Anand P., Kunnumakkara A.B., Newman R.A., Aggarwal B.B. Bioavailability of curcumin: problems and promises. Mol Pharm 2007, 4, 807-818.

Araújo J., Nikolic S., Egea M.A., Souto E.B., Garcia M.L. Nanostructured lipid carriers for triamcinolone acetonide delivery to the posterior segment of the eye. Colloids Surf B Biointerfaces 2011, 88, 150–157. DOI: 10.1016/j.colsurfb.2011.06.025

Arranja A., Gouveia L.F., Gener P., Rafael D.F., Pereira C., Schwartz S.J., Videira M.A. Self-assembly PEGylation assists SLN-paclitaxel delivery inducing cancer cell apoptosis upon internalization. Int J Pharm 2016, 501, 180-9.

Ausborn M., Nuhn P., Schreier H. Stabilization of liposomes by freeze–thaw and lyophilization techniques: problems and opportunities, Eur. J. Pharm. Biopharm., 1992; 38:133–139.

Awika J.M., Rooney L.W., Wu X., Prior R.L., Cisneros-Zevallos L. Screening methods to measure antioxidant activity of sorghum (sorghum bicolor) and sorghum products. J. Agric. Food Chem. 2003, 51, 6657–6662.

Balguri S.P., Adelli G.R., Majumdar S. (2016). Topical ophthalmic lipid nanoparticle formulations (SLN, NLC) of indomethacin for delivery to the posterior segment ocular tissues. Eur. J. Pharm. Biopharm. 109, 224–235.

Banks W.A. Characteristics of compounds that cross the blood-brain barrier. BMC Neurology 2009, 9 (Suppl 1), S3.

Basso L., Aboushousha R., Fan C.Y., Iftinca M., Melo H., Flynn R., Agosti F., Hollenberg M.D., Thompson R., Bourinet, E. TRPV1 promotes opioid analgesia during inflammation. Sci. Signal 2019, 12, eaav0711.

Basso L.G.M., Rodrigues R.Z., Naal R.M.Z.G., Costa Filho A. G. Effects of the antimalarial drug primaquine on the dynamic structure of lipid model membranes. Biochim. Biophys. Acta 2011, 1808, 55−64.

Battaglia L., Serpe L., Foglietta F., Muntoni E., Gallarate M., Del Pozo Rodriguez A., Solinis M.A. Application of lipid nanoparticles to ocular drug delivery. Expert Opin Drug Deliv 2016, 13, 1743–1757. DOI: 10.1080/17425247.2016.1201059

Beebe D.C., Holekamp N.M., Shui Y.B. 2010. Oxidative damage and the prevention of age-related cataracts. Ophthalmic Res 2010, 44, 155–165. DOI: 10.1159/000316481

Bellucci A., Luccarini I., Scali C., Prosperi C., Giovannini M.G., Pepeu G., Casamenti F. Cholinergic dysfunction, neuronal damage and axonal loss in TgCRND8 mice. Neurobiol Dis 2006; 23, 260-272.

Bensouda Y., Cave´ G., Seiller M., Puisieux F. Freeze drying of emulsions influence of congealing on granulometry research of a cryoprotectant agent, Pharm. Acta Helv.,1989; 64:40–44.

Betancourt, T., Byrne J. D., Sunaryo N., Crowder S.W., Kadapakkam M., Patel S., Casciato S., Brannon-Peppas L. PEGylation strategies for active targeting of PLA/PLGA nanoparticles. J. Biomed. Mater. Res. A 2009, 91 (1), 263−276.

Bhatt P.C., Srivastava P., Pandey P., Khan W., Panda B.P. Nose to brain delivery of astaxanthin loaded solid lipid nanoparticles: fabrication, radio labeling, optimization and biological studies. RSC Advances (2015) RA-ART-09-2015-019113.R1.

Bilia A.R., Nardiello P., Piazzini V., Leri M., Bergonzi M.C., Bucciantini M., Casamenti F. Successful Brain Delivery of Andrographolide Loaded in Human Albumin Nanoparticles to TgCRND8 Mice, an Alzheimer's Disease Mouse Model. Front. Pharmacol. 2019; 10:910. doi: 10.3389/fphar.2019.00910.

Bley K.R. TRPV1 agonist approaches for pain management. In Vanilloid Receptor TRPV1 in Drug Discovery: Targeting Pain and Other Pathological Disorders; Gomtsyan, A., Faltynek, C.R., Eds.; Wiley: New York, NY, USA, 2010; pp. 325–347.

Bode A.M., Cho Y.Y., Zheng D., Zhu F., Ericson M.E., Ma W.Y., Yao K., Dong Z. Transient receptor potential type vanilloid 1 suppresses skin carcinogenesis. Cancer Res. 2009, 69, 905–913.

Bonaventura G., Incontro S., Iemmolo R., La Cognata V., Barbagallo I., Costanzo E., Barcellona M.L., Pellitteri R., Cavallaro S. Dental mesenchymal stem cells and neuro-regeneration: a focus on spinal cord injury. Cell Tissue Res 2019, 67, 84–93.

Brederson J.D., Kym P.R., Szallasi A. Targeting TRP channels for pain relief. Eur. J. Pharmacol. 2013, 716, 61–76.

Brigger I., Dubernet C., Couvreur P. Nanoparticles in Cancer Therapy and Diagnosis. Advanced Drug Delivery Reviews, 2002,54: 631–651.

Brugè F., Damiani E., Puglia C., Offerta A., Armeni T., Littarru G.P., Tiano L. Nanostructured lipid carriers loaded with CoQ10: Effect on human dermal fibroblasts under normal and UVA-mediated oxidative conditions. Int J Pharm 2013, 455, 348–356. DOI: 10.1016/j.ijpharm.2013.06.075

Bucolo C., Drago F., Salomone S. Ocular drug delivery: a clue from nanotechnology. Front Pharmacol 2012, 3. DOI: 10.3389/fphar.2012.00188

Bucolo C., Marrazzo G., Platania C.B.M., Drago F., Leggio G.M., Salomone S. Fortified extract of red berry, ginkgo biloba, and white willow bark in experimental early diabetic retinopathy. J Diabetes Res. 2013; 2013:432695.

Caddeo C., Pons R., Carbone C., Fernandez-Busquets X., Cardia M.C., Maccioni A.M., Fadda A.M., Manconi M. Physico-chemical characterization of succinyl chitosan-stabilized liposomes for the oral co-delivery of quercetin and resveratrol. Carbohydr. Polym. 2017, 157, 1853–1861.

Calderon G.D., Juarez O.H., Hernandez G.E., Punzo S.M., De la Cruz Z.D. Oxidative stress and diabetic retinopathy: development and treatment. Eye (Lond) 2017; 31(8):1122-1130.

Campisi A., Spatuzza M., Russo A., Raciti G., Vanella A., Stanzani S., Pellitteri R. Expression of tissue transglutaminase on primary olfactory ensheathing cells cultures exposed to stress conditions. Neurosci Res 72:89–295, 2012.

Cao G., Alessio H.M., Cutler R.G. Oxygen-radical absorbance capacity assay for antioxidants. Free Radic. Biol. Med. 1993, 14, 303–311.

Caracciolo P.C., Rial-hermida M.I., Montini-ballarin F., Abraham G.A., Concheiro A., Alvarez-Lorenzo C. Surface-modified bioresorbable electrospun scaffolds for improving hemocompatibility of vascular grafts. Mater Sci Eng C 2017, 75,1115–27. DOI: 10.1016/j.msec.2017.02.151

Carbone C., Campisi A., Manno D., Serra A., Spatuzza M., Musumeci T., Bonfanti R., Puglisi G. The critical role of didodecyldimethylammonium bromide on physico-chemical, technological and biological properties of NLC. Colloids Surf. B Biointerfaces 2014, 121, 1–10.

Carbone C., Fuochi V., Zielińska A., Musumeci T., Souto E.B., Bonaccorso A., Puglia C., Petronio Petronio G., Furneri P.M. Dual-drugs delivery in solid lipid nanoparticles for the treatment of Candida albicans mycosis. Colloids Surf. B Biointerfaces 2020, 186, 110705.

Carbone C.; Caddeo C., Grimaudo M.A., Manno D.E., Serra A., Musumeci T. Ferulic Acid-NLC with Lavandula Essential Oil: A Possible Strategy for Wound-Healing? Nanomaterials 2020, 10, 898–916.

Cardoso A.M., Guedes J.R., Cardoso A.L., Morais C., Cunha P., Viegas A.T., Costa R., Jurado A., Pedroso de Lima M.C. Recent Trends in Nanotechnology Toward CNS Diseases: Lipid-Based Nanoparticles and Exosomes for Targeted Therapeutic Delivery. Int Rev Neurobiol 2016; 130:1-40. doi: 10.1016/bs.irn.2016.05.002. Epub 2016 Jun 21.

Caterina M.J., Leffler A., Malmberg A.B., Martin W.J., Trafton J., Petersen-Zeitz K.R., Koltzenburg M., Basbaum A.I., Julius D. Impaired nociception and pain sensation in mice lacking the capsaicin receptor. Science 2000, 288, 306–313.

Caterina, M.J. Transient receptor potential ion channels as participants in thermosensation and thermoregulation. Am. J. Physiol. Regul. Integr. Comp. Physiol. 2007, 292, R64–R76.

Chattopadhyay I., Biswas K., Bandyopadhyay U., Banerjee R.K. Turmeric and curcumin. Biological actions and medicinal applications. Curr Sci 2004, 87, 44-50

Chen C., Cheng Y.C., Yu C.H., Chan S.W., Cheung M.K., Yu P.H.F. In vitro cytotoxicity, hemolysis assay, and biodegradation behavior of biodegradable poly (3- hydroxybutyrate) –poly (ethylene glycol)-poly(3-hydroxybutyrate) nanoparticles as potential drug carriers. J Biomed Mater Res A 2008, 87, 290-298. DOI: 10.1002/jbm.a.31719

Chishti M.A. , Yang D. S., Janus C., Phinney A. L., Horne P., Pearson J., Strome R., Zuker N., Loukides J., French J., Turner S., Lozza G., Grilli M., Kunicki S., Morissette C., Paquette J., Gervais F., Bergeron C., Fraser P.E., Carlson G.A., George-Hyslop P.S., Westaway D. Early-

onset amyloid deposition and cognitive deficits in transgenic mice expressing a double mutant form of amyloid precursor protein 695. J Biol Chem 2001;276(24):21562-70. doi: 10.1074/jbc.M100710200.

Choongjin B., Seokwon L., Pahn-Shick C., Young J.C. Enhancing the stability of lipid nanoparticle systems by sonication during the cooling step and controlling the liquido oil content. J Agric Food Chem 2014;62(47):11557-67.

Chorover, S. L., & Schiller, P. H. (1965). Short-term retrograde amnesia in rats. *Journal of Comparative and Physiological Psychology, 59*(1), 73–78. doi:10.1037/h0021606.

Chow B.W., Gu C. (2015). The molecular constituents of the blood-brain barrier. Trends in Neurosciences, 38, 598–608.

Clapham D.E., Runnels L.W., Strubing C. The TRP ion channel family. Nat. Rev. Neurosci. 2001, 2, 387–396.

Coburn O.H., Graham C.E., Haninger J. The effect of egg yolk in diets on anaphylactic arthritis (passive Arthus phenomenon) in the guinea pig. Journal of Experimental Medicine, 100 (5) (1954), pp. 425-435.

Coffin M.D., McGinity J.W. Biodegradable pseudolatexes: the chemical stability of poly (D, L-lactide) and poly(epsilon-caprolactone) nanoparticles in aqueous media. Pharm Res 1992, 9, 200–205.

Corrias F., Lai F. New methods for lipid nanoparticles preparation. Recent Pat. Drug Deliv. Formul., 2011, 5(3),201-213. http://dx.doi.org/10.2174/187221111797200597

Costagliola C., Romano M. R., Dell'Omo R., Russo A., Mastropasqua R., Semeraro F. Effect of palmitoylethanolamide on visual field damage progression in normal tension glaucoma patients:

results of an open-label six-month follow-up. J. Med. Food 2014, 17, 949–954. doi: 10.1089/jmf.2013.0165.

Crascì L., Cardile V., Longhitano G., Nanfitò F., Panico A. Anti-degenerative effect of Apigenin, Luteolin and Quercetin on human keratinocyte and chondrocyte cultures: SAR evaluation. Drug Res (Stuttg) 2018, 68, 132-138.

Crowe L.M., Crowe J.H. Stabilization of dry liposomes by carbohydrates, Dev. Biol. Stand.,1992; 74:285–294.

Crowe L.M., Womersley C., Crowe J.H., Reid D., Appel L., Rudolph A. Prevention of fusion and leakage in freeze-dried liposomes by carbohydrates, Biochim. Biophys. Acta,1986; 861:131–140.

D'Agostino G., La Rana G., Russo R., Sasso O., Iacono A., Esposito E., Raso G.M., Cuzzocrea S., Lo Verme J., Piomelli D., Meli R., Calignano A. Acute intracerebroventricular administration of palmitoylethanolamide, an endogenous peroxisome proliferator-activated receptor-alpha agonist, modulates carrageenan-induced paw edema in mice. J Pharmacol Exp Ther. 2007; 322(3):1137-1143.

Damiani E., Astolfi P., Giesinger J., Ehlis T., Herzog B., Greci L., Baschong W. 2010, Assessment of the photo-degradation of UV-filters and radical-induced peroxidation in cosmetic sunscreen formulations, Free Radic Res 44:304–312

Das S., Chaudhury A. Recent advances in lipid nanoparticle formulations with solid matrix for oral drug delivery. AAPS PharmSciTech, 2011, 12(1), 62-76. http://dx.doi.org/10.1208/s12249-010-9563-0

Davis C.B., Markey C.E., Busch M.A., Busch K.W. Determination of capsaicinoids in habanero peppers by chemometric analysis of UV spectral data. J Agric Food Chem 2007, 55, 5925-5933.

Del Amo E.M., Urtti A. Current and future ophthalmic drug delivery systems. A shift to the posterior segment. Drug Discov Today 2008, 13, 135–143. DOI: 10.1016/j.drudis.2007.11.002

Devchand P.R., Hihi A.K., Perroud M., Schleuning W.D., Spiegelman B.M., Wahli W. Chemical probes that differentially modulate peroxisome proliferator-activated receptor alpha and BLTR, nuclear and cell surface receptors for leukotriene B(4), J Biol Chem, 274 (1999) 23341-23348.

Dhananjaya B.L., Shivalingaiah S. The anti-inflammatory activity of standard aqueous stem bark extract of Mangifera indica L. as evident in inhibition of Group IA sPLA2. An. Acad. Bras. Cienc. 2016;88: 197–209. doi: 10.1590/0001-3765201620140574

Doebbler G.F. Cryoprotective compounds, Cryobiology,1966; 3:2–11.

Dong Z., Guo J., Xing X., Zhang X., Du Y., Lu Q. RGD modified and PEGylated lipid nanoparticles loaded with puerarin: Formulation, characterization and protective effects on acute myocardial ischemia model Biomedicine & Pharmacotherapy 89 (2017) 297–304.

Duan Y., Cai X., Du H., Zhai G. (2015). Novel in situ gel systems based on P123/TPGS mixed micelles and gellan gum for ophthalmic delivery of curcumin. Colloids Surf. B Biointerfaces 128, 322–330.

Ellison N., Loprinzi C.L., Kugler J., Hatfield A.K., Miser A., Sloan J.A., Wender D.B., Rowland K.M., Molina R., Cascino T.L. Phase III placebo-controlled trial of capsaicin cream in the management of surgical neuropathic pain in cancer patients. J. Clin. Oncol. 1997, 15, 2974–2980.

Engels C., Knödler M., Zhao Y.Y., Carle R., Gänzle M.G., Schieber A. Antimicrobial activity of gallotannins isolated from mango (Mangifera indica L.) kernels. J Agric Food Chem 2009, 57, 7712–7718. DOI: 10.1021/jf901621m.

Ennaceur A., Delacour J. A new one-trial test for neurobiological studies of memory in rats. 1: Behavioral data. Behav Brain Res 1988;31(1):47-59. DOI: 10.1016/0166-4328(88)90157-x.

Esposito E., Drechsler M., Mariani P., Carducci F., Servadio M., Melancia F., Ratano P., Campolongo P., Trezza V., Cortesi R., Nastruzzi C. Lipid nanoparticles for administration of poorly water soluble neuroactive drugs. Biomed Microdevices 2017; 19: 44.

Esposito E., Ravani L., Mariani P., Contado C., Drechsler M., Puglia C., Cortesi R. Curcumin containing monoolein aqueous dispersions: a preformulative study. Mater Sci Eng C Mater Biol Appl 2013, 33, 4923-34.

Esposito, E. Innovative Nanotechnology Based Systems for Dermal Application, 2005, http://www.pharmainfo.net

Fairless R., Barnett S.C. (2005) Olfactory ensheathing cells: their role in central nervous system repair. Int J Biochem Cell Biol 37:693–699.

Fakhri S., Aneva I.Y., Farzaei M.H., Sobarzo-Sánchez E. The Neuroprotective Effects of Astaxanthin: Therapeutic Targets and Clinical Perspective. Molecules 2019;24(14):2640.

Ferrer-Montiel A., Garcia-Martinez C., Morenilla-Palao C.; Garcia-Sanz N., Fernandez-Carvajal A., Fernandez-Ballester G., Planells-Cases R. Molecular architecture of the vanilloid receptor. Insights for drug design. Eur. J. Biochem. 2004, 271, 1820–1826.

Fonseca-Santos B., Bento Silva P., Balasin Rigon R., Rillo Sato M., Chorilli M. Formulating SLN and NLC as Innovative Drug Delivery Systems for Non-Invasive Routes of Drug Administration. Current Medicinal Chemistry, 2020, 27, 3623-3656.

Frank M.M., Fries L.F. The role of complement in inflammation and phagocytosis. Frank MM1, Fries LF. Immunol Today 1991, 12, 322-6.

Freitas C., Lucks J.S., Muller R.H. Effect of storage condition on long-term stability of solid lipid nanoparticles (SLNs) in aqueous dispersion. Proceedings of 1st World Meeting on Pharmaceutics,

Biopharmaceutics, Pharmaceutical Technology, APGI/APV, Budapest, 9 to 11 May 1995, 493-494.

http://www.muller-berlin.com/publicat.htm

Freitas C., Muller R.H. Correlation between long-term stability of solid lipid nanoparticles (SLNs) and crystallinity of lipid phase. Eur. J. Pharm. Biopharm. 1999, 47, 125–132.

Fu M., Xie Z., Zuo H. TRPV1: A potential target for antiepileptogenesis. Med. Hypotheses 2009, 73, 100–102.

Galano A., Martinez A. Capsaicin, a tasty free radical scavenger: Mechanism of action and kinetics. J. Phys. Chem. 2012, 116, 1200–1208.

Ganley O.H., Graessle O.E., Robinson H.J. Anti-inflammatory activity of compounds obtained from egg yolk, peanut oil, and soybean lecithin. Translational Research 1958, 51 (5):709-714. doi:10.5555/uri:pii:0022214358902063.

Gaspar D.P., Gaspar M.M., Eleutério C.V., Grenha A., Blanco M., Gonçalves L.M.D., Taboada P., Almeida A.J., Remuñán-López C. Microencapsulated Solid Lipid Nanoparticles as a Hybrid Platform for Pulmonary Antibiotic Delivery. Mol Pharm. 2017 Sep 5;14(9):2977-2990. doi: 10.1021/acs.molpharmaceut.7b00169.

Geszke-Moritz M., Moritz M. (2016). Solid lipid nanoparticles as attractive drug vehicles: Composition, properties and therapeutic strategies. Mater Sci. Eng. C. Mater Biol. Appl. 68, 982–994. doi: 10.1016/j.msec.2016.05.119

Ghosh I., Bose S., Vippagunta R., Harmon F. Nanosuspension for improving the bioavailability of a poorly soluble drug and screening of stabilizing agents to inhibit crystal growth. Int J Pharm 2011, 409, 260–268. DOI: 10.1016/j.ijpharm.2011.02.051

Gökçe E.H., Sandri G., Egrilmez S., Bonferoni M.C., Guneri T., Caramella C. Cyclosporine a-loaded solid lipid nanoparticles: ocular tolerance and in vivo drug release in rabbit eyes. Curr Eye Res 2009, 34, 996–1003. DOI: 10.3109/02713680903261405

Göppert T.M., Müller R.H. Polysorbate-stabilized solid lipid nanoparticles as colloidal carriers for intravenous targeting of drugs to the brain: Comparison of plasma protein adsorption patterns. J. Drug Target. 13, 179–187 (2005)

Gowda N.K., Ledoux D.R., Rottinghaus G.E., Bermudez A.J., Chen Y.C. Antioxidant Efficacy of Curcuminoids From Turmeric (Curcuma Longa L.) Powder in Broiler Chickens Fed Diets Containing Aflatoxin B1. Br J Nutr 2009 Dec;102(11):1629-34. doi: 10.1017/S0007114509990869.

Gref R., Domb A., Quellec P., Blunk T., Muller R.H., Verbavatz J.M., Langer R. The controller intravenous delivery of drugs using PEG-coated sterically stabilized nanospheres. Adv Drug Deliv Rev 1995, 16, 215-233.

Gref R., Minamitake Y., Peracchia M.T., Trubetskoy V., Torchilin V., Langer R. Biodegradable long circulating polymeric nanospheres. Science 1994, 263, 1600–1603.

Gronthos S., Mankani M., Brahim J., Robey P.G., Shi S. Postnatal human dental pulp stem cells (DPSCs) in vitro and in vivo. Proc. Natl. Acad. Sci. USA 2000, 97, 13625–13630.

Hanafy A., Spahn-Langguth H., Vergnault G., Grenier P., Tubic Grozdanis M., Lenhardt T., Langguth P. Pharmacokinetic evaluation of oral fenofibrate nanosuspensions and SLN in comparison to conventional suspensions of micronized drug. Adv Drug Deliv Rev 2007; 419-426.

Hatcher H., Planalp R., Cho J., Torti F.M., Torti S.V. Curcumin: from ancient medicine to current clinical trials. Cell Mol Life Sci 2008, 65, 1631-52.

Hauser H., Strauss G. Stabilization of small, unilamellar phospholipid vesicles by sucrose during freezing and dehydration, Adv. Exp. Med. Biol., 1988; 238:71–80.

Higuera-Ciapara I., Félix-Valenzuela L., Goycoolea F.M. Astaxanthin: A Review of Its Chemistry and Applications. Crit Rev Food Sci Nutr. 2006;46(2):185-96. doi: 10.1080/10408690590957188.

Holzer P. The pharmacological challenge to tame the transient receptor potential vanilloid-1 (TRPV1) nocisensor. Br. J. Pharmacol. 2008, 155, 1145–1162.

Hu X., Kang X., Ying X., Wang L., Du Y. Enhanced oral absorption of saquinavir mediated by PEGylated solid lipid nanoparticles. RSC Adv 2015, 5, 40341.

Illum L., Hunneyball I.M., Davis S.S. The effect of hydrophilic coating on the uptake of the colloidal particles by the liver and by peritoneal-macrophages. Int J Pharm 1986; 29, 53-65.

Impellizzeri D., Talero E., Siracusa R., Alcaide A., Cordaro M., Maria Zubelia J., Bruschetta G., Crupi R., Esposito E., Cuzzocrea S., et al. Protective effect of polyphenols in an inflammatory process associated with experimental pulmonary fibrosis in mice. Br. J. Nutr. 2015; 114:853–865. doi: 10.1017/S0007114515002597.

Jenning V., Gohla S.H. Encapsulation of retinoids in solid lipid nanoparticles (SLN), J. Microencapsul. 18 (2001) 149 – 158.

Jenning V., Mader K., Gohla S.H. Solid lipid nanoparticles (SLN) based on binary mixtures of liquid and solid lipids: a 1H-NMR study, Int. J. Pharm. 205 (2000) 15 – 21.

Jenning V., Thunemann A.F., Gohla S.H. Characterisation of a novel solid lipid nanoparticle carrier system based on binary mixtures of liquid and solid lipids, Int. J. Pharm. 1999 (2000) 167 – 177.

Jiang T., Liao W., Charcosset C. Recent advances in encapsulation of curcumin in nanoemulsions: A review of encapsulation technologies, bioaccessibility and applications. Food Res Int 2020, 132:109035.

Jin L., Miyamoto O., Toyoshima T., Kobayashi R., Murakami T.H., Itano T. Localization of calbindin-D28k in normal and incised mouse skin: immunohistochemical and immunoblot analysis. Arch Dermatol Res 1997, 289, 578-584.

Johnson R.J. The complement system. In Biomaterials Science: An Introduction to Materials in Medicine, 2nd ed.; Ratner, B.D., Hoffman, A.S., Schoen, F.J., Lemons J.E. Elsevier Academic Press, Amsterdam, 2004; 318-328.

Joubert E., Richards E.S., Merwe J.D., De Beer D. Manley M. Gelderblom W.C. Effect of species variation and processing on phenolic composition and in vitro antioxidant activity of aqueous extracts of Cyclopia spp. (Honeybush Tea). J Agric Food Chem 2008, 56, 954–963. DOI: 10.1021/jf072904a

Kastantin M., Ananthanarayanan B., Karmali P., Ruoslahti E., Tirrell M. Effect of the Lipid Chain Melting Transition on the Stability of DSPE-PEG (2000) Micelles. Langmuir 2009, 25, 7279–7286.

Kaul G., Amiji M. Long-circulating poly(ethylene glycol)-modified gelatin nanoparticles for intracellular delivery. Pharm. Res. 2002; 19: 1061-1067.

Kedei, N., Szabo T., Lile J.D., Treanor J.J., Olah Z., Iadarola M.J., Blumberg P.M. Analysis of the native quaternary structure of vanilloid receptor 1. J. Biol. Chem. 2001, 276, 28613–28619.

Kesslak J.P., Cotman C.W., Chui H.C., Van den Noort S., Fang H., Pfeffer R., Lynch G. Olfactory tests as possible probes for detecting and monitoring Alzheimer's disease. Neurobiol Aging 1988; 9:399–403.

Kim C.S., Kawada T., Kim B.S., Han I.S., Choe S.Y. Capsaicin exhibits anti-inflammatory property by inhibiting IkB-a degradation in LPS-stimulated peritoneal macrophages. Cell Signal. 2003, 15, 299–306.

Kim S.J., Sung M.S., Heo H, Lee J.H., Park S.W. Mangiferin Protects Retinal Ganglion Cells in Ischemic Mouse Retina via SIRT1. Curr Eye Res 2016, 41, 844-55. DOI: 10.3109/02713683.2015.1050736

Kommareddy S., Amiji M. Biodistribution and pharmacokinetic analysis of long-circulating thiolated gelatin nanoparticles following systemic administration in breast cancer-bearing mice. J Pharm Sci 2007, 96, 397-407.

Koss E., Weiffenbach J.M., Haxby J.V., Friedland R.P. Olfactory detection and recognition in Alzheimer's disease. Lancet 1987; 1:622.

Koss E., Weiffenbach J.M., Haxby J.V., Friedland R.P. Olfactory detection and identification performance are dissociated in early Alzheimer's disease. Neurology 1988; 38:1228–32.

Kostadinova R., Wahli W., Michalik L. PPARs in diseases: control mechanisms of inflammation, Curr Med Chem, 12 (2005) 2995-3009.

Kubanis, P., Zornetzer, S. F. Age-related behavioral and neurobiological changes: A review with an emphasis on memory. *Behavioral & Neural Biology 1981, 31*(2), 115–172. doi:10.1016/S0163-1047(81)91195-X.

Lazzeri M., Vannucchi M.G., Spinelli M., Bizzoco E., Beneforti P., Turini D., Faussone-Pellegrini M.S. Transient receptor potential vanilloid type 1 (TRPV1) expression changes from normal urothelium to transitional cell carcinoma of human bladder. Eur. Urol. 2005, 48, 691–698.

Lee H., Ahn S., Ann J., Ha H., Yoo Y.D., Kim Y.H., Hwang J.Y., Hur K.H., Jang C.G., Pearce L.V. Discovery of dual-acting opioid ligand and TRPV1 antagonists as novel therapeutic agents for pain. Eur. J. Med. Chem. 2019, 182, 111634.

Lee H.Y., Kim S.W., Lee G.H., Choi M.K., Chung H.W., Lee Y.C., Kim H.R., Kwon H.J., Chae H.J. Curcumin and Curcuma longa L. extract ameliorate lipid accumulation through the regulation of the endoplasmic reticulum redox and ER stress. Sci Rep 2017, 7: 6513.

Leonardi A., Bucolo C., Romano G.L., Platania C.B., Drago F., Puglisi G., Pignatello R. Influence of different surfactants on the technological properties and in vivo ocular tolerability of lipid nanoparticles. Int J Pharm 2014, 470, 133–140. DOI: 10.1016/j.ijpharm.2014.04.061

Li M., Zahi M.R., Yuan Q., Tian F., Liang H. Preparation and stability of Astaxanthin solid lipid nanoparticles based on stearic acid. Eur. J. Lipid Sci. Technol. 2016, 118, 592–602.

Li Y., Huang T.H., Yamahara J. Salacia root, a unique Ayurvedic medicine, meets multiple targets in diabetes and obesity. Life Sci 2008, 82, 1045–1049. DOI: 10.1016/j.lfs.2008.03.005

Li Y.Z., Sun X., Gong T., Liu J., Zuo J., Zhang Z.R. Inhalable microparticles as carriers for pulmonary delivery of thymopentin- loaded solid lipid nanoparticles. Pharm. Res, 2010; 1977-1986.

Li Z., Dong X., Liu H., Chen X., Shi H., Fan Y., Hou D., Zhang X. Astaxanthin protects ARPE-19 cells from oxidative stress via upregulation of Nrf2-regulated phase II enzymes through activation of PI3K/Akt. Mol Vis. 2013 Jul 25;19:1656-66.

Lim S-J., Lee M-K., Kim C-K. Altered chemical and biological activities of all-trans retinoic acid incorporated in solid lipid nanoparticle powders. J. Control. Release, 2004, 100(1), 53-61. http://dx.doi.org/10.1016/j.jconrel.2004.07.032

Limb G. A., Webster L., Soomro H., Janikoun S., Shilling J. "Platelet expression of tumour necrosis factor-alpha (TNF-α), TNF receptors and intercellular adhesion molecule-1 (ICAM-1) in patients with proliferative diabetic retinopathy," Clinical and Experimental Immunology, vol. 118, no. 2, pp. 213–218, 1999.

Liparulo A., Esposito R., Santonocito D., Muñoz-Ramírez A., Spaziano G., Bruno F., Xiao J., Puglia C., Filosa R., Berrino L., D'Agostino B. Formulation and Characterization of Solid Lipid Nanoparticles Loading RF22-c, a Potent and Selective 5-LO Inhibitor, in a Monocrotaline-Induced Model of Pulmonary Hypertension. Front Pharmacol 2020 Feb 28;11:83. doi: 10.3389/fphar.2020.00083.

Liu R., Liu Z., Zhang C., Zhang B. Nanostructured Lipid Carriers As Novel Ophthalmic Delivery System for Mangiferin: Improving In Vivo Ocular Bioavaibility. J Pharm Sci 2012, 101, 3833-44. DOI: 10.1002/jps.23251

Lo Verme J., Fu J., Astarita G., La Rana G., Russo R., Calignano A., Piomelli D. The Nuclear Receptor Peroxisome Proliferator-Activated Receptor Mediates the Anti-Inflammatory Actions of Palmitoylethanolamide. Mol Pharmacol. 2005; 67(1):15–19.

Lorenzo-Veiga B., Sigurdsson H.H., Loftsson T., Alvarez-Lorenzo C. Cyclodextrin‾Amphiphilic Copolymer Supramolecular Assemblies for the Ocular Delivery of Natamycin. Nanomaterials 2019, 9, 745. DOI: 10.3390/nano9050745

Loureiro J.A., Andrade S., Duarte A., Neves A.R., Queiroz J.F., Nunes C., Sevin E., Fenart L., Gosselet F., Coelho M.A.N., Pereira M.C. Resveratrol and Grape Extract-loaded Solid Lipid Nanoparticles for the Treatment of Alzheimer's Disease. Molecules 2017, 22, 277.

Lucas-Abellan C., Mercader-Ros M.T., Zafrilla M.P., Gabaldon J.A., Nunez-Delicado E. Comparative study of different methods to measure antioxidant activity of resveratrol in the presence of cyclodextrins, Food Chem Toxicol 2011, 49, 1255-1260. DOI: 10.1016/j.fct.2011.03.004

Lui X., Li L., Su H., Zhou D., Hongmei S., Wang L., Jiang E.X. Poly (ethylene glycol)-block-poly(ε-caprolactone)– and phospholipid-based stealth nanoparticles with enhanced therapeutic efficacy on murine breast cancer by improved intracellular drug delivery. International Journal of Nanomedicine 2015:10 1791–1804.

Luo C.F., Hou N., Tian J., Yuan M., Liu S.M., Xiong L.G., Luo J.D., Chen M.S. Metabolic profile of puerarin in rats after intragastric administration of puerarin solid lipid nanoparticles. Int. J. Nanomed. 2013, 8, 933–940.

Luo Q., Zhao J., Zhang X., Pan, W. (2011). Nanostructured lipid carrier (NLC) coated with Chitosan Oligosaccharides and its potential use in ocular drug delivery system. Int. J. Pharm. 403, 185–191.

Madden T., Bally M., Hope M., Cullis P., Schieren H., Janoff A. Protection of large unilamellar vesicles by trehalose during dehydration: retention of vesicle contents, Biochim. Biophys. Acta, 1985; 817:67–74.

Maheshwari R.K., Singh A.K., Gaddipati J., Srimal R.C. Multiple biological activities of curcumin: a short review. Life Sci 2006, 78, 2081-7.

Mandal M., Jaiswal P., Mishra A. Role of curcumin and its nanoformulations in neurotherapeutics: A comprehensive review. J Biochem Mol Toxicol 2020, e22478.

Matias I., Wang J.W., Schiano Moriello A., Nieves A., Woodward D.F., Di Marzo V. Changes inendocannabinoid and palmitoylethanolamide levels in eye tissues of patients with diabetic retinopathy and age-related macular degeneration. Prostaglandins, Leukotrienes and Essential Fatty Acids 2006, 75, 413–418.

Mehnert W., K. Mader K. Solid lipid nanoparticles: production, characterization and applications. Adv. Drug Deliv. Rev., 2001; 47 (2-3): 165-96.

Mehnert W.Z., Muhlen A., Weyhers H., Muller R.H. Solid lipid nanoparticles (SLN)-ein neuartiger Wirkstoff-Carrier fur Kosmetika und Pharmazeutika. II. Wirkstoff-Inkorporation, Freisetzung und Sterilizierbarkeit. Pharm Ind, 1997, 59, 511.

Michael G.J., Priestley J.V. Differential expression of the mRNA for the vanilloid receptor subtype 1 in cells of the adult rat dorsal root and nodose ganglia and its downregulation by axotomy. J. Neurosci. 1999, 19, 1844–1854.

Moberg P.J., Pearlson G.D., Speedie L.J., Lipsey J.R., Strauss M.E., Folstein S.E. Olfactory recognition: differential impairments in early and late Huntington's and Alzheimer's diseases. J Clin Exp Neuropsychol 1987; 9:650–64.

Mohammadi M., Pezeshk A., Abbasi M.M., Ghanbarzadeh B., Hamishehkar H. Vitamin D3-Loaded Nanostructured Lipid Carriers as a Potential Approach for Fortifying Food Beverages; in Vitro and in Vivo Evaluation. Adv Pharm Bull 2017, 7, 61–71. DOI: 10.15171/apb.2017.008

Montenegro L., Ottimo S., Puglisi G., Castelli F., Sarpietro M.G. Idebenone Loaded Solid Lipid Nanoparticles Interact with Biomembrane Models: Calorimetric Evidence. Mol. Pharmaceutics 2012, 9, 2534−2541.

Morgan C.D., Nordin S., Murphy C. Odor identification as an early marker for Alzheimer's disease: impact of lexical functioning and detection sensitivity. J Clin Exp Neuropyschol 1995; 17:793–803.

Müller R.H., Mäder K., Gohla S. Solid lipid nanoparticles (SLN) for controlled drug delivery - a review of the state of the art. Eur. J. Pharm. Biopharm., 2000, 50(1), 161-177. Doi:10.1016/S0939-6411(00)00087-4

Muller R.H., Radtke M., Wissing S.A. Nanostructured lipid matrices for improved microencapsulation of drugs. Int J Pharm 2002, 242, 121–128. DOI: 10.1016/S0378-5173(02)00180-1.

Muller R.H., Souto E.B., Mehnert W. Solid Lipid Nanoparticles (SLN) and Nanostructured Lipid Carriers (NLC) for Dermal Delivery.Percutaneous Absorption; CRC Press, 2005, pp. 719-738.

Murphy C. Loss of olfactory function in dementing disease. Physiol Behav 1999; 66:177–82.

Musumeci T., Leonardi A., Bonaccorso A., Pignatello R., Puglisi G. Tangential Flow Filtration Technique: An Overview on Nanomedicine Applications. Pharm Nanotechnol. 2018;6(1):48-60. doi: 10.2174/2211738506666180306160921.

Naguib Y.W., Rodriguez B.L., Li X., Hursting S.D., Williams III R.O., Cui. Solid Lipid Nanoparticle Formulations of Docetaxel Prepared With High Melting Point Triglycerides: In Vitro and in Vivo Evaluation. Mol Pharm 2014 Apr 7;11(4):1239-49. doi: 10.1021/mp4006968. Epub 2014 Mar 12.

Nastruzzi, C. Lipospheres in drug targets and delivery: approaches, methods, and applications; CRC Press, 2004. http://dx.doi.org/10.1201/9780203505281

Naveen, P., Lingaraju H.B., Shyam Prasad K. Rapid Development and Validation of Improved Reversed-Phase High-performance Liquid Chromatography Method for the Quantification of Mangiferin, a Polyphenol Xanthone Glycoside in Mangifera indica. Pharmacognosy Res 2017, 9, 215- 219. DOI: 10.4103/0974-8490.204652.

Netto C.A., Izquierdo I.   On how passive is inhibitory avoidance. Behavioral and Neural Biology 1985; 43 (3), 327-330. Doi: 10.1016/S0163-1047(85)91697-8.c

Ninfali P., Mea G., Giorgini S., Rocchi M., Bacchiocca M. 2005. Antioxidant capacity of vegetables, spices and dressings relevant to nutrition. Br J Nutr 2005, 93, 257–266.

Nordin S., Murphy C. Odor memory in normal aging and Alzheimer's disease. Ann NY Acad Sci 1998; 855:686–93.

Ou B., Hampsch-Woodill M., Prior R.L. Development and validation of an improved oxygen radical absorbance capacity assay using fluorescein as the fluorescent probe. J. Agric. Food Chem. 2001, 49, 4619–4626.

Owens III D.E., Peppas N.A. Opsonization, biodistribution, and pharmacokinetics of polymeric Nanoparticles. Int. J. of Pharm. 2006; 307: 93-102.

Pal R., Larsen J.P., Moller S.G. The potential of proteomics in understanding neurodegeneration, Int. Rev. Neurobiol. 121 (2015) 25e58.

Palozza P., Torelli C., Boninsegna A., Simone R., Catalano A., Mele M.C., Picci N. Growth-inhibitory effects of the astaxanthin-rich alga Haematococcus pluvialis in human colon cancer cells. Cancer Letters 2009, 283 (1), 108-117.doi: 10.1016/j.canlet.2009.03.031

Panagi Z., Beletsi A., Evangelatos G., Livaniou E., Ithakissios D.S., Avgoustakis K. Effect of dose on the biodistribution and pharmacokinetics of PLGA and PLGA-mPEG nanoparticles. Int J Pharm 2001, 221, 143-152.

Panaro M.A., Corrado A., Benameur T., Paolo C.F., Cici D., Porro C. The Emerging Role of Curcumin in the Modulation of TLR-4 Signaling Pathway: Focus on Neuroprotective and Anti-Rheumatic Properties. Int J Mol Sci 2020, 21, 2299.

Panico A., Maccari R., Cardile V., Avondo S., Crascì L., Ottanà R. Evaluation of the anti-inflammatory/chondroprotective activity of aldose reductase inhibitors in human chondrocyte cultures. Med Chem Commun 2015, 6, 823-830.

Paolino D., Accolla M.L., Cilurzo F., Cristiano M.C., Cosco D., Castelli F., Sarpietro M.G., Fresta M., Celia C. Interaction between PEG lipid and DSPE/DSPC phospholipids: An insight of PEGylation degree and kinetics of de-PEGylation. Colloids Surf. B Biointerfaces 2017, 155, 266–275.

PardeikeJ., Hommoss A., Müller R.H. Lipid nanoparticles (SLN, NLC) in cosmetic and pharmaceutical dermal products. Int J pharm 2009;366 170-184.

Pardo-Andreu G.L., Sánchez-Baldoquín C., Avila-González R., Delgado R., Naal Z., Curti C. Fe^{3+} improves antioxidant and cytoprotecting activities of mangiferin. Eur J Pharmacol. 2006;547(1-3):31–6.

Paterniti, I., Di Paola, R., Campolo, M., Siracusa, R., Cordaro, M., Bruschetta, G., et al. (2015). Palmitoylethanolamide treatment reduces retinal inflammation in streptozotocin-induced diabetic rats. Eur. J. Pharmacol. 769, 313–323.

Pescosolido N., Librando A., Puzzono M., Nebbioso M. Palmitoylethanolamide Effects on Intraocular Pressure After Nd:YAG Laser Iridotomy: An Experimental Clinical Study. J Ocul Pharmacol Ther 2011 Dec;27(6):629-35. doi: 10.1089/jop.2010.0191. Epub 2011 Aug 10.

Petrosino S., Iuvone T., Di Marzo V. N-palmitoyl-ethanolamine: Biochemistry and new therapeutic

Piermarocchi S., Saviano S., Parisi V., Tedeschi M., Panozzo G., Scarpa G., Boschi G., Lo Giudice G.; Carmis Study Group. Carotenoids in Age-related Maculopathy Italian Study (CARMIS). Eur J Ophthalmol. 2012 Mar-Apr;22(2):216-25.

Pignatello R., Puglisi, G. (2011). Nanotechnology in ophthalmic drug delivery: a survey of recent developments and patenting activity. Recent Patents Nanomed. 1:13.

Pikal M.J., Shah S. The collapse temperature in freeze drying: Dependance on measurement methodology and rate of water removal from the glassy state. Int J Pharm, 1990; 62:165-86.

Pison U., Welte T., Giersig M., Groneberg D.A. Nanomedicine for respiratory diseases. Eur J Pharmacol. 2006; 341- 350.

Platania C.B.M., Fidilio A., Lazzara F., Piazza C., Geraci F., Giurdanella G., Leggio G.M., Salomone S., Drago F., Bucolo C. Retinal Protection and Distribution of Curcumin in Vitro and in Vivo. Front Pharmacol. 2018; 9:670.

Pleguezuelos-Villa M., Nácher A., Hernández M.J., Vila Buso M.A.O., Ruiz Sauri A., Díez-Sales O. Mangiferin nanoemulsions in treatment of inflammatory disorders and skin Regeneration. Int J Pharm 2019, 564, 299–307. DOI: 10.1016/j.ijpharm.2019.04.056

Prabhu P.N., Ashokkumar P., Sudhandiran G. Antioxidative and Antiproliferative Effects of Astaxanthin During the Initiation Stages of 1,2-dimethyl Hydrazine Induced Experimental Colon Carcinogenesis. Fundam Clin Pharmacol 2009 Apr;23(2):225-34. doi: 10.1111/j.1472-8206.2009.00669.x.

Prasad S., Tyagi A.K. Curcumin and its analogues: a potential natural compound against HIV infection and AIDS. Food Funct 2015, 6, 3412-9.

Prevarskaya N., Zhang L., Barritt G. TRP channels in cancer. Biochim. Biophys. Acta 2007, 1772, 937–946.

Prior R.L., Wu X., Schaich K. Standardized methods for the determination of antioxidant capacity and phenolics in foods and dietary supplements. J. Agric. Food Chem. 2005, 53, 4290–4302.

Puglia C., Blasi P., Ostacolo C., Sommella E., Bucolo C., Platania C.B.M., Romano G.L., Geraci F., Drago F., Santonocito D., Albertini B., Campiglia P., Puglisi, G., Pignatello R. Innovative Nanoparticles Enhance N-Palmitoylethanolamide Intraocular Delivery; Front Pharmacol 2018, 9, 285. DOI: 10.3389/fphar.2018.00285

Puglia C., Blasi P., Rizza L., Schoubben A., Bonina F., Rossi C., Ricci M. Lipid nanoparticles for prolonged topical delivery: An in vitro and in vivo investigation. Int. J. Pharm. 2008, 357, 295–304.

Puglia C., Lauro M.R., Offerta A., Crascì L., Micicchè L., Panico A., Bonina F., Puglisi G. Nanostructured Lipid Carriers (NLC) as Vehicles for Topical Administration of Sesamol: In Vitro Percutaneous Absorption Study and Evaluation of Antioxidant Activity. Planta Med. 2017 Mar;83(5):398-404. doi: 10.1055/s-0042-105293.

Puglia C., Offerta A., Carbone C., Bonina F., Pignatello R., Puglisi G. Lipid nanocarriers (LNC) and their applications in ocular drug delivery. Curr Med Chem 2015, 22, 1589–1602. DOI: 10.2174/0929867322666150209152259

Puglia C., Offerta A., Rizza L., Zingale G., Bonina F., Ronsisvalle S. Optimization of curcumin loaded lipid nanoparticles formulated using high shear homogenization (HSH) and ultrasonication (US) methods. J Nanosci Nanotechnol. 2013;13(10):6888-6893.

Puglia C., Offerta A., Tirendi G.G., Tarico M.S., Curreri S., Bonina F., Perrotta R.E. Design of solid lipid nanoparticles for caffeine topical administration. Drug Deliv. 2016; 23(1):36-40.

Puglia C., Santonocito D., Musumeci T., Cardile V., Graziano A.C.E., Salerno L., Raciti G., Crascì L., Panico A., Puglisi G. Nanotechnological Approach to Increase the Antioxidant and Cytotoxic Efficacy of Crocin and Crocetin. Planta Med. 2019 Feb;85(3):258-265. doi: 10.1055/a-0732-5757;

Puglia C., Santonocito D., Ostacolo C., Sommella E.M., Campiglia P., Carbone C., Drago F., Pignatello R., Bucolo C. Ocular Formulation Based on Palmitoylethanolamide-Loaded Nanostructured Lipid Carriers: Technological and Pharmacological Profile. Nanomaterials (Basel) 2020 Feb 8;10(2):287.doi: 10.3390/nano10020287.

Puri D., Bhandari A., Sharma P. and Choudhary D. Lipid nanoparticles (SLN, NLC): a novel approach for cosmetic and dermal pharmaceutical. Journal of Global Pharma Technology. 2010; 2(5):1-15.

Rajashree H., Harshal G., Vilasrao K. Solid lipid nanoparticles and nanostructured lipid carriers: a review. Curr. Drug Ther., 2011, 6(4), 240-250.doi: 10.2174/157488511798109637

Ramon-Cueto A., Avila J. (1998) Olfactory ensheathing cells: properties and function. Brain Res Bull 46:175–187.

Rasool M., Malik A., Qureshi M.S., Manan A., Pushparaj P.N., Asif M., Qazi M.H., Qazi A.M., Kamal M.A., Gan S.H., Sheikh I.A. Recent Updates in the Treatment of Neurodegenerative Disorders Using Natural Compounds. Evid Based Complement Alternat Med 2014; 2014:979730. doi: 10.1155/2014/979730.

Rigon R.B., Fachinetti N., Severino P., Santana M.H., Chorilli M. Skin delivery and in vitro biological evaluation of trans-resveratrol-loaded solid lipid nanoparticles for skin disorder therapies. Molecules, 2016, 21(1), E116. http://dx.doi.org/10.3390/molecules21010116

Rodríguez J., Di Pierro D., Gioia M., Monaco S., Delgado R., Coletta M., Marini S. Effects of a natural extract from Mangifera indica L, and its active compound, mangiferin, on energy state and lipid peroxidation of red blood cells. Biochim Biophys Acta. 2006;1760(9):1333–42

Romero-Aroca P., de la Riva-Fernandez S., Valls-Mateu A., Sagarra-Alamo R., Moreno-Ribas A., Soler N., Puig D. Cost of diabetic retinopathy and macular oedema in a population, an eight year follow up, BMC Ophthalmology (2016) 16:136.

Ruozi B., Tosi G., Forni F., Fresta M., Vandelli M.A. Atomic force microscopy and photon correlation spectroscopy: Two techniques for rapid characterization of liposomes. Eur. J. Pharm. Sci. 2005, 25, 81–89.

Sampat K.M., Garg S.J. Complications of intravitreal injections. Curr Opin Ophthalmol 2010;21:178–83.

Sanchez-Lopez E., Espina M., Doktorovova S., Souto E.B., Garcia, M.L. (2017). Lipid nanoparticles (SLN, NLC): overcoming the anatomical and physiological barriers of the eye - Part II - Ocular drug-loaded lipid nanoparticles. Eur. J. Pharm. Biopharm. 110, 58–69.

Sansone F., Mencherini T., Picerno P., D'Amore M., Aquino R.P., Lauro M.R. Maltodextrin/pectin microparticles by spray-drying as carrier for nutraceutical extracts. J. Food Eng., 2011, 105, 468-476. doi:10.1016/j.jfoodeng.2011.03.004.

Sá-Nunes A., Rogerio A.P., Medeiros A.I., Fabris V.E., Andreu G.P., Rivera D.G., Delgado R., Faccioli L.H. Modulation of eosinophil generation and migration by Mangifera indica L. extract (Vimang®). Int Immunopharmacol 2006, 6, 1515–1523. DOI: 10.1016/j.intimp.2006.04.008.

Sarkar A., Sreenivasan Y., Ramesh G.T., Manna S.K. β-D-Glucoside Suppresses Tumor Necrosis Factor-induced Activation of Nuclear Transcription Factor κB but Potentiates Apoptosis. August 6, 2004 The Journal of Biological Chemistry 279, 33768-33781 doi: 10.1074/jbc.M403424200

Sarpietro M.G., Accolla M.L., Celia C., Grattoni A., Castelli F., Fresta M., Ferrari M., Paolino D. Differential scanning calorimetry as a tool to investigate the transfer of anticancer drugs to biomembrane model. Curr. Drug Targets 2013, 14, 1053–1060.

Satoh A., Tsuji S., Okada Y., Murakami N., Urami M., Nakagawa K., Ishikura M., Katagiri M., Koga Y., Shirasawa T. Preliminary Clinical Evaluation of Toxicity and Efficacy of A New Astaxanthin-rich Haematococcus Pluvialis Extract. J Clin Biochem Nutr 2009 May;44(3):280-4. doi: 10.3164/jcbn.08-238.

Schubert M.A., Muller-Goymann C.C. Solvent injection as a new approach for manufacturing lipid nanoparticles – evaluation of the method and process parameters. Eur J Pharm Biopharm 2003, 55, 125–131.

Schwarz C., Mehnert W. Freeze- drying of drug- free and drug- loaded solid lipid nanoparticles (SLN). Int. J. Pharm,1997; 157:171-179.

Schwarz C., Mehnert W. Solid lipid nanoparticles (SLN) for controlled drug delivery. II. Drug incorporation and physicochemical characterization. J. Microencapsul., 1999, 16(2), 205-213. Doi:10.1080/026520499289185

Seite S., Moyal D., Richard S., de Rigal J., Leveque J.L., Hourseau C., Fourtanier A.J. 1998, Mexoryl SX: A broad absorption UVA filter protects human skin from the effects of repeated suberythemal doses of UVA, Photochem Photobiol B 44:69–76

Sentjurc M., Ahlin P., Strancar J., Kristl J. Eur. J. Pharm. Sci., 2003, 19(4), 181.

Sharma A., Jindal M., Aggarwal G., Jain S. 2010. Development of a Novel Method for Fabrication of Solid Lipid Nanoparticles: using High Shear Homogenization and Ultrasonication. Biological and Chemical Sciences 1, 265-274.

Shidhaye S.S., Vaidya R., Sutar S., Patwardhan A., Kadam V.J. Solid Lipid Nanoparticles and Nanostructured Lipid Carriers – Innovative Generations of Solid Lipid Carriers. Current Drug Delivery, 2008, 5, 324-331.

Shimojo A.A.M., Fernandes A.R.V., Ferreira N.R.E., Sanchez-Lopez E., Santana M.H.A., Souto E.B. Evaluation of the Influence of Process Parameters on the Properties of Resveratrol-Loaded NLC Using 22 Full Factorial Design. Antioxidants 2019, 8, 272. DOI: 10.3390/antiox8080272

Shuhendler A.J., Prasad P., Leung M., Rauth A.M., Dacosta R.S., Wu X.Y. A novel solid lipid nanoparticle formulation for active targeting to tumor $\alpha(v)$ $\beta(3)$ integrin receptors reveals cyclic RGD as a double-edged sword. Adv. Healthc. Mater. 2012, 1,600–608.

Shulkin P., Seltzer S., Davis M., Adams D. Lyophilized liposomes: a new method for long-term vesicular storage, J. Microencapsul., 1984; 1:73–80.

Shytle R.D., Bickford P.C., Rezai-zadeh K., Hou L., Zeng J., Tan J., Sanberg P.R., Sanberg C.D., Jr B.R., Fink R.C., Alberte R.S. Optimized Turmeric Extracts Have Potent Anti-Amyloidogenic Effects. Curr Alzheimer Res 2009 Dec;6(6):564-71. doi: 10.2174/156720509790147115.

Siewert M., Dressman J., Brown C.K., Shah V.P. FIP/AAPS guidelines to dissolution/in vitro release testing of novel/special dosage forms. AAPS Pharm Sci Tech 2003, 4, E7.

Silva B.A., Oliveira P.J., Dias A.C.P., Malva J.O., 2007. Mitochondria as targets for neuronal protection against excitotoxicity: a role for phenolic compounds? Cent. Nerv. Syst. Agents Med. Chem. 7, 205–222.

Simone D.A., Baumann T.K., LaMotte R.H. Dose-dependent pain and mechanical hyperalgesia in humans after intradermal injection of capsaicin. Pain 1989, 38, 99–107.

Simone D.A., Ngeow J.Y.F., Putterman G.J., La Motte R.H. Hyperalgesia to heat after intradermal injection of capsaicin. Brain Res. 1987, 418, 201–203.

Simone D.A., Nolano M., Johnson T., Wendelschafer-Crabb G., Kennedy W.R. Intradermal injection of capsaicin in humans produces degeneration and subsequent reinnervation of epidermal nerve fibers: Correlation with sensory function. J. Neurosci. 1998, 18, 8947–8959.

Souza L.G., Silva E.J., Martins A.L., Mota M.F., Braga R.C., Lima E.M., Valadares M.C., Taveira S.F., Marreto R.N. Development of topotecan loaded lipid nanoparticles for chemical stabilization and prolonged release. Eur. J. Pharm. Biopharm. 2011, 79, 189–196.

Spampinato S., Trabucco A., Biasiotta A., Biagioni F., Cruccu G., Copani A., ColledgeW.H., Sortino M.A., Nicoletti F., Chiechio S. Hyperalgesic activity of kisspeptin in mice. Mol. Pain 2011, 7, 1744–8069.

Srivastava P., Yadav R.S. Efficacy of Natural Compounds in Neurodegenerative Disorders. Adv Neurobiol 2016; 12:107-23. doi: 10.1007/978-3-319-28383-8_7.

Strauss G. Freezing and thawing of liposomes suspensions, in: G. Gregoriadis (Ed.), Liposome Technology, Preparation of Liposomes, 1984; 1: 197-219, CRC Press, Boca Raton.

Strauss G., Schurtenberger P., Hauser H. The interaction of saccharides with lipid bilayer vesicles: stabilization during freeze-thawing and freeze-drying, Biochim. Biophys. Acta, 1986; 858:169–180.

Tang J., Kern T.S. Inflammation in diabetic retinopathy. Prog Retin Eye Res. 2011; 30(5):343– 358.

Tang M., Taghibiglou C. The Mechanisms of Action of Curcumin in Alzheimer's Disease. Journal of Alzheimer's Disease 58 (2017) 1003–1016.

Tharanathan R.N., Yashoda H.M., Prabha T.N. 2006. Mango (Mangifera indica L.), "The king of fruits" - An overview. Food Rev Int 2006, 22, 95–123. DOI: 10.1080/87559120600574493

Thau L., Asuka E., Mahajan K. Physiology, Opsonization. 2020 May 24. In: StatPearls [Internet]. Treasure Island (FL): StatPearls Publishing; 2020.

Thresh J.C. Isolation of capsaicin. Pharm J Trans 1876, 6:941-947.

Tripathi D.N., Jena G.B. Astaxanthin Intervention Ameliorates Cyclophosphamide-Induced Oxidative Stress, DNA Damage and Early Hepatocarcinogenesis in Rat: Role of Nrf2, p53, p38 and phase-II Enzymes. Mutat Res 2010 Feb;696(1):69-80. doi: 10.1016/j.mrgentox.2009.12.014.

Tronino D., Offerta A., Ostacolo C., Russo R., De Caro C., Calignano A., Puglia C., Blasi P. Nanoparticles prolong N-palmitoylethanolamide anti-inflammatoryand analgesic effects in vivo. Colloids Surf B Biointerfaces 2016, 141, 311–317.

Trotta M., Debernardi F., Caputo O. Preparation of solid lipid nanoparticles by a solvent emulsification-diffusion technique. Int J Pharm 2003, 257, 153–160. DOI: 10.1016/S0378-5173(03)00135-2

Ueda T., Inden M., Ito T., Kurita H., Hozumi I. Characteristics and Therapeutic Potential of Dental Pulp Stem Cells on Neurodegenerative Diseases. Front. Neurosci. 2020, 14, 407.

Varela-Garcia A., Concheiro A., Alvarez-Lorenzo C. Cytosine-functionalized bioinspired hydrogels for ocular delivery of antioxidant transferulic acid. Biomater Sci 2020, 8, 1171-1180. DOI: 10.1039/c9bm01582e.

Varela-Garcia A., Concheiro A., Alvarez-Lorenzo C. Soluplus micelles for acyclovir ocular delivery: Formulation and cornea and sclera permeability. Int J Pharm 2018, 552, 39-47. DOI: 10.1016/j.ijpharm.2018.09.053.

Vega-Villa K., Takemoto J.K., Yáñez J.A. Clinical toxicities of nanocarrier systems. Adv Drug Deliver Rev 2008, 60: 929-938.

Vemuri S., Yu C.D., DeGroot J., Wangsatornthnakum V., Venkataram S. Effect of sugars on freeze–thaw and lyophilization of liposomes, Drug Dev. Ind. Pharm., 1991; 17:327–348.

Vighi E., Ruozi B., Montanari M., Battini R., Leo E. Re-dispersible cationic solid lipid nanoparticles (SLNs)freeze-dried without cryoprotectors: Characterization and ability to bind the pEGFP-plasmid. Eur. J. Pharm.Biopharm. 2007, 67, 320–328.

Vijayan V., Aafreen S., Sakthivel S., Reddy K.R. Formulation and characterization of solid lipid nanoparticles loaded Neem oil for topical treatment of acne. J. Acute Dis., 2013, 2(4), 282-286.

Vilceanu D., Honore P., Hogan Q.H., Stucky C.L. Spinal nerve ligation in mouse upregulates TRPV1 heat function in injured IB4-positive nociceptors. J. Pain 2010, 11, 88–99.

Vonarbourg A., Passirani C., Saulnier P., Benoit J.P. Parameters influencing the stealthiness of colloidal drug delivery systems, Biomaterials 27 (2006) 4356–4373.

Wang H.-Q., Sun X.-B., Xu Y.-X., Zhao H., Zhu Q.-Y., Zhu C.-Q. Astaxanthin upregulates heme oxygenase-1 expression through ERK1/2 pathway and its protective effect against beta-amyloid-induced cytotoxicity in SH-SY5Y cells. Brain Res. 2010, 1360, 159–167.

Wang Y., Kho K., Cheow W.S., Hadinoto K. A comparison between spray drying and spray freeze drying for dry powder inhaler formulation of drug-loaded lipid-polymer hybrid nanoparticles. Int. J. Pharm. 2012, 424, 98–106.

Warner M.D., Peabody C.A., Flattery J.J., Tinklenberg J.R. Olfactory deficits and Alzheimer's disease. Biol Psychiatry 1986; 21:116–8.

Watson C.P., Evans R.J., Watt V.R. Post-herpetic neuralgia and topical capsaicin. Pain 1988, 33, 333–340.

Weber M., Steinle H., Golombek S., Hann L., Schlensak C., Wendel H.P., Avci-Adal M. Blood-Contacting Biomaterials: In Vitro Evaluation of the Hemocompatibility. Front Bioeng Biotechnol 2018, 6, 99. DOI: 10.3389/fbioe.2018.00099

Williams R., Airey M., Baxter H., Forrester J., Kennedy-Martin T., Girach A. Epidemiology of diabetic retinopathy and macular oedema: a systematic review. Eye. 2004; 18:963–983.

Wissing S.A., Kayser O., Müller R.H. Solid lipid nanoparticles for parenteral drug delivery. Adv. Drug Deliv. Rev.,2004, 56(9), 1257-1272. http://dx.doi.org/10.1016/j.addr.2003.12.002

Yamagishi R., Aihara M. Neuroprotective effect of astaxanthin against rat retinal ganglion cell death under various stresses that induce apoptosis and necrosis. Molecular Vision 2014; 20:1796-1805.

Yang F., Zheng J. Understand spiciness: Mechanism of TRPV1 channel activation by capsaicin. Protein Cell2017, 8, 169–177.

Yu S., Wang Q.M., Wang X., Liu D., Zhang W., Ye T. (2015). Liposome incorporated ion sensitive in situ gels for opthalmic delivery of timolol maleate.Int. J. Pharm. 480, 128–136.

Yuan H., Chen C.Y., Chai G.H., Du Y.Z., Hu F.Q. Improved Transport and Absorption Through Gastrointestinal Tract by PEGylated Solid Lipid Nanoparticles. Mol Pharm 2013 May 6;10(5):1865-73. doi: 10.1021/mp300649z. Epub 2013 Apr 5.

Zanforlin E., Zagotto G., Ribaudo G. An Overview of New Possible Treatments of Alzheime r's Disease, Based on Natural Products and Semi-Synthetic Compounds. Current Medicinal Chemistry, 2017, 24, 3749-3773.

Zhang J., He Y., Jiang X., Jiang H., Shen J. Nature Brings New Avenues to the Therapy of Central Nervous System diseases-An Overview of Possible Treatments Derived From Natural Products. Sci China Life Sci 2019 Oct;62(10):1332-1367. doi: 10.1007/s11427-019-9587-y.

Zhang Z., Lv H., Zhou J. Novel solid lipid nanoparticles as carriers for oral administration of insulin. Pharmazie 2009; 574-578.

Zhao Y., Zhao B (2013). Oxidative stress and the pathogenesis of Alzheimer's disease. Oxid Med Cell Longev 2013, 1-10

Zheng K., Dai X., Xiao N., Wu X., Wei Z., Fang W., Zhu Y., Zhang J., Chen X. (2017) Curcumin ameliorates memory decline via inhibiting BACE1 Eexpression and –amyloid pathology in 5×FAD transgenic mice. Mol Neurobiol 54, 1967-1977.

Zhuang C.Y., Li N., Wang M., Zhang X.N., Pan W.S., Peng J.J., Pan J.S., Tang X. Preparation and characterization of vinpocetine loaded nanostructured lipid carriers (NLC) for improved oral bioavailability. Int J Pharm 2010; 179-185.

Zur Mühlen A, Schwarz C, Mehnert W. Solid lipid nanoparticles (SLN) for controlled drug delivery– drug release and release mechanism. Eur J Pharm Biopharm. 1998;45(2):149–155

Curriculum Vitae and Doctoral Activities

PhD candidate: DEBORA CONCETTA SANTONOCITO

Doctor of Philosophy Thesis

"Lipid Nanoparticles as Tools for the Administration of Active Natural Products Aimed to the Treatment of Nervous System Disorders"

International PhD in Chemical Sciences, XXXIII Cycle, 2017-2020

University of Catania, Department of Chemical Sciences-Italy

Short CV

Debora Concetta Santonocito was born on February 2nd, 1990 in Catania (Italy).

She graduated in Chemistry and Pharmaceutical Technology at University of Catania (Italy) in 2016 with a final work concerning the *Evaluation of antioxidant and anticancer activity of compounds extracted from Crocus Sativus L. through lipid nanoparticles*.

In the same university she obtained a contract as research collaborator (2 months) and she won a scholarship grant (3 months) to work in a project related to "*Optimization of the formulation process of lipid nanoparticles containing crocin and crocetin*".

The following year, she started the PhD course in Chemical Sciences where she worked in the Department of Drug Sciences under the supervision of Prof. Puglia. Moreover, she spent of her PhD course (4 months) at Departamento de Farmacia y Tecnología Farmacéutica-University of Santiago di Compostela (Spain), under the supervision of Prof. Carmen Alvarez Lorenzo. During the latter period, she acquired skills about toxicity and ophthalmology studies and participated at the following

seminars: "*Caracterizacìon de particulas Ambivalue Eye Tech*" and "*Bioimpresiòn con equipo BIO X de CELLINK*".

During the PhD course, she presented the results of her research activity through poster contributions at several conferences. Furthermore, she is author or co-author of several pubblications. She also member of the CRS Italy Chapter.

The main scientific interests are focused on nanotechnology and natural compouds.

Finally, in order to improve her writing skills she is following an online course "English for Research Publication Purposes Specialization" through the Coursera platform.

Doctoral Activities

During her PhD course, Debora Concetta Santonocito worked on the research project "*Lipid Nanoparticles as Tools for the Administration of Active Natural Products Aimed to the Treatment of Nervous System Disorders*", under the supervision of Prof. Puglia at Department of Drug Sciences (University of Catania).

She studied many strategies in order to formulate stable lipid nanoparticles loaded with natural compounds, suitable for parenteral/ocular administration, for the potential treatment of nervous system disorders.

Along this period, she has acquired skills on preparation and characterization of different lipid nanocarriers. Moreover thanks to the Prof. Carmen Alvarez Lorenzo, the candidate learnt many skills about toxicity and ophthalmology studies.

During the PhD period, she was co-supervisor of six experimental theses in Pharmaceutical Technology and laboratory assistant of "Tecnologia socioeconomia e legislazione farmaceutica e laboratorio di tecnica" course of Prof. Carmelo Puglia.

Furthermore, she attended numerous PhD courses kept by international researcher such as:

- "*Project writing*" kept by Prof. J. Silberring (University of Krakow, Poland), March 2018;

- "*The role of dioxygen in the biosphere*" kept by Prof. O. Hansson (University of Gothenburg, Sweden), July 2018.

As part of her educational activity, she gave an oral presentation "*Novel strategies to optimize dermal and transdermal delivery of active pharmaceutical ingredients (API)*".

The scientific actitivies (pubblications, posters and conferences) are summarized in the following list.

- **Pubblications**

1. *Cosmeceuticals: Nanotechnology-Based Strategies for the Delivery of Phytocompounds*. Puglia C, **Santonocito D**. Curr Pharm Des. 2019;25(21):2314-2322. doi: 10.2174/1381612825666190709211101.

2. *Innovative Nanoparticles Enhance N-Palmitoylethanolamide Intraocular Delivery*. Puglia C, Blasi P, Ostacolo C, Sommella E, Bucolo C, Platania CBM, Romano GL, Geraci F, Drago F, **Santonocito D**, Albertini B, Campiglia P, Puglisi G, Pignatello R. Front Pharmacol. 2018 Mar 28; 9:285. doi: 10.3389/fphar.2018.00285.

3. *Lipid Nanoparticles and Active Natural Compounds: A Perfect Combination for Pharmaceutical Applications*. Puglia C, Pignatello R, Fuochi V, Furneri PM, Lauro MR, **Santonocito D**, Cortesi R, Esposito E. Curr Med Chem. 2019;26(24):4681-4696. doi: 10.2174/0929867326666190614123835.

4. *Nanotechnological Approach to Increase the Antioxidant and Cytotoxic Efficacy of Crocin and Crocetin*. Puglia C, **Santonocito D**, Musumeci T, Cardile V, Graziano ACE, Salerno L, Raciti G, Crascì L, Panico AM, Puglisi G. Planta Med. 2019 Feb;85(3):258-265. doi: 10.1055/a-0732-5757.

5. *Lipid Nanoparticle Inclusion Prevents Capsaicin-Induced TRPV1 Defunctionalization.* Puglia C, **Santonocito D**, Bonaccorso A, Musumeci T, Ruozi B, Pignatello R, Carbone C, Parenti C, Chiechio S. Pharmaceutics. 2020 Apr 10;12(4):339. doi: 10.3390/pharmaceutics12040339.

6. *Curcumin Containing PEGylated Solid Lipid Nanoparticles for Systemic Administration: A Preliminary Study.* **Santonocito D,** Sarpietro MG, Carbone C, Panico A, Campisi A, Siciliano EA, Sposito G, Castelli F, Puglia C. Molecules. 2020 Jun 30;25(13): E2991. doi: 10.3390/molecules25132991.

7. *Ocular Formulation Based on Palmitoylethanolamide-Loaded Nanostructured Lipid Carriers: Technological and Pharmacological Profile.* Puglia C, **Santonocito D**, Ostacolo C, Maria Sommella E, Campiglia P, Carbone C, Drago F, Pignatello R, Bucolo C. Nanomaterials (Basel). 2020 Feb 8;10(2):287. doi: 10.3390/nano10020287.

8. *Optimization of Curcumin Nanocrystals as Promising Strategy for Nose-to-Brain Delivery Application.* Bonaccorso A, Gigliobianco MR, Pellitteri R, **Santonocito D**, Carbone C, Di Martino P, Puglisi G, Musumeci T. Pharmaceutics. 2020 May 23;12(5):476. doi: 10.3390/pharmaceutics12050476.

9. *Formulation and Characterization of Solid Lipid Nanoparticles Loading RF22-c, a Potent and Selective 5-LO Inhibitor, in a Monocrotaline-Induced Model of Pulmonary Hypertension.* Liparulo A, Esposito R, **Santonocito D**, Muñoz-Ramírez A, Spaziano G, Bruno F, Xiao J, Puglia C, Filosa R, Berrino L, D'Agostino B. Front Pharmacol. 2020 Feb 28; 11:83. doi: 10.3389/fphar.2020.00083.

- Posters

1. *Lipid nanoparticles based on crocin and crocetin: antioxidant activities and anticancer properties.* Puglia; **Santonocito**; Musumeci; Crascì; Panico; Cianciolo; Siracusa; Pignatello

and Puglisi. 11th World Meeting on Pharmaceutics, Biopharmaceutics and Pharmaceutical Technology; Granada, Spain, March 19-22, 2018

2. *Freeze drying optimization of lipid nanoparticles for naproxen delivery: formulation, characterization and effect of cryoprotectant agents*. **Santonocito**, Puglia and Puglisi. 18th School for Doctorate in Pharmaceutical Technology "Innovation in local drug delivery"; Como, September 25-28, 2018.

3. *Formulation and Characterization In Monocrotaline-Induced Pulmonary Hypertension Of Solid Lipid Nanoparticles Loaded RF-22c, A Potent And Selective 5-LO Inhibitor*. Liparulo, Esposito, **Santonocito**, Muñoz-Ramírez, Spaziano, Bruno, Xiao, Berrino, Puglia, Filosa and D'Agostino. 19th Advanced Course in Pharmaceutical Technology "Characterization of Colloidal Nanocarriers"; Soverato (CZ), September 9-12, 2019.

4. *Ocular Formulation Based On Palmitoylethanolamide-Loaded Nanostructured Lipid Carriers: Technological And Pharmacological Profile*. Puglia, **Santonocito**, Ostacolo, Sommella, Campiglia, Carbone, Drago, Pignatello and Bucolo. 19th Advanced Course in Pharmaceutical Technology "Characterization of Colloidal Nanocarriers"; Soverato (CZ), September 9-12, 2019.

5. *Astaxanthin Loaded Stealth Solid Lipid Nanoparticles (S-SLN) Interact with Biomembrane Models: Calorimetric Evidence*. **Santonocito**, Puglia, Sarpietro and Castelli. CRS Italy Chapter Annual Workshop di Catania, Catania, November 7-9, 2019.

6. *Mangiferin-loaded nanostructured lipid carriers (NLC) with antioxidant activity*. **Santonocito** and Puglia. Nanoinnovation 2020, Rome 15-18 September 2020.

- **Oral discussion**

Astaxanthin Loaded Stealth Solid Lipid Nanoparticles (S-SLN) Interact with Biomembrane Models: Calorimetric Evidence. CRS Italy Chapter Annual Workshop di Catania, Catania, November 7-9, 2019.